Study on Water Management to Suppress the Hysteresis Phenomenon in Anion Exchange Membrane Fuel Cells

A Doctoral Thesis Presented to Special Doctoral Program for Green Energy Conversion Science and Technology

The Integrated Graduate School of Medicine, Engineering and Agricultural Science

University of Yamanashi

March 2022

G19DTE01 Kanji Otsuji

Contents

Chapter 3 Two approaches to suppress the performance hysteresis phenomenon in anion exchange membrane fuel cells with Fe-N-C cathode catalysts

Chapter 4 General conclusions and Future prospects

Chapter 1

General Introduction

1.1 Background

Japan is an island country that is geographically isolated from other continents and has scarce energy resources. Japan relies on the energy resources produced in other countries; About 10 years ago, the self-sufficiency rate was 20.3% in 2010, but due to various factors, the self-sufficiency rate of Japan's primary energy supply is only 11.8% in the 2018 forecast [1]. Japan relies heavily on fossil fuels such as coal, oil and natural gases as its primary energy resources. The energy dependency of the fossil fuels was 81.2% in 2010, which increased to 85.5% in 2018 because of the Great East Japan Earthquake in 2011 [2]. Fossil fuels such as coal, oil, natural gas and uranium which is a fuel for nuclear power generation, are limited and will be depleted in the remaining 50 to 130 years [3, 4]. And the use of large amounts of fossil fuels inevitably causes serious environmental problems such as global warming and atmospheric pollution. For future generations, we need to prepare an alternative energy source for fossil fuels. As a low-emission power source for a sustainable society, there is a strong demand for the establishment of power generation methods such as solar power generation, wind power generation, hydroelectric power generation, and geothermal power generation. The problem with these energy sources is that unpredictable weather and geodynamic impacts make it difficult to meet rapid fluctuations in electricity demand. Electricity is generally stored in batteries to provide balanced power, but batteries are not suitable for large/long-term power storage.

To solve these problems, hydrogen is attracting attention as a promising candidate for storage and transportation carriers, which is generated from the electricity generated by the use of renewable energy. Hydrogen is used and produced in a variety of ways. For example, it can be produced by reforming fossil fuels, by-products of industrial processes, biomass production by microorganisms and water electrolysis [5]. The produced hydrogen is converted to electricity by using fuel cells.

Fuel cells are devices that converts chemical energy into electricity through the reaction of oxygen (in the air) with fuel (usually hydrogen) and was first put to practical use by Sir William Robert Grove in 1839. The fuel cells can be typically classified into four types by electrolytes and operating temperatures: polymer electrolyte fuel cells (PEFCs), solid oxide fuel cells (SOFCs), molten carbonate fuel cells (MCFCs) and phosphoric acid fuel cells (PAFCs). Fuel cells have major advantages such zero emission, high efficiency, compactness and quietness. Among the fuel cells, PEFCs and SOFCs are actively studied and developed for vehicle and residential use. In 2009, a residential co-generation fuel cell system named “ENE-FARM” was released by electronic manufactures and gas companies. Fuel cell vehicles (FCVs) has stated to sell under the name of “CLARITYFUEL CELL” by Honda Motor Co., Ltd in 2016 and renewed “MIRAI” by Toyota Motor Co., Ltd. in 2020.

1.2 Polymer electrolyte fuel cells (PEFCs)

Among the fuel cells, PEFCs have attracted most attention and are intensively studied because of their advantages, such as high power density, low operating temperature, quick start-up and shut-down, and easy maintenance [4, 5]. PEFCs can be further categorized into two types by electrolyte membranes: proton exchange membrane fuel cells

(PEMFCs) and anion exchange membrane fuel cells (AEMFCs) [6-9]. For PEFCs, polymer electrolyte membrane is one of the key materials. Currently, proton exchange membranes (PEMs), perfluorosulfonated acid membranes such as Nafion (Du Pont) as an example, are mostly used in PEFCs due to their high proton conductivity and chemical/mechanical stability [10, 11]. For PEFCs using PEMs with a strong acidic nature, the electrodes are exposed to acid environments. Such acidic condition requires platinum for the electrocatalysts. This is a serious drawback for wide-spread practical applications. For the last decade, replacing the PEMs with anion exchange membranes (AEMs) have attracted considerable attentions as an approach to reduce the cost of electrocatalysts by replacing platinum [7, 12].

1.3 Anion exchange membrane fuel cells (AEMFCs)

In recent years, AEMFCs have been actively studied [6-9, 13]. Figure 1-1 shows a schematic drawing of an AEMFCs, which generally consists of two conductive separators with gas flow channels and membrane electrode assemblies (MEAs). MEAs are constructed with AEMs, the two catalyst layers (CLs) and two gas diffusion layers (GDLs) both at the cathode and the anode. The CL is composed of highly distributed Pt-based nanoparticles (2-5 nm in diameter supported on carbon black (ca. <10 nm in diameter) of anion conductive electrolyte ionomer binders (Figure 1-2 [14]). Non-Pt-based catalysts are extensively studied, too, but the performance is still lower. GDL is a porous material typically consisting of a microporous fibrous material (carbon fiber paper) and a microporous layer (MPL) containing poly tetrafluoroethylene (PTFE). A GDL allows an effective diffusion of gases (hydrogen and oxygen), a prpper water management and an electronic connection between the separator and electrode. In

AEMFCs, hydrogen and oxygen are supplied into the CLs through gas flow channels and the GDLs at the anode and cathode, respectively. During the AEMFC operation, the oxygen reduction reaction (ORR) and the hydrogen oxidation reaction (HOR) take place at the cathode (Eq. 1-1) and anode (Eq. 1-2), respectively, and only H_2O is generated at the anode (Eq. 1-3).

$$\text{Cathode: } O_2 + 2H_2O + 4e^- \rightarrow 4OH^- \qquad E^0_a = -0.83\ V \qquad \text{(Eq. 1-1)}$$

$$\text{Anode: } 4OH^- + 2H_2 \rightarrow 4e^- + 4H_2O \qquad E^0_c = 0.40\ V \qquad \text{(Eq. 1-2)}$$

$$\text{Overall reaction: } 2H_2 + O_2 \rightarrow 2H_2O \qquad E^0 = 1.23\ V \qquad \text{(Eq. 1-3)}$$

Hydroxide ions are generated from oxygen, water and electron on the triple phase boundary, where contact ionomers, reactions and catalyst (Figure 1-2), and transferred to the anode through the membrane. Subsequently, hydrogen and hydroxide ion react and produce water on the triple phase boundary at the anode.

AEMFCs have been investigated as a low-cost fuel cell alternative to PEMFCs due to the potential use of non-platinum group metal (PGM) catalysts and the enhanced oxygen reduction kinetics on non-PGM catalysts under alkaline conditions. [13, 15-21]

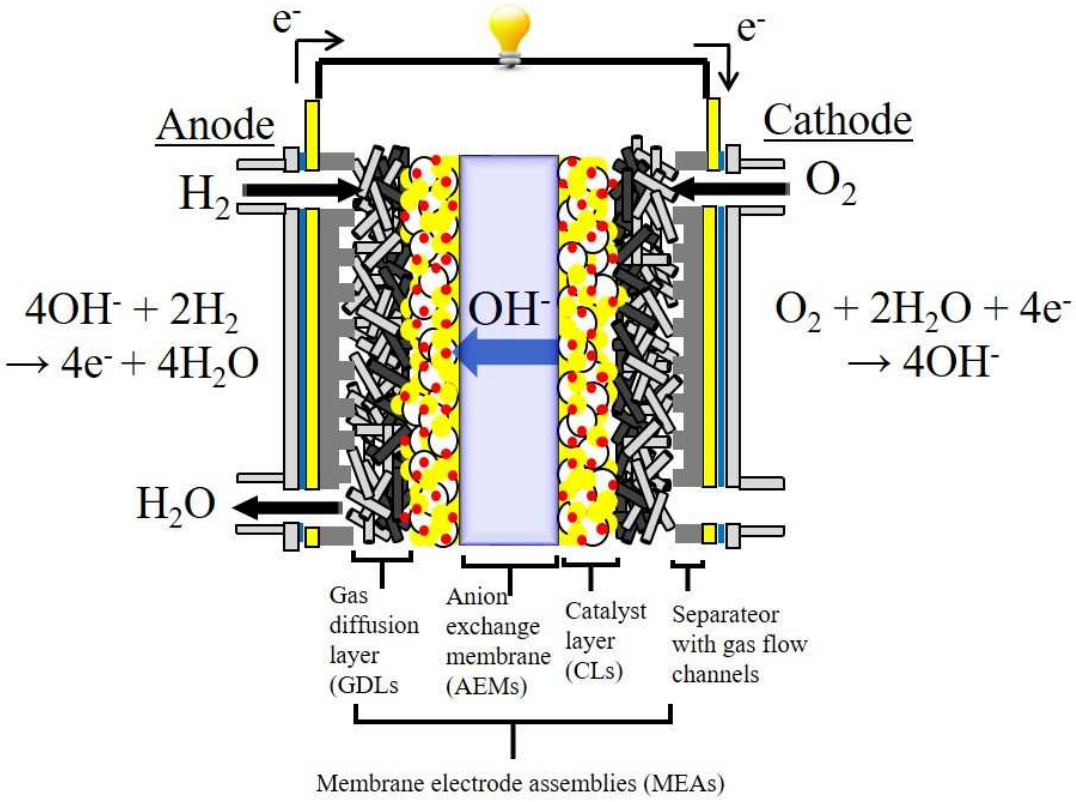

Figure 1-1. Schematic diagram of AEMFCs

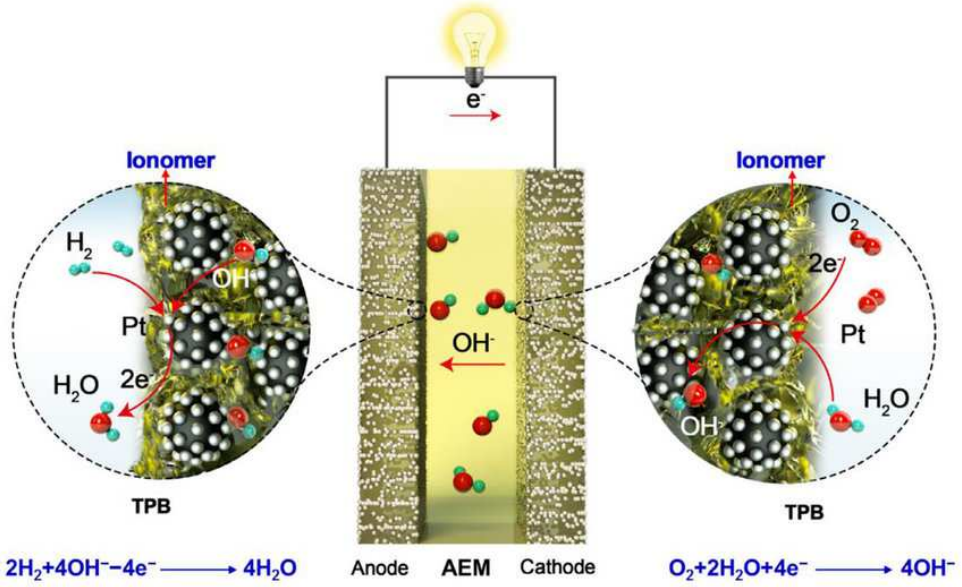

Figure 1-2. Schematic diagram of the triple-phase boundary for AEMFCs

1.4 Technical challenges of AEMFCs

The technical challenge for AEMFCs is that there is still much room for improvement in both performance and durability compared to PEMFCs. To obtain high performance and durability for AEMFCs, the chemical / mechanical stability and anion conductivity of the AEMs continue to be improved. [22-30] In recent years, various strategies have been devised to overcome these problems, such as microphase separation, cross-linking, and organic-inorganic composites. [9, 14, 30] This means that AEMs can be manufactured with higher anion conductivity while maintaining the same ion exchange capacity (IEC). [25, 31] In addition, Mandal et al. reported a high performance AEMFC with an anionic conductivity of 212 mS cm^{-1}, cell performance of 3.5 W cm^{-2}, and cell durability of more than 545 hours at 80 ^{o}C due to the introduction of cross-linking and long alkyl spacers. [32]

Other important factors are the development of effective non-PGM catalysts. For anodes, mainly Ni-based non-PGM catalysts have been reported. [16, 18, 33] For cathodes, mainly non-PGM catalysts based on Fe, Co and other transition metals have been reported. [6, 34-40] Among these, Hossen et al. reported the remarkable result that an Fe-N-C catalyst had the same performance as that of platinum-supported carbon (Pt/C), by combining the N-C materials used in the synthesis of catalysts and optimizing the ionomer content of the cathode catalyst layers (CLs). [37]

In addition to the above components, water management of the anode and cathode is also an important factor in AEMFCs. For the anion transport n the anion conductive ionomer membranes, three types of hydroxide ion transfer mechanisms (surface site hopping, Grotthuss mechanism and Vehicle mechanism) have been manly suggested and discussed (Figure 1-3). [41] The surface site hopping with hydroxide ions proceeds on

quaternized ammonium groups in the ionomer membranes. The Grotthuss mechanism is based on a hopping process though the hydrogen bond network of water molecules, and considered to be the dominant transport mechanisms for hydroxide ion transport though anion conductive ionomers. The Vehicle mechanism is based on molecular diffusion process of hydrated hydroxide ion. In both cases, water is an important factor in AEMFCs. Moreover, water is produced at the anode by the HOR and consumed at the cathode by the ORR of AEMFCs. Also, water moves from the cathode to the anode, due to the electroosmotic drag associated with the movement of OH^-, and moves from the anode to the cathode due to back-diffusing water. [42-54] In other words, the AEMFC must provide sufficient water to maintain hydration of the AEMs and electrodes, without flooding the anode or drying the cathode. Kaspar et al. reported improvement of flooding and drying for CLs by controlling the use of MPLs associated with the GDLs and the humidification of the feed gases. [45]. In another recent study, Mustain et al. reviewed the water management of AEMFCs in detail [46]. Peng et al. reported suppression of flooding by lowering the humidification temperature to the extent that ionomer decomposition did not occur and increasing the hydrophobicity of the GDL and CL [55]. Dekel et al. also reported, by means of simulation, that the water required for the cathodic reaction increases with increasing current density and that the lack of water shortens the AEMFC life [47, 48]. Recently, Omasta et al. reported that back-diffusing water is the main source for maintaining the hydrated state of AEMs during cell operation, in addition to being an important water source for the cathodic reaction [49, 50].

One of the problems that can be predicted for water management in AEMFCs is, for example, the I-V hysteresis phenomenon. In PEMFCs, it was concluded that this hysteresis phenomenon was due to the increased gas diffusion overvoltage caused by

cathodic flooding and can be improved by optimizing the water management of PEMFCs. [51] On the other hand, AEMFCs require water for the cathodic reaction and produce water in the anodic reaction, which may lead to hysteresis phenomena at both the anode and cathode. This is estimated to be due to lack of water at the cathode and blockage of water at the anode. I-V hysteresis causes the power output of the fuel cell to fluctuate, which may cause an imbalance in the power supply. In a large-scale system such as a stack, water management such as water supply and removal is very difficult. Suppression of the hysteresis phenomenon is essential to equalize the power supply and demand, and it is necessary to evaluate the water management of the AEMFC from a bird's eye view.

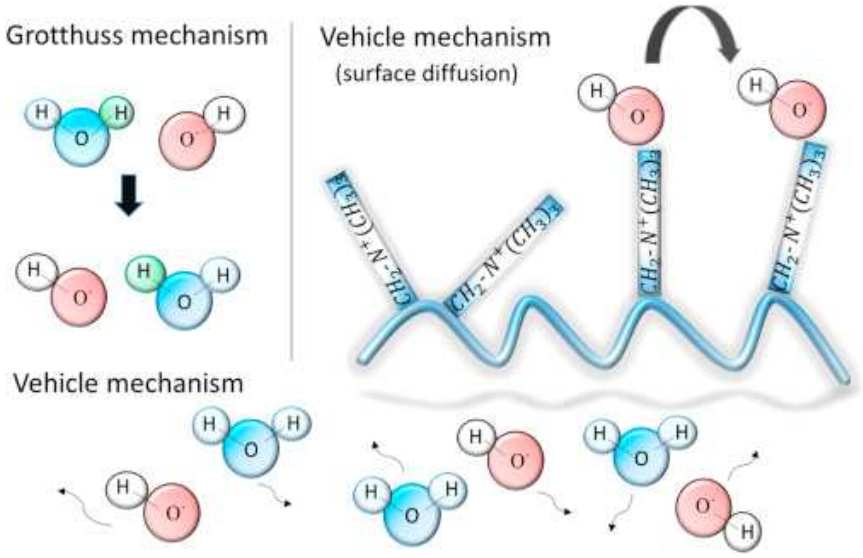

Figure 1-3. Schematic of hydroxide transport mechanisms in AEMs and ionomers.

While studies are conducted on water management of various AEMFCs, the overall number of studies on water management of AEMFCs are very low. (Figure 1-4. [52]). In addition, a limitation of these studies on water management has been that the cells were evaluated under unrealistic conditions involving the use of high gas flow rates (e.g., 1 L min^{-1} for 4~5 cm^2 cell) in order to achieve maximum power density [49-50, 52-56]. This is quite low in terms of hydrogen and oxygen flow rate utilization, 3% for hydrogen (stoichiometric ratio = 33.3) and 1.5% (stoichiometric ratio = 66.6) for oxygen at 1 A cm^{-2} [38, 49, 50], which are difficult to be implemented in practical fuel cell systems. Chen et al. have proposed a new normalized efficiency metric of W cm^{-2} divided by the flow rate, W s cm^{-2} L^{-1}. [58] As a result, AEMFCs with low flow rates can be compared with AEMFCs with high power generation performance at high flow rates, and our understanding of the water management of AEMFCs for practical applications has been enhanced. The maximum power of the current cell is about 210 W s cm^{-2} L^{-1} using Pt-Ru/C and Pt/C catalysts. [29]

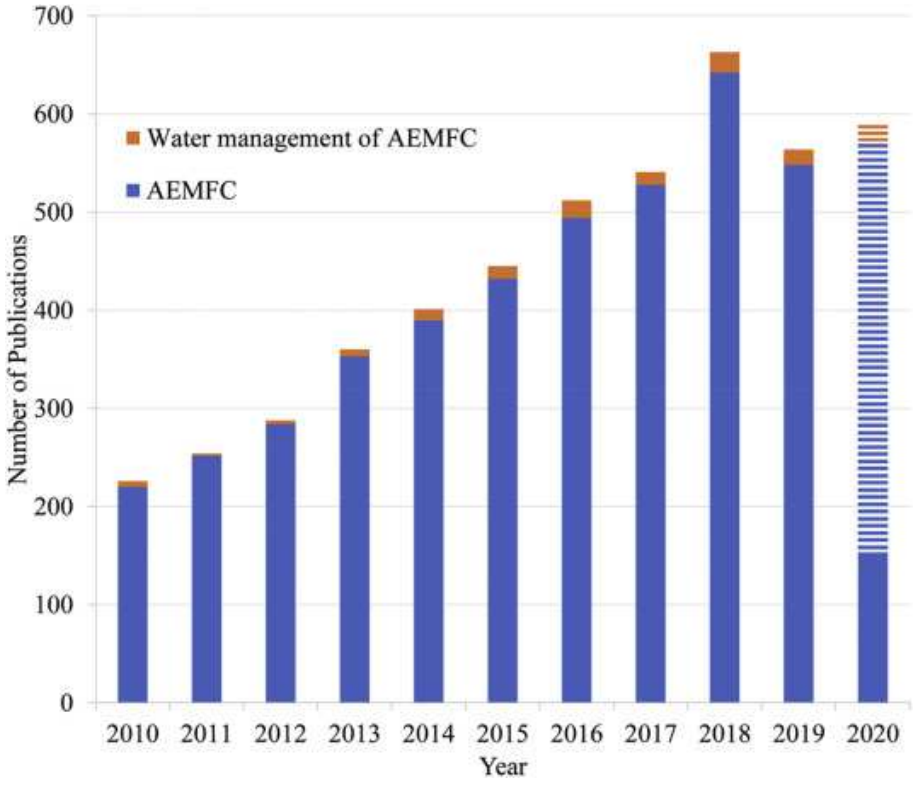

Figure 1-4. Year wise number of publications appeared in AEMFC and water management in the last ten years from Web of Science using the key words “AEMFC” or “water management and “AEMFC”.

1.5 Objective of this research

The stable operation of AEMFCs is an integral part of the overall stability and performance of hydrogen energy systems. That is, they require dynamic transient responses that are fast and stable so that they can quickly respond to increases in power demand. As mentioned in the previous section, when water is the cause of the I-V performance mismatch, or hysteresis phenomenon, it is estimated to occur in both the anode and cathode electrocatalyst layers. At the anode, power generation performance is degraded due to inhibition of the fuel, H_2, by water formation, called flooding, i.e., increased diffusion overvoltage. At the cathode, the lack of water leads not only to a decrease in power generation performance but also to a decrease in durability.

As described above, improving the water management of AEMFCs is an important research to improve the performance and durability of power generation. The purpose of this paper is to evaluate the performance of AEMFCs under low flow conditions and with non-precious metal cathode catalysts, and to obtain a deeper understanding of water management in AEMFCs. This thesis consists of two chapters: water management affecting cells with low flow rate and cathodic non-PGMs catalysts leading to higher performance of AEMFCs, and investigation and suggestion of ways to improve the water management.

In Chapter 2, the importance of water management for high performance AEMFCs are discussed through various power generation tests and analysis of the catalyst layer (Tafel slope component analysis and nitrogen adsorption, etc.). The importance of this Current-Voltage (I-V) hysteresis phenomenon is first raised in this thesis.

In Chapter 3, two approaches are investigated to suppress the I-V hysteresis phenomenon that occurred in Chapter 2, that is, to improve the water management

capability: Specifically, (i) Improve water diffusion by using a thinner AEM and hydrophilization of the membrane to increase the flux of back-diffusing water from the anode. (ii) Fabrication of a highly ORR-active catalyst layer with macro/mesopore layers accessible to both oxygen gas and water to improve the supply of water to the active site of the cathodic non-PGMs catalysts. These approaches are analyzed by current-sensing atomic force microscopy (CS-AFM) and contact angle measurement for hydrophilized membranes, and nitrogen adsorption and cell-based power generation evaluation for cathodic non-precious metal catalyst layers, and their effects are discussed.

Finally, in Chapter 4, the result are summarized and future prospects are overviewd.

References

[1] International Energy Agency (IEA), “World Energy Balances 2019”.

[2] Agency for Natural Resources and Energy of Japan "Comprehensive Energy Statistics".

[3] BP Statistical Review of World Energy 2018.

[4] Organisation for Economic Cooperation and Development (OECD) and the International Atomic Energy Agency (IAEA), “Uranium 2018”.

[5] Hydrogen energy white paper published by New Energy and Industrial Technology Development Organization (NEDO).

[6] G. Couture, A. Alaaeddine, F. Boschet, B. Ameduri, “Polymeric materials as anion-exchange membranes for alkaline fuel cells,” *Progress in Polymer Science,* 36 (2011) 1521-1557. DOI: 10.1016/j.progpolymsci.2011.04.004

[7] G. Merle, M. Wessling, K. Nijmeijer, “Anion exchange membranes for alkaline fuel cells: a review,” *Journal of Membrane Science,* 377 (2011) 1-35. DOI: 10.1016/j.memsci.2011.04.043

[8] M. A. Hickner, A. M. Herring, E. B. Coughlin, “Anion Exchange Membranes: Current Status and Moving Forward,” *Journal of Polymer Science Part B,* 51 (2013) 1727-1735. DOI: 10.1002/polb.23395

[9] J. R. Varcoe, P. Atanassov, D. R. Dekel, A. M. Herring, M. A. Hickner, P. A. Kohl, A. R. Kucernak, W. E. Mustain, K. Nijmeijer, K. Scott, T. Xu, L. Zhuang, “Anion-exchange membranes in electrochemical energy systems,” *Energy & Environmental Science*, 7 (2014) 3135-3191. DOI: 10.1039/C4EE01303D

[10] A. Kraytsuberg, Y. Ein-Eli, “Review of Advanced Materials for Proton Exchange Membrane Fuel Cells”, *Energy Fuels* 28 (2014) 7303-7330. DOI: 10.1021/ef501977k

[11] A. Kusoglu, A. Z. Weber, “New Insights into Perfluorinated Sulfonic-Acid Ionomers”, *Chem. Rev.,* 117 (2017) 987−1104. DOI: 10.1021/acs.chemrev.6b00159

[12] D. R. Dekel, “Review of cell performance in anion exchange membrane fuel cells,” *Journal of Power Sources,* 375 (2018) 158-169. DOI: 10.1016/j.jpowsour.2017.07.117

[13] J. R. Varcoe, R. C. T. Slade, G. L. Wright, Y. Chen, “Steady-State dc and

Impedance Investigations of H2/O2 Alkaline Membrane Fuel Cells with Commercial Pt/C, Ag/C, and Au/C Cathodes", *The Journal of Physical Chemistry B,* , 110 (2006) 21041-21049. DOI: 10.1021/jp064898b

[14] N. Chen, Y. M. Lee, "Anion exchange polyelectrolytes for membranes and ionomers", *Progress in Polymer Science,* 113 (2021) 101345. DOI: 10.1016/j.progpolymsci.2020.101345

[15] M.A. Hickner, B.S. Pivovar, "The Chemical and Structural Nature of Proton Exchange Membrane Fuel Cell Properties," *Fuel Cells,* 5 (2005) 213-229. DOI: 10.1002/fuce.200400064

[16] D. R. Dekel, "Unraveling mysteries of hydrogen electrooxidation in anion exchange membrane fuel cells," *Current Opinion in Electrochemistry*, 12 (2018) 182-188. DOI: 10.1016/j.coelec.2018.11.013

[17] W. E. Mustain, "Understanding how high-performance anion exchange membrane fuel cells were achieved: Component, interfacial, and cell-level factors," *Current Opinion in Electrochemistry*, 12 (2018) 233-239. DOI: 10.1016/j.coelec.2018.11.010

[18] S. T. Thompson, D. Peterson, D. Ho, D. Papageorgopoulos, "Perspective—The Next Decade of AEMFCs: Near-Term Targets to Accelerate Applied R&D," *Journal of The Electrochemical Society*, 167 (2020) 084514. DOI: 10.1149/1945-7111/ab8c88

[19] M. Tanaka, K. Fukasawa, E. Nishino, S. Yamaguchi, K. Yamada, H. Tanaka, B. Bae, K. Miyatake, M. Watanabe, "Anion Conductive Block Poly(arylene ether)s: Synthesis, Properties, and Application in Alkaline Fuel Cells", *Journal of the American Chemical Society,* 133 (2011) 10646-10654. DOI: 10.1021/ja204166e

[20] A. Fazil, R. Chetty, "Synthesis and Evaluation of Carbon Nanotubes Supported Silver Catalyst for Alkaline Fuel Cell", *Electroanalysis,* 26 (2014) 2380-2387. DOI: 10.1002/elan.201400246

[21] R. Janarthanan, A. Serov, S. K. Pilli, D. A.Gamarra, P. Atanassov, M. R. Hibbs, A. M. Herring, "Direct Methanol Anion Exchange Membrane Fuel Cell with a Non-Platinum Group Metal Cathode based on Iron-Aminoantipyrine Catalyst", *Electrochimica Acta,* 175 (2015) 202-208. DOI: 10.1016/j.electacta.2015.03.209

[22] C. G. Arges, L. Zhang, "Anion Exchange Membranes' Evolution toward High Hydroxide Ion Conductivity and Alkaline Resiliency," *ACS Applied Energy Materials,* 1 (2018) 2991-3012. DOI: 10.1021/acsaem.8b00387

[23] J. Pan, C. Chen, L. Zhuang, J. Lu, "Designing Advanced Alkaline Polymer Electrolytes for Fuel Cell Applications," *Accounts of Chemical Research,* 45 (2012) 473-481. DOI: 10.1021/ar200201x

[24] J. Ponce-González, I. Ouachan, J. R. Varcoe, D. K. Whelligan, "Radiation-induced grafting of a butyl-spacer styrenic monomer onto ETFE: the synthesis of the most alkali stable radiation-grafted anion-exchange membrane to date," *Journal of Materials Chemistry A,* 6 (2018) 823-827. DOI: 10.1039/c7ta10222d

[25] H. Ono, T. Kimura, A. Takano, K. Asazawa, J. Miyake, J. Inukai, K. Miyatake, "Robust anion conductive polymers containing perfluoroalkylene and pendant ammonium groups for high performance fuel cells," *Journal of Materials Chemistry A,* 5 (2017) 24804-24812. DOI: 10.1039/c7ta09409d

[26] A. M. A. Mahmoud, A. M. M. Elsaghier, K. Otsuji, K. Miyatake, "High Hydroxide Ion Conductivity with Enhanced Alkaline Stability of Partially Fluorinated and Quaternized Aromatic Copolymers as Anion Exchange Membranes," *Macromolecules,* 50 (2017) 4256-4266. DOI: 10.1021/acs.macromol.7b00401

[27] D. Koronka, A. M. A. Mahmoud, K. Miyatake, "Partially fluorinated copolymers containing pendant piperidinium head groups as anion exchange membranes for alkaline fuel cells," *Journal of Polymer Science Part A,* 57 (2019) 1059-1069. DOI: 10.1039/c9ra07775h

[28] D. Koronka, A. Matsumoto, K. Otsuji, K. Miyatake, "Effect of Crosslinking on the Properties of Partially Fluorinated Anion Exchange Membranes," *RSC Advances,* 9 (2019) 37391-37402. DOI: 10.1002/pola.29360

[29] N. U. Hassan, M. Mandal, G. Huang, H. A. Firouzjaie, P. A. Kohl, W. E. Mustain, "Achieving High-Performance and 2000 h Stability in Anion Exchange Membrane Fuel Cells by Manipulating Ionomer Properties and Electrode Optimization," *Advanced Energy Materials*, 10, (2020) 2001986, DOI: 10.1002/aenm.202001986

[30] F. Xu, Y. Su, B. Lin, "Progress of Alkaline Anion Exchange Membranes for Fuel Cells: The Effects of Micro-Phase Separation", *Frontiers in Materials,* 7 (2020) 4.

DOI: 10.3389/fmats.2020.00004

[31] T. Kimura, A. Matsumoto, J. Inukai, K. Miyatake, "Highly Anion Conductive Polymers: How Do Hexafluoroisopropylidene Groups Affect Membrane Properties and Alkaline Fuel Cell Performance?", *ACS Applied Energy Materials,* 3, 1, (2020) 469-477. DOI: 10.1021/acsaem.9b01733

[32] M. Mandal, G. Huang, N. U. Hassan, X. Peng, T. Gu, A. H. Brooks-Starks, B. Bahar, W. E. Mustain, P. A. Kohl, "The Importance of Water Transport in High Conductivity and High-Power Alkaline Fuel Cells", *Journal of The Electrochemical Society,* 167 (2020) 054501. DOI: 10.1149/2.0022005JES

[33] A. Roy, M. R. Talarposhti, S. J. Normile, I. V. Zenyuk, V. D. Andrade, K. Artyushkova, A. Serov, P. Atanassov, "Nickel–copper supported on a carbon black hydrogen oxidation catalyst integrated into an anion-exchange membrane fuel cell," *Sustainable Energy Fuels,* 2 (2018) 2268-2275. DOI: 10.1039/c8se00261d

[34] V. M. Truong, J. R. Tolchard, J. Svendby, M. Manikandan, H. A. Miller, S. Sunde, H. Yang, D. R. Dekel, A. O. Barnett, "Platinum and Platinum Group Metal-Free Catalysts for Anion Exchange Membrane Fuel Cells," *Energies,* 13 (2020) 582. DOI: 10.3390/en13030582

[35] X. Peng, V. Kashyap, B. Ng, S. Kurungot, L. Wang, J. R. Varcoe, W. E. Mustain, "High-Performing PGM-Free AEMFC Cathodes from Carbon-Supported Cobalt Ferrite Nanoparticles," *Catalysts.,* 9 (2019) 264. DOI: 10.3390/catal9030264

[36] Y. Yang, H. Peng, Y. Xiong, Q. Li, J. Lu, L. Xiao, F. J. DiSalvo, L. Zhuang, H. D. Abruña, "High-Loading Composition-Tolerant Co–Mn Spinel Oxides with Performance beyond 1 W/cm^2 in Alkaline Polymer Electrolyte Fuel Cells," *ACS Energy Letters,* 4 (2019) 1251-1257. DOI: 10.1021/acsenergylett.9b00597

[37] M. M. Hossen, K. Artyushkova, P. Atanassov, A. Serov, "Synthesis and characterization of high performing Fe-N-C catalyst for oxygen reduction reaction (ORR) in Alkaline Exchange Membrane Fuel Cells," *Journal of Power Sources,* 375 (2018) 214-221. DOI: 10.1016/j.jpowsour.2017.08.036

[38] K. Tammeveski, J. H. Zagal, "Electrocatalytic oxygen reduction on transition metal macrocyclic complexes for anion exchange membrane fuel cell application," *Current Opinion in Electrochemistry*, 9 (2018) 207-213. DOI:

10.1016/j.coelec.2018.04.001

[39] P. Song, H. M. Barkholtz, Y. Wang, W. Xu, D. Liu, L. Zhuang, "High-performance oxygen reduction catalysts in both alkaline and acidic fuel cells based on pre-treating carbon material and iron precursor", *Science Bulletin,* 62 (2017) 1602–1608. DOI: 10.1016/j.scib.2017.10.020

[40] K. Kisand, A. Sarapuu, D. Danilian, A. Kikas, V. Kisand, M. Rähn, A. Treshchalov, M. Käärik, M. Merisalu, P. Paiste, J. Aruväli, J. Leis, V. Sammelselg, S. Holdcroft, K. Tammeveski, "Transition metal-containing nitrogen-doped nanocarbon catalysts derived from 5-methylresorcinol for anion exchange membrane fuel cell application", *Journal of Colloid and Interface Science,* 584 (2021) 263-274. DOI: 10.1016/j.jcis.2020.09.114

[41] H. Takaba, T. Hisabe, T. Shimizu, Md. K. Alam, "Molecular modeling of OH– transport in poly(arylene ether sulfone ketone)s containing quaternized ammonio-substituted fluorenyl groups as anion exchange membranes", *Journal of Membrane Science,* 522 (2017) 237-244. DOI: 10.1016/j.memsci.2016.09.019

[42] C. E. Diesendruck, D. R. Dekel, "Water – A key parameter in the stability of anion exchange membrane fuel cells," *Current Opinion in Electrochemistry,* 9 (2018) 173-178. DOI: 10.1016/j.coelec.2018.03.019

[43] W. Youa, K. J. T. Noonan, G. W. Coates, "Alkaline-stable anion exchange membranes: A review of synthetic approaches," *Progress in Polymer Science*, 100 (2020) 101177 DOI: 10.1016/j.progpolymsci.2019.101177

[44] R. Gutru, Z. Turtayeva, F. Xu, G. Maranzana, B. Vigolo, A. Desforges, "A comprehensive review on water management strategies and developments in anion exchange membrane fuel cells," *International Journal of Hydrogen Energy,* 45 (2020) 19642-19663. DOI: 10.1016/j.ijhydene.2020.05.026

[45] R. B. Kaspar, M. P. Letterio, J. A. Wittkopf, K. Gong, S. Gu, Y. Yan, "Manipulating Water in High-Performance Hydroxide Exchange Membrane Fuel Cells through Asymmetric Humidification and Wetproofing," *Journal of The Electrochemical Society*, 162 (2015) F483-F488. DOI: 10.1149/2.0131506jes

[46] W. E. Mustain, M. Chatenet, M. Page, Y. S. Kim, "Durability challenges of anion exchange membrane fuel cells," *Energy & Environmental Science,* 13 (2020) 2805-

2838, DOI: 10.1039/d0ee01133a

[47] D. R. Dekel, S. Willdorf, U. Ash, M. Amar, S. Pusara, S. Dhara, S. Srebnik, C. E. Diesendruck, "The critical relation between chemical stability of cations and water in anion exchange membrane fuel cells environment," *Journal of Power Sources,* 375 (2018) 351-360. DOI: 10.1016/j.jpowsour.2017.08.026

[48] D. R. Dekel, I. G. Rasin, M. Page, S. Brandon, "Steady state and transient simulation of anion exchange membrane fuel cells," *Journal of Power Sources,* 375 (2018) 191-204. DOI: 10.1016/j.jpowsour.2017.07.012

[49] T. J. Omasta, L. Wang, X. Peng, C.A. Lewis, J.R. Varcoe, W.E. Mustain, "Importance of balancing membrane and electrode water in anion exchange membrane fuel cells," *Journal of Power Sources,* 375 (2018) 205-213. DOI: 10.1016/j.jpowsour.2017.05.006

[50] T. J. Omasta, A. M. Park, J. M. LaManna, Y. Zhang, X. Peng, L. Wang, D. L. Jacobson, J. R. Varcoe, D. S. Hussey, B. S. Pivovar, W. E. Mustain, "Beyond catalysis and membranes: visualizing and solving the challenge of electrode water accumulation and flooding in AEMFCs," *Energy & Environmental Science*, 11 (2018) 551-558. DOI: 10.1039/c8ee00122g

[51] K. Park, J. Lee, H. Kim, K. Choi, G. Hwang, "Discrete regenerative fuel cell reduces hysteresis for sustainable cycling of water", *Nature Scientific Reports,* 4 (2014) 4592. DOI: 10.1038/srep04592

[52] R. Gutru, Z. Turtayeva, F. Xu, G. Maranzana, B. Vigolo, A. Desforges, "A comprehensive review on water management strategies and developments in anion exchange membrane fuel cells", *International Journal of Hydrogen Energy,* 45 (2020) 19642-19663. DOI: 10.1016/j.ijhydene.2020.05.026

[53] M. Mamlouk, J. A. Horsfall, C. Williams, K. Scott, "Radiation grafted membranes for superior anion exchange polymer membrane fuel cells performance," *International Journal of Hydrogen Energy,* 37 (2012) 11912-11920. DOI: 10.1016/j.ijhydene.2012.05.117

[54] J. Ponce-González, D. K. Whelligan, L. Wang, R. Bance-Soualhi, Y. Wang, Y. Peng, H. Peng, D. C. Apperley, H. N. Sarode, T. P. Pandey, A. G. Divekar, S. Seifert, A. M. Herring, L. Zhuang, J. R. Varcoe, "High performance aliphatic-heterocyclic

benzyl-quaternary ammonium radiation-grafted anion-exchange membranes," *Energy & Environmental Science*, 9 (2016) 3724-3735. DOI: 10.1039/c6ee01958g

[55] L. Wang, E. Magliocca, E. L. Cunningham, W. E. Mustain, S. D. Poynton, R. Escudero-Cid, M. M. Nasef, J. Ponce-González, R. Bance-Souahli, R. C. T. Slade, Da. K. Whelligan, J. R. Varcoe, "An optimised synthesis of high performance radiation-grafted anion-exchange membranes," *Green Chemistry,* 19 (2017) 831-843. DOI: 10.1039/c6gc02526a

[56] Y. Wang, G. Wang, G. Li, B. Huang, J. Pan, Q. Liu, J. Han, L. Xiao, J. Lu, L. Zhuang, "Pt–Ru catalyzed hydrogen oxidation in alkaline media: oxophilic effect or electronic effect?," *Energy & Environmental Science,* 8 (2015) 177-181. DOI: 10.1039/c4ee02564d

[57] X. Peng, D. Kulkarni, Y. Huang, T. J. Omasta, B. Ng, Y. Zheng, L. Wang, J. M. LaManna, D. S. Hussey, J. R. Varcoe, I. V. Zenyuk, W. E. Mustain, "Using operando techniques to understand and design high performance and stable alkaline membrane fuel cells," *Nature Communications,* 11 (2020) 3561, DOI: 10.1038/s41467-020-17370-7

[58] N. Chen, S. P. Kim, C. Hu, H. H. Wang, J. H. Park, H. M. Kim, Y. M. Lee, "High-performance poly(fluorenyl aryl piperidinium)-based anion exchange membrane fuel cells with realistic hydrogen supply", *Journal of Power Sources,* 512 (2021) 230474. DOI: 10.1016/j.jpowsour.2021.230474

Chapter 2

Performance hysteresis phenomena of anion exchange membrane fuel cells using an Fe-N-C cathode catalyst

2.1 Introduction

To deeply understand the water management of AEMFCs with low flow rates and non-precious metal catalysts at the cathode, it is necessary to test AEMs with various structures such as hydrocarbon-based membranes, cross-linking, and microphase separation. In this thesis, an anion conductive electrolyte (quaternized poly(arylene perfluoroalkylene), QPAF-4), which was developed by the University of Yamanashi and Takahata Precision Co., Ltd. [1], was used as the electrolyte membrane and binder. The QPAF-4 AEM with the molecular structure shown in Figure 2-1 is suitable for this study because of its excellent microphase molecular structure, high gas permeability, high alkaline stability and high membrane mechanical strength. QPAF-4 is also soluble in methanol, which is highly volatile and minimizes the effect of the catalyst layer preparation. In this Chapter 2, using practical gas flow conditions (0.1 L min^{-1} hydrogen, 0.1 L min^{-1} oxygen), and in order to focus on the issue of water management in the low flow rate and cathodic non-PGMs catalyst as described in Chapter 1, a MEA was fabricated using a commercial non-PGM catalyst (Fe-N-C) as the cathode and this QPAF-4 as both the membrane and CL binder. With these, the effects of AEMFCs on water management under near-practical conditions were investigated. Also, while the amount of supplied water vapor depends exponentially on the temperature, too high temperature

increases the aggressiveness of the anion OH^- on the membrane molecules, and furthermore, the durability of AEMFCs decreases rapidly when the water vapor supply is stagnant. In this thesis, the power generation performance was evaluated at 60 °C and 100% relative humidity (RH) so that the temperature was neither too high nor too low and could be compared with other AEMFC researches.

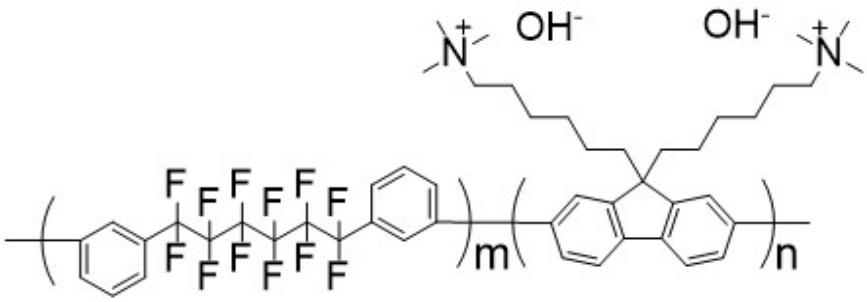

Figure 2-1. Chemical structure of quaternized poly(arylene perfluoroalkylene), QPAF-4.

2.2 Experimental

Preparation of MEAs

QPAF-4 was synthesized based on the synthetic procedure of Ono et al. [1].

The catalyst inks for the anodes were prepared with Pt catalyst supported on carbon black (Pt/CB: TEC10E50E, Tanaka Kikinzoku Kogyo, K. K.), methanol and pure water by use of a planetary ball mill for 30 min. Subsequently, 5 wt.% QPAF-4-MeOH (ion exchange capacity (IEC) = 2.0 meq g^{-1}) binder solution was added to the slurry, and the mixture was further stirred with a planetary ball mill for 30 min. The weight ratio of QPAF-4 binder to support carbon was adjusted to 0.8. In the same way, the catalyst inks for the cathodes were prepared with the Fe-N-C catalyst (XPMF2000E, Pajarito Powder), 5 wt.% QPAF-4-MeOH binder solution (IEC = 2.0 meq g^{-1}), methanol and pure water by use of a planetary ball mill. The weight ratio of QPAF-4 binder to support catalyst was adjusted to 0.43. These catalyst inks were directly sprayed onto the microporous layers (MPL) of the gas diffusion layer (GDL) as the anode (Carbon cloth GDL, GDL with MPL formed after water repellent treatment of PANEX30 PW03 from Zoltek) and cathode (29BC, SGL Carbon Group Co., Ltd.) by the pulse-swirl-spray (PSS, Nordson Co. Ltd.) technique in order to prepare the gas diffusion electrodes (GDEs). The electrode areas were 4.41 cm^2, the Pt loading of the catalyst layers (CLs) was 0.50 ± 0.02 mg cm^{-2}, and the Fe-N-C loading of the CLs was 0.50 ± 0.05 mg cm^{-2}. The prepared GDEs were immersed in 1 M KOH 80 ◦C for 2 days before measurement in order to ion-exchange to the OH^- form. Similarly, the QPAF-4 electrolyte membranes (IEC = 2.0 meq g^{-1}, average thickness = 30 μm) were also immersed in 1M KOH at 80 °C for 2 days before measurement. Excess aqueous KOH and water were removed from the GDEs and membranes with a laboratory cloth prior to assembly. Each set of GDEs and QPAF-4

membrane was pressed together in-cell to form the membrane electrode assembly (MEA) without hot pressing. The MEAs were sandwiched between two single serpentine flow graphite plates and 200 μm silicone/poly(ethyl benzene-1, 4-dicarboxylat/silicone gaskets (SB50A1P, Maxell Kureha Co., Ltd.) and were fastened to10 kgf cm^{-2} with four springs.

Performance test of single cells

The cell voltages (V) as a function of current density (I) were measured with hydrogen and oxygen at 60 °C at various pressures. The back-pressure (BP) was controlled at 0 to 100 kPa (gauge: kPa_g). Hydrogen and oxygen gases were supplied to the anode and the cathode at a flow rate of 100 mL min^{-1}. The flow rates of all gases were controlled by mass flow controllers. These gases were humidified at 80 to 100% relative humidity (RH) by bubbling through a hot water reservoir. The I-V curves were galvanostatically measured under steady-state operation by use of an electronic load (PLZ664WA and KFM2150, Kikusui Electronics Corp.) controlled by a measurement system (fuel cell characteristic evaluation device, Netsuden Kogyo Corp.). The measurement times in the direction of increasing current were 1 minute up to 0.02 A cm^{-2}, 3 minutes up to 0.1 A cm^{-2}, 5 minutes up to 0.2 A cm^{-2}, 7 minutes up to 0.3 A cm^{-2}, and 10 minutes up to 1.0 A cm^{-2}. The measurement times in the direction of decreasing current were just half those used for increasing current. Also, since resistances are difficult to measure with Alternating Current (AC) impedance at current densities below 0.1 A cm^{-2} (KFM2150, Kikusui Electronics Corp.), they were measured with a 1 kHz external resistance meter (MODEL 3566, Tsuruga Electric Corp.) For current densities of 0.1 A cm^{-2} or more, the membrane resistance was measured by AC impedance. In the hydrogen pump test, hydrogen was flowed through both electrodes at 60 °C 100% RH and 100 mL min^{-1}, and

the anode overpotential was measured by use of an Automatic Polarization System (HZ-5000, Hokuto Denko Co.) at the same current density positions and stabilization times as those used in the I-V measurements.

Characterization of catalyst layers

For a more detailed comparison of the CLs using Fe-N-C and Pt/CB, they were investigated by use of various analytical methods, as follows. The cross-sections of the CLs on GDEs were observed by FIB-SIM (FB2200 and SU3500, HITACHI High-Tech Corp.). The wettability of the CL surfaces was investigated by contact angle measurement (DM-501, Kyowa Interface Science Co., Ltd.). Reagents (wetting tension test mixture, Kanto Chemical Co., Inc.) having different surface tensions of 30, 40, 50, and 73 mN m^{-1} were pipetted on the CL surfaces, and the contact angles were measured. The above reagent was pipetted on each CL formed on 29BC GDL, and the contact angle between the reagent and the CLs was measured with analysis software (FAMAS, Kyowa Interface Science Co., Ltd.).

To investigate the pore structure of the CLs, N_2 adsorption was carried out. The N_2 physisorption experiments were measured at 77 K by use of an automated gas sorption analyzer (Autosorb iQ, Anton-Paar GmbH). All of the samples (0.1 g or more) were degassed at 60 °C for 24 h in an onboard degassing port, prior to the adsorption experiments. The N_2 adsorption measurements were conducted in the P/P_0 range 0.025-0.997, where P represents the gas pressure and P_0 the saturation pressure. The specific surface areas and pore volume distributions were calculated by the Brunauer-Emmett-Teller (BET) and Barrett-Joyner-Halenda (BJH) methods, respectively. In the case of the catalyst powders, the powders were directly filled in the spherical cells. The N_2 adsorption

values of the GDLs were larger than those of the CLs. In order to obtain precise measurements of the values of the CLs and avoid the influence of the values of GDLs, catalyst-coated membranes (CCMs) were prepared by coating the catalysts on the QPAF-4 electrolyte membrane by the PSS method. The CCMs (5 cm × 5 cm) were divided into three parts and placed in the measurement cell. The specific surface area and pore size distribution were calculated from the obtained adsorption isotherm curves.

Water vapor adsorption was also carried out to investigate the pore structure of CLs. The experiments of water vapor physisorption were measured at 60 °C with water vapor sorption analyzers (Vstar, Anton-Paar GmbH). All of the samples (0.1 g or more) were degassed at 60 °C for 24 h in an onboard degassing port prior to the adsorption experiments. The values of water vapor adsorption were measured in the P/P_0 range 0.05-0.95. The catalyst powders were directly filled in the spherical cells. In the case of the CLs, these were formed on a PP film by the PSS method and were removed and filled into the cell.

2.3 Results and Discussions

Polarization performance of MEAs using the Fe-N-C cathode catalyst

In Figure 2-2, the polarization curves and ohmic resistance changes of the cell using Fe-N-C CL and Pt/CB CL (as reference) as the cathode CL are shown. Figure 2-2(a) shows time courses of voltage and current density with increasing and decreasing current for each cathode CL. The polarization curves and Tafel plots shown in Figure 2-2(b) and 2-2(d) were drawn using the quasi-steady-state voltage data, i.e., the final values observed during each period of current density in Figure 2-2(a). The cell using the Fe-N-C CL exhibited large hysteresis in the I-V curve, i.e., a large difference in potential between the increasing and decreasing current curves. In the case of the Pt/CB CL, the hysteresis was very small. The ohmic resistance of the cell using the Fe-N-C CL increased with increasing current density; however, in the low current density region, the change with decreasing current density decreased, and hysteresis was observed in this region. The Tafel slopes of the cell using Fe-N-C CL were very different for increasing and decreasing current density. The change of the slope with increasing current density was larger than that with decreasing current density.

The Tafel slopes were analyzed with a component analysis technique developed in our laboratory (Figures 2-2(d), (e)) [2]. This technique involves fitting the I-V curves with a primary Tafel slope, typically corresponding to a transfer coefficient α of 1.0, which would be 66 mV dec^{-1} at 60 °C, typically together with doubled (132 mV) and quadrupled (264) slopes. Perry et al. have shown that either gas mass transport or ionic transport limitations can lead to Tafel slope doubling, and the combination of the two can lead to quadrupling [3]. That analysis is based on the hydrogen anode being essentially nonpolarized under acidic conditions. For the AEMFC, it is well known that the hydrogen

anode is significantly polarized [4, 5, 6]. As shown in the Supporting Information, an MEA operated under hydrogen pump conditions exhibited a rather small polarization at low current densities, which would not perturb the low current density region of the H_2-O_2 cell. However, at high current density, the Tafel slope was 476 mV, corresponding to quadrupling, approximately half of which (238 mV) can be assigned to the hydrogen anode. Thus, an approximate I-V curve for the hydrogen anode can be generated and used to correct the observed cell voltages. The corrected I-V curves for the Pt/CB (Figure 2-2(d)) and Fe-N-C (Figure 2-2(e)) CLs are shown for increasing and decreasing current density. The apparent (uncorrected) slope of 532 mV for the Pt/CB H_2-O_2 cell was decreased to approximately 294 mV (532 – 238 = 294), i.e., more consistent with a quadrupled slope (264 mV). The additional 30 mV polarization is small but might possibly be due to the additional coupling of water mass transport with gas and ionic transport. The precisely quadrupled slopes, although not observed, are also shown in Figures 2-2(d), (e) for reference. For both Pt/CB and Fe-N-C catalysts, the low current density region, with an initial Tafel slope of 56.0 mV, can be assigned to pure kinetic control. Even though there is curvature, the curve-fitting allows us to clearly determine the slopes precisely. For Pt/CB, with both increasing and decreasing current density, the behavior transitioned directly to the quadrupled slope, with additional polarization, bypassing the doubled slope. For Fe-N-C during increasing current density, the I-V curve increased to a significantly higher value, 448 mV, corresponding precisely to slope octupling, most likely due to a strong effect of limited water transport. At high current density, the behavior became unstable, with the potential increasing chaotically, presumably due to the influx of generated water from the anode, giving rise to a deviation from the slope of 448 mV (Figure 2-2(e)); this behavior was time-dependent, as seen from

Figure 2-2(a). During the decreasing-current portion, the I-V curve for the Fe-N-C CL became less steeply sloped (269 mV), i.e., consistent with slope quadrupling, which is most likely due to the relaxation of one of the three types of transport limitation (principally water transport).

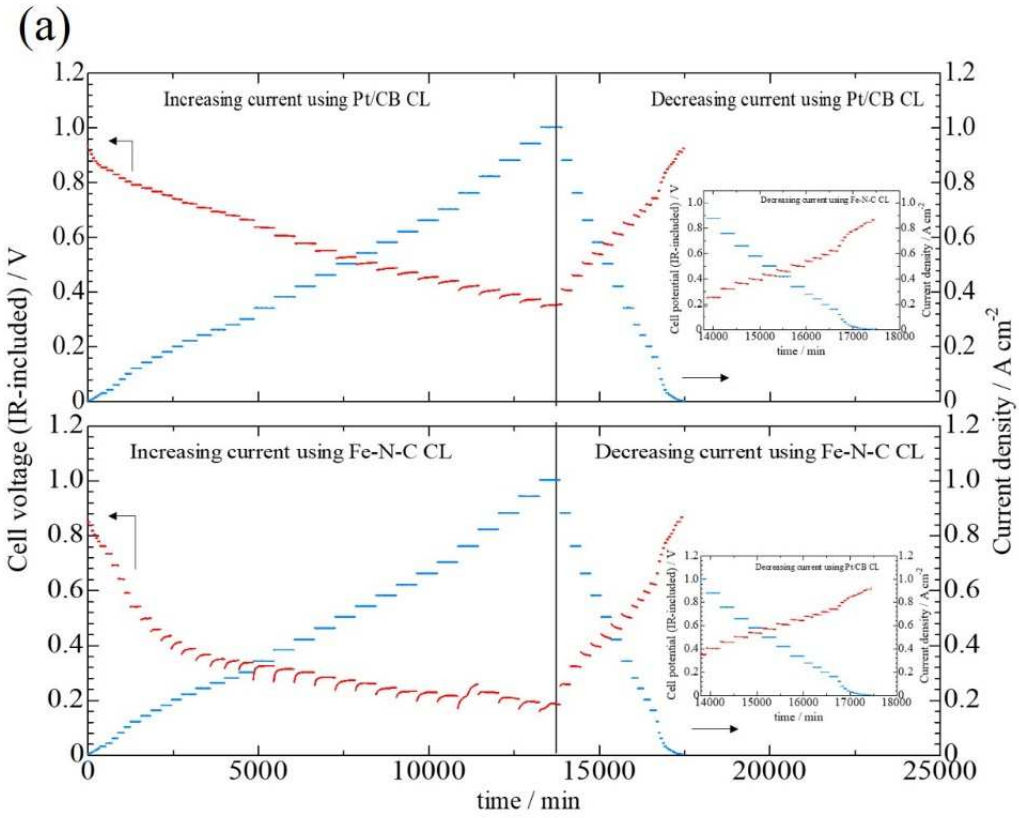
(a)
Increasing current using Pt/CB CL
Decreasing current using Pt/CB CL
Increasing current using Fe-N-C CL
Decreasing current using Fe-N-C CL
Cell voltage (IR-included) / V
Current density / A cm-2
time / min

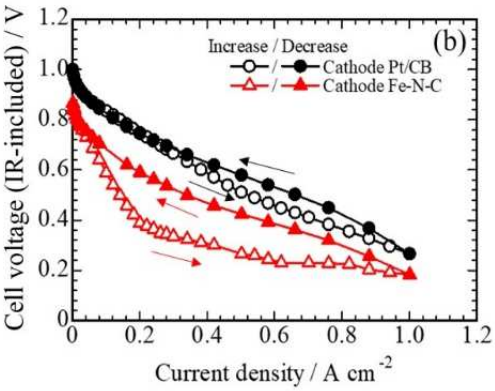
(b)
Increase / Decrease
Cathode Pt/CB
Cathode Fe-N-C
Cell voltage (IR-included) / V
Current density / A cm-2

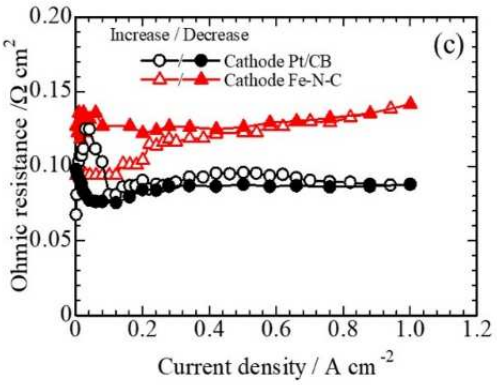
(c)
Increase / Decrease
Cathode Pt/CB
Cathode Fe-N-C
Ohmic resistance /Ω cm2
Current density / A cm-2

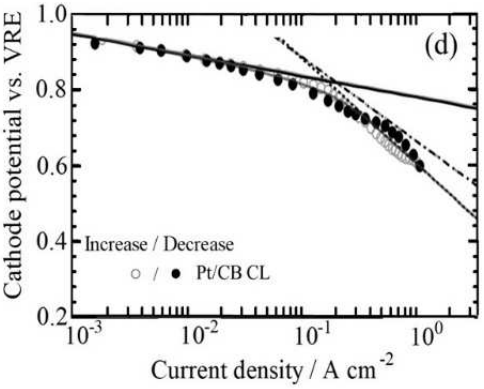
(d)
Increase / Decrease
Pt/CB CL
Cathode potential vs. VRE
Current density / A cm-2

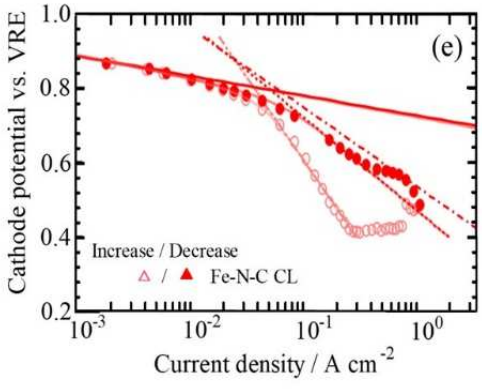
(e)
Increase / Decrease
Fe-N-C CL
Cathode potential vs. VRE
Current density / A cm-2

Figure 2-2. (a) Time courses of cell voltage and current density, (b) polarization curves, (c) ohmic resistances, and Tafel plots versus a "virtual" reference electrode (1/2 polarization of a hydrogen pump cell) for (d) a Pt/CB CL and (e) and an Fe-N-C CL at 60 °C, 100% RH; anode H_2 (100 mL min^{-1}, 0 kPa_g); cathode O_2 (100 mL min^{-1}, 0 kPa_g).

Polarization performance of MEA using Fe-N-C cathode catalyst under various gas conditions

In order to investigate the factors controlling the I-V hysteresis, the effect of the BPs of the supply gases on performances were evaluated (Figures 2-3(a-d)). In the case of the cell using Fe-N-C CL, the degree of I-V hysteresis decreased as the BPs on both electrodes increased from 0 to 50, and 100 kPa_g (Figure 2-3(a)). Under 100 kPa_g BP on both electrodes, the cell performances for the Fe-N-C CL and Pt/CB CL were comparable, and there was negligible I-V hysteresis (Figure 2-3(b)). Figures 2-3(c) and 2-3(d) show I-V curves with BP applied to only one side, i.e., anode and cathode, respectively. Despite the presence or absence of BP at the anode, I-V hysteresis was observed but was not observed when only the cathode was pressurized to 100 kPa_g. These results indicate that the I-V hysteresis occurs only in the cell using Fe-N-C CL as the cathode, and the degree of the hysteresis is reduced by applying BP to the cathode.

With increasing BP, the amount of water vapor in the gas decreases, the oxygen partial pressure increases, and the amount of liquid water also increases in the CL. The effects of oxygen partial pressure and water vapor pressure are shown in Figures 2-3(e) and 2-3(f), respectively. The performance of the cell under air was lower than that under O_2, but the I-V hysteresis was hardly observed (Figure 2-3(e)). The I-V hysteresis increased with lowering the relative humidity of the gas supplied to the cathode, namely, lowering the water vapor pressure (Figure 2-3(f)).

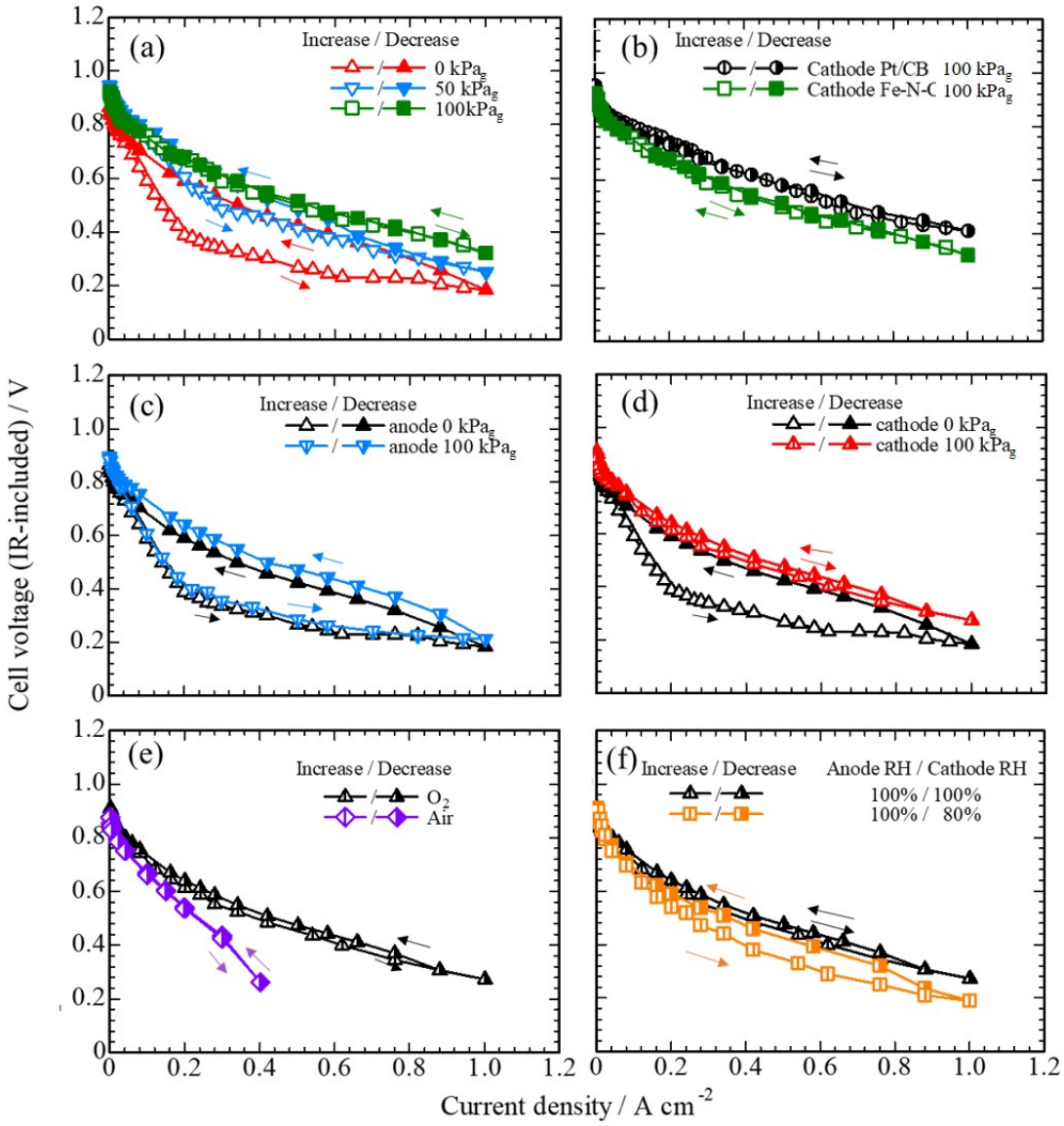

Figure 2-3. I-V curves at 60 ºC, 100% RH using Fe-N-C CL: (a) anode H_2 (0-100 kPa_g), cathode O_2 (0-100 kPa_g), (b) comparison of I-V curves using Pt/CB CL, anode H_2 (100 kPa_g) and cathode O_2 (100 kPa_g), (c) anode H_2 (0 and 100 kPa_g), cathode O_2 (0 kPa_g), (d) anode H_2 (0 kPa_g), cathode O_2 (0 and 100 kPa_g). Gas flow rates were 100 mL min^{-1}, (e)

I-V curves using Fe-N-C CL at 60 °C, 100% RH ; anode H_2 (100 mL min^{-1}, 0 kPa_g); cathode air (100 mL min^{-1}, 100 kPa_g), (f) I-V curves using Fe-N-C CL at 60 °C, different relative humidities; anode H_2 (100 mL min^{-1}, 0 kPa_g); cathode O_2 (100 mL min^{-1}, 100 kPa_g).

Figure 2-4 shows Tafel plots and ohmic resistances with 0 kPa_g at both electrodes, 100 kPa_g and 100% RH at the cathode, 100 kPa_g and 80%RH at the cathode. In the part deviating from the Tafel slope in Figure 2-4(a), the voltages for both increasing and decreasing current decreased in the order of 100 kPa_g + 100% RH at the cathode > 100 kPa_g + 80% RH at the cathode > 0 kPa_g, and the I-V hysteresis decreased in that order. On the other hand, for the ohmic resistance (Figure 2-4(b)), the values decreased in the order of 100 kPa_g + 80% RH at the cathode > 100 kPa_g + 100% RH at the cathode > 0 kPa_g. The results of Figure 2-4 show that the I-V hysteresis occurred in the mass transport region at high current density, but little ohmic resistance hysteresis was observed in this region. In the cathode, a decreasing amount of liquid water due to a decrease of BP and relative humidity increased the ohmic resistance because of decreasing water content in the cathode ionomer and membrane. In the high current density region of AEMFCs, the increased reaction increases the amount of water produced at the anode, but also increases the water consumption at the cathode. These results suggest that the I-V hysteresis is caused by a deficiency of liquid water at cathode reaction sites with increasing current density.

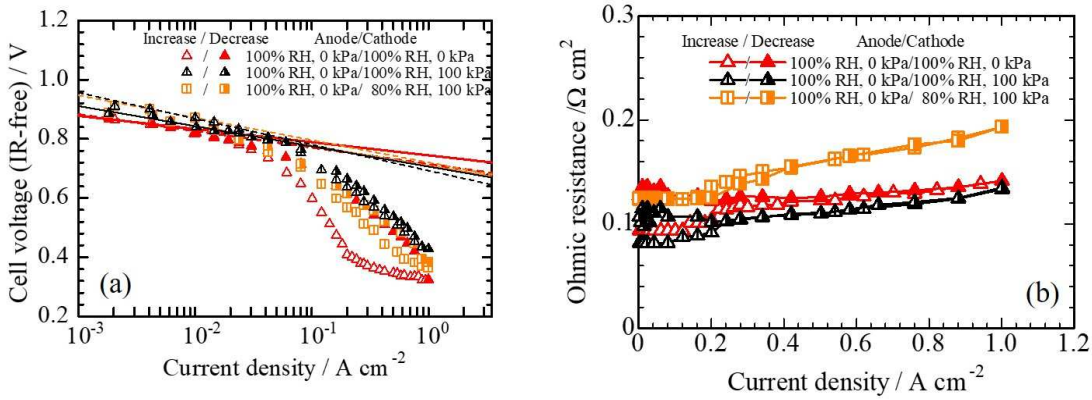

Figure 2-4. (a) Tafel plots using Fe-N-C at 60 °C; anode H_2 (100 mL min^{-1}, 100% RH, 0 kPa_g); cathode O_2 (100 mL min^{-1}, 80-100% RH, 0-100 kPa_g), (b) ohmic resistances using Fe-N-C at 60 °C; anode H_2 (100 mL min^{-1}, 100% RH, 0 kPa_g); cathode O_2 (100 mL min^{-1}, 80-100% RH, 0-100 kPa_g).

In the reaction in the cathode of the AEMFC, water is also essential to the reaction. These results indicate that the key factor controlling the hysteresis is water concentration in the cathode, not oxygen concentration. The lack of water supply in the cathode led to the hysteresis and also the increased resistance of the electrolyte membrane. The results of the BP changes also suggest that the increased amount of liquid water associated with increasing BP suppressed the hysteresis. During increasing current density, the void volume of the CL is large but decreased at high current density due to the voids becoming occupied with liquid water, which is supplied by both the cathode gas and back-diffusing

water generated in the anode. These hysteresis phenomena were highly significant in the Fe-N-C CL but were hardly observed in the Pt/CB CL.

Therefore, these results suggest that the difference of these hysteresis phenomena might arise from a difference in the absorption capacity of liquid water for both CLs, thus affecting the supply of water at reaction sites in the cathode. In order to suppress the hysteresis in the cell using Fe-N-C at the cathode, it is necessary to find ways to better manage the water supply so as to optimize the trade-off between the number of effective reaction sites and the void volume, which accompany the appropriate types of mass transport at the various current densities.

Microstructure analysis for CL using Fe-N-C and Pt/CB

In the contact angle changes for various reagents with different surface tensions, using both CLs (Figure 2-5), the values for the Fe-N-C CL were approximately 10° lower than those for the Pt/CB CL at each measurement point. This result indicates that the Fe-N-C CL was more hydrophilic than the Pt/CB CL. In a comparision between the Fe-N-C catalyst and the Fe-N-C CL coated with QPAF-4 (Figure 2-6(a)), the volume for pores below 20 nm decreased 84% as a result of QPAF-4 addition. In a comparison between thePt/CB catalyst and the Pt/CB CL coated with QPAF-4 (Figure 2-6(b)), the volume for pores below 100 nm decreased 85% as a result of QPAF-4 addition. These results show that the Fe-N-C CL pores in the range of 20-100 nm were relatively empty compared to those in the Pt/CB CL, despite the addition of QPAF-4. In comparing the water vapor adsorption isotherms of Fe-N-C and Fe-N-C CL (Figure 2-7(a)) and Pt/CB and Pt/CB CL (Figure 2-7(b)), the total volume of water vapor adsorption for Fe-N-C was approximately a factor of two larger than that for the Pt/CB, irrespective of the presence or absence of

QPAF-4. These results regarding the microstructure and hydrophilicity indicate that the Fe-N-C CL had many hydrophilic voids in the range of 20-100 nm and that the capacity for water absorption was much higher than that for Pt/CB. Both MEAs used the same fabrication technique, binder, and membrane; however, the catalysts differed. Thus, the differences in the porosity characteristics in the CL are due to the differences in the carbon structures of Fe-N-C and Pt/CB.

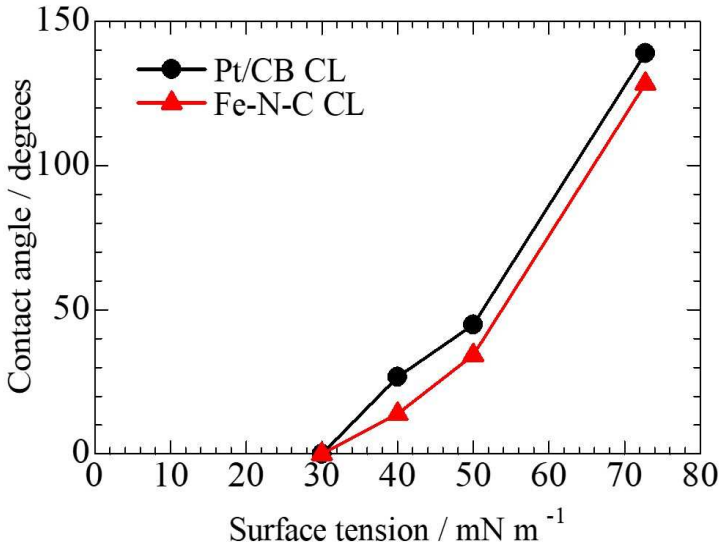

Figure 2-5. Contact angle changes for various reagents with different surface tensions with the Fe-N-C CL and Pt/CB CL.

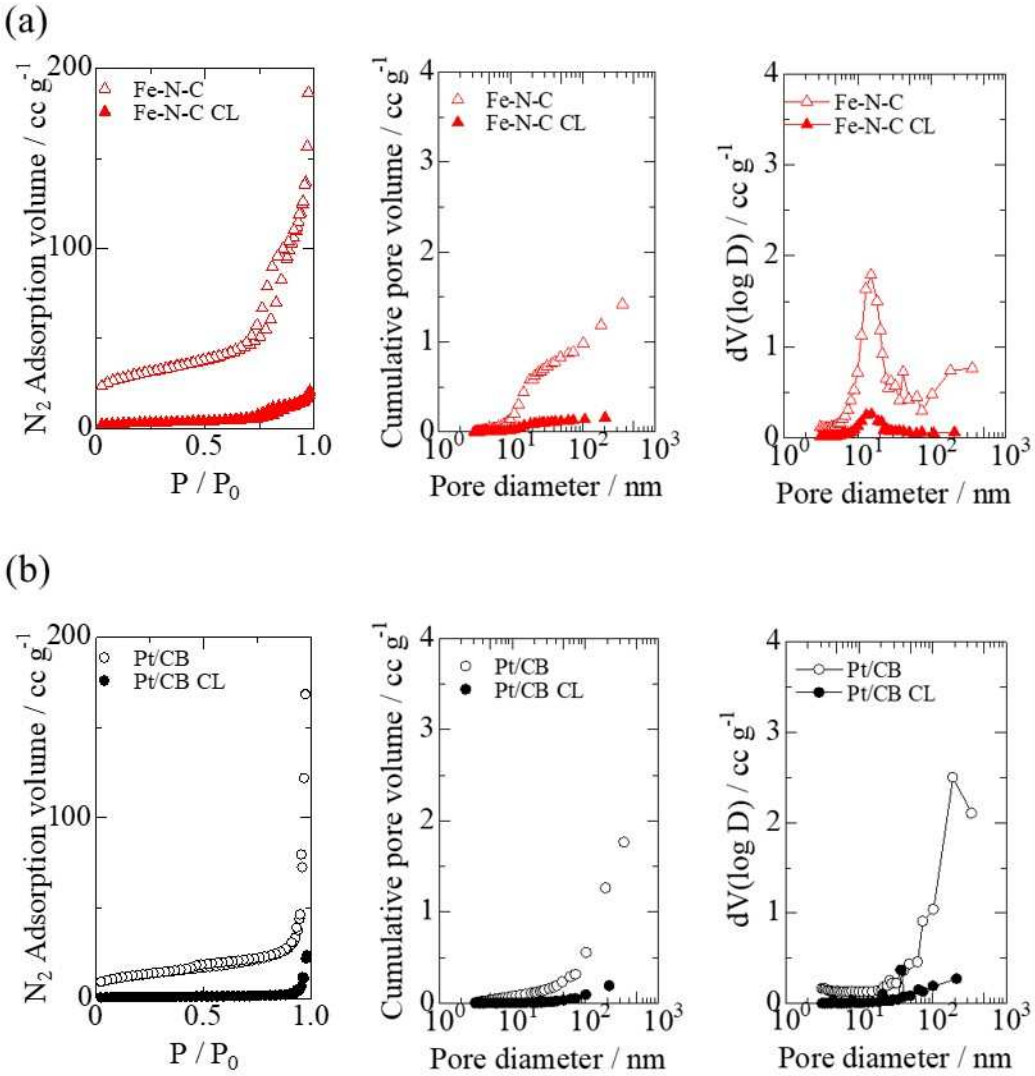

Figure 2-6. (a) N_2 adsorption isotherms of Fe-N-C catalyst and Fe-N-C CL, and pore size distribution calculated by the BJH method. (b) N_2 adsorption isotherms of the Pt/CB catalyst and Pt/CB CL, and pore size distribution calculated by the BJH method.

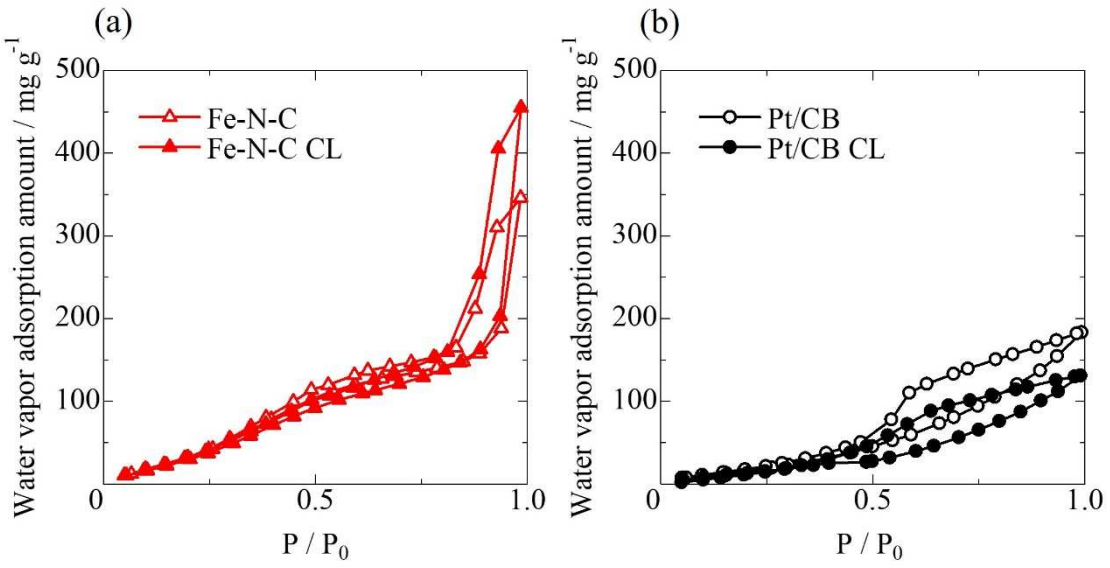

Figure 2-7. (a) Water vapor adsorption isotherms of Fe-N-C catalyst and Fe-N-C CL, (b) water vapor adsorption isotherms of Pt/CB catalyst and Pt/CB CL.

Consequently, it can be suggested as a major difference between Fe-N-C and Pt/CB from the morphology analysis that the void volume of the Fe-N-C catalyst absorbed the water generated during increasing current density, and this led to the lack the reactant water at the cathode reaction sites, thus contributing to the I-V hysteresis.

Mechanisms of hysteresis phenomena in the cell using Fe-N-C cathode

The comparison of the cross-sectional structure images in Figure 2-8(a) and 2-8(b) shows that the Fe-N-C CL was about 15 μm in thickness and had larger pores than the Pt/CB CL, and the Fe-N-C CL contained micrometer-order and submicrometer-order pores. On the other hand, the thickness of the Pt/CB CL was approximately 5 μm and contained fine pores of 1 μm or less.

Figure 2-8(c), d schematically depicts the behavior of the water distribution in the Fe-N-C CL during increasing current density, together with the corresponding Tafel plots. I divided the regions acording to the values of current density in the Tafel plots. Region a' corresponds to reaction kinetics control (56 mV), and the cell voltage undergoes abrupt changes in the degree of decrease with increasing current density in regions a to c. In region a (low current density, Figure 2-8(c)), the potential drops as the supply of water starts to become a limiting factor. The reactant water supplied from Fe-N-C CL pores, originating from water supplied by back-diffusion from the anode, is relatively balanced with the reaction. At that time, the ohmic resistace of cell is maintained at low values, as shown in Figure 2-4(b) (100% RH, 0 kPa_g). In region b (mid-range current density, Figure 2-8(d)), the cell voltage enters the high-slope regime due to the coupling of all three types of mass transport, i.e., gas, ions, and water, with the latter being the most important. I consider that the reactant water supply from Fe-N-C CL pores becomes a limiting factor for the reaction, due to the insufficiency of water generated at the anode. At that time, the ohmic resistace of the cell also increases due to decreasing membrane water content, as shown in Figure 2-4(b) (100% RH, 0 kPa_g). In region c (high current density, Figure 2-8(e)), the slope deviates from 448 mV and decreases markedly at current densities over 0.2 A cm^{-2}. The reactant water supplied from Fe-N-C CL pores becomes sufficient, so

that water mass transport becomes less of a limiting factor for the cathode reaction, due to the large amount of water generated at the anode. At that time, the increase of the ohmic resistance is reversed due to the rehydration of the membrane from the water generated in anode, as shown in Figure 2-4(b) (100% RH, 0 kPa_g). In the case of the decreasing current density, going back from region c to a, there was no sudden slope increase of the cell voltage. I consider that the water transport, although still a factor, was less limiting, due to a sufficient supply at reaction sites, because the balance between the water supply from back-diffusion and the reaction demand was maintained as a result of the large water volume in the Fe-N-C CL. These results also show that the cell potentials in region a' for both increasing and decreasing current density did not change. These indicate that there were negligible changes in the number of reaction sites, and basically, the behavior in regions a, b and c can be explained by combinations of various types mass transport, with water playing a major role. In the case of the Pt/CB cathode CL, the ohmic resistance in the current density range over 0.2 A cm^{-2} hardly changed with increasing current density, as shown in Figure 2-2(c). In the case of the Fe-N-C cathode CL, however, the values of the ohmic resistances were larger than those of the Pt/CB cathode CL and increased with increasing current density. These results also suggest that the water content of the membrane with the Fe-N-C cathode CL was lower than that of the Pt/CB cathode CL and continued to decrease, and thus, the water permeability in the membrane was also insufficient. More specifically, in the case of Fe-N-C, the total water consumption of the cathode used for the water absorption and reaction of the CL is larger than that of the water back-diffusing from the anode. The large void volume of Fe-N-C is concluded to lead to a decreased number of contact points at the interface between the membrane and the CL, and also a decreased number of supply pathways for back-diffusing water from

the anode. These conditions lead to an increased cathode-ionomer interfacial resistance in the high current density region. These results indicate the importance of providing the cathode reactant water with the back-diffusing water from the anode [6] [7], while maintaining liquid water at a level that does not cause flooding. I also found that lowering the humidity of the anode increased the hysteresis, not only in Fe-N-C but also in Pt/CB (Figure 2-9). Interestingly, it was found that lowering the humidity of the anode increased the hysteresis, not only in Fe-N-C but also in Pt/CB (Figure 2-9). This proves that the supply of water to the reaction sites of the cathode via the back-diffusion of water from the anode is essential. In order to reduce the hysteresis, it is necessary to enhance the membrane water permeability, thus increasing the amount of back-diffusing water and forming a homogeneous interface between the membrane and the CL.

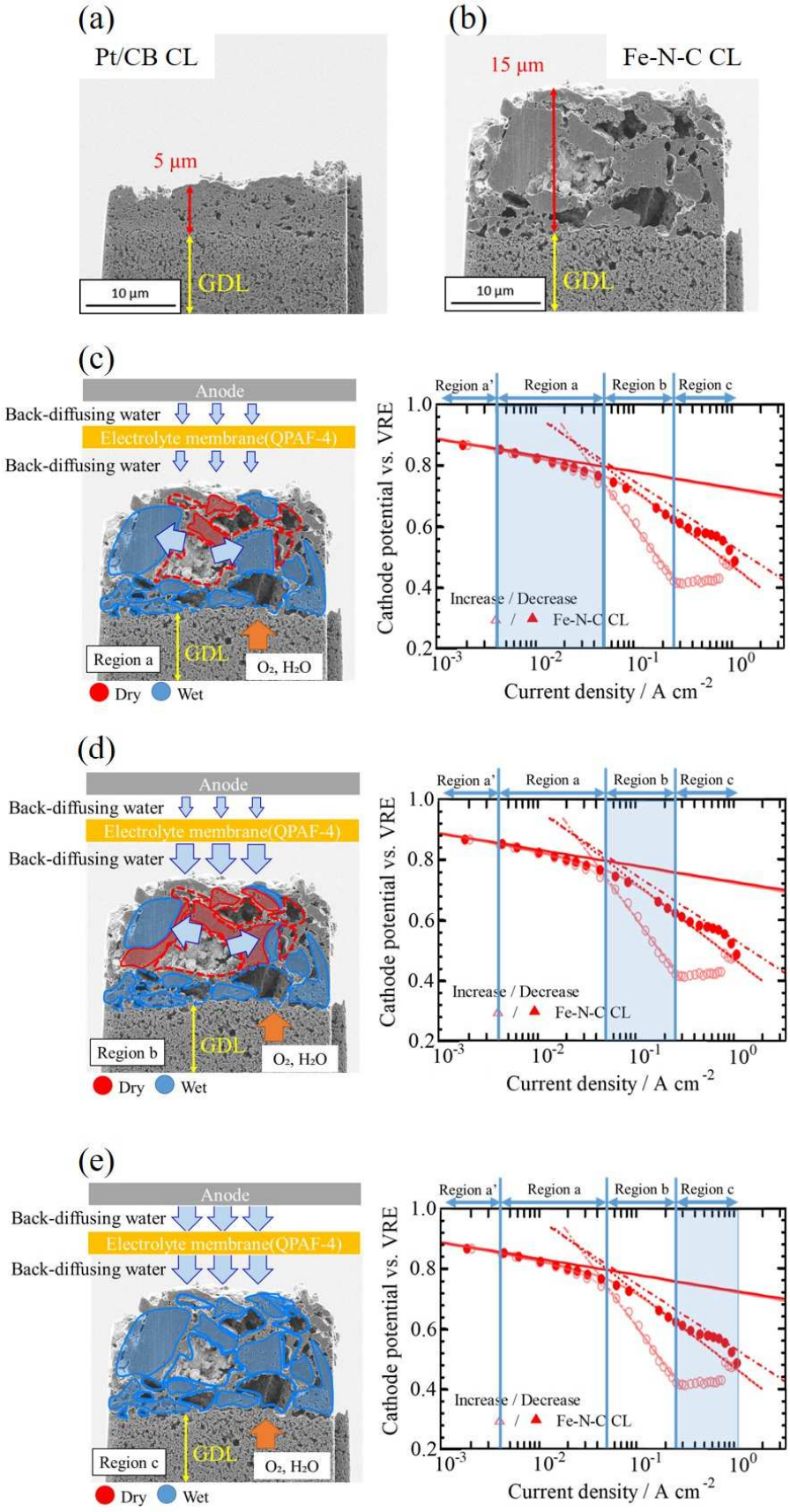
(a)
Pt/CB CL
5 μm
10 μm
GDL
(b)
15 μm
Fe-N-C CL
10 μm
GDL
(c)
Anode
Back-diffusing water
Electrolyte membrane(QPAF-4)
Back-diffusing water
Region a
GDL
O2, H2O
Dry
Wet
Region a'
Region a
Region b
Region c
Cathode potential vs. VRE
Increase / Decrease
Fe-N-C CL
Current density / A cm-2
(d)
Anode
Back-diffusing water
Electrolyte membrane(QPAF-4)
Back-diffusing water
Region b
GDL
O2, H2O
Dry
Wet
Region a'
Region a
Region b
Region c
Cathode potential vs. VRE
Increase / Decrease
Fe-N-C CL
Current density / A cm-2
(e)
Anode
Back-diffusing water
Electrolyte membrane(QPAF-4)
Back-diffusing water
Region c
GDL
O2, H2O
Dry
Wet
Region a'
Region a
Region b
Region c
Cathode potential vs. VRE
Increase / Decrease
Fe-N-C CL
Current density / A cm-2

Figure 2-8. Images of cross-sectional structure with (a) Pt/CB and (b) Fe-N-C CL by FIB-SIM. Schematic depiction of water management in the electrolyte membrane and CL at (c) low, (d) middle, and (e) high current density, with the corresponding Tafel plots.

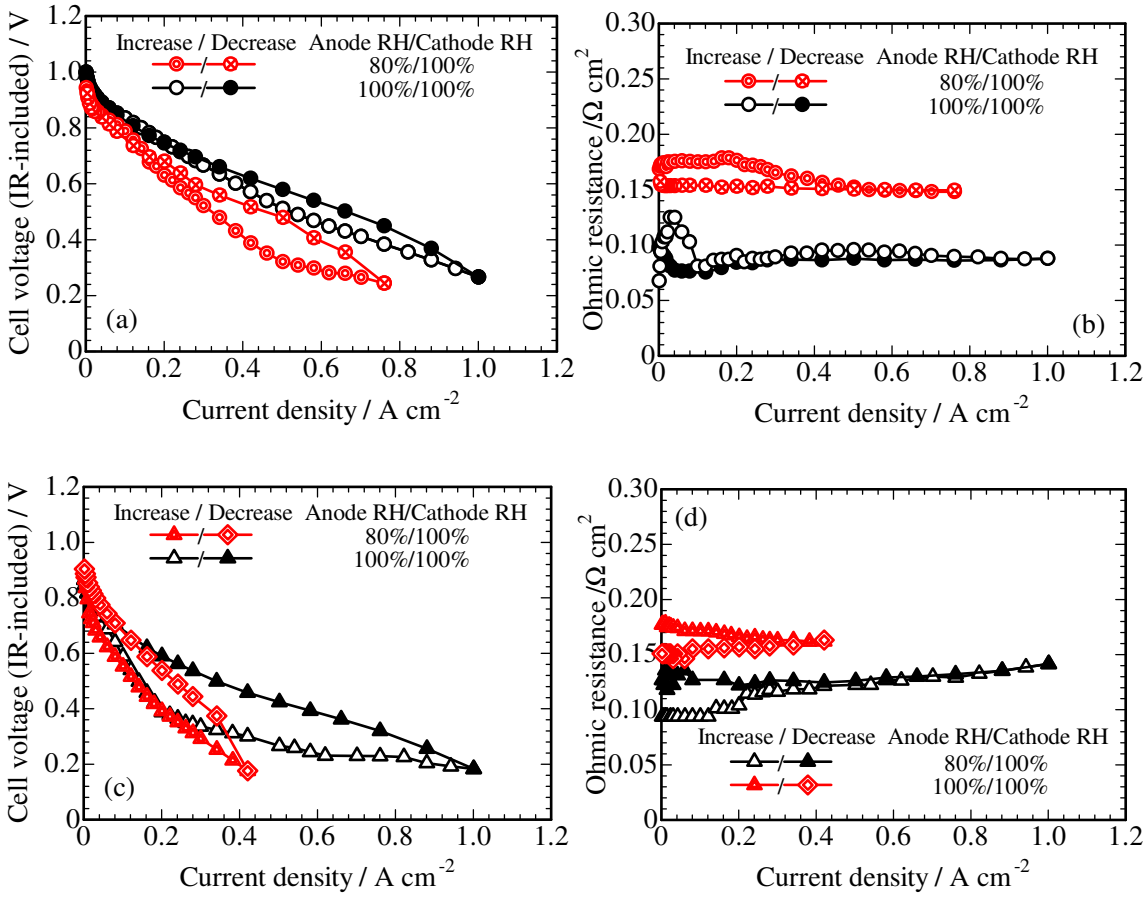

Figure 2-9. (a) I-V curves and (b) ohmic resistances using Pt/CB CL at 60 °C, various relative humidities; anode H_2 (100 mL min^{-1}, 0 kPa_g); cathode O_2 (100 mL min^{-1}, 0 kPa_g), (c) I-V curves and (d) ohmic resistances using Fe-N-C CL at 60 °C, various relative humidities; anode H_2 (100 mL min^{-1}, 0 kPa_g); cathode O_2 (100 mL min^{-1}, 0 kPa_g).

2.4 Conclusions

I focus on the water management challenges on the improvements of cell performance for anion exchange membrane fuel cells (AEMFCs) using a non-PGM catalyst (Fe-N-C) for the cathode and an in-house-developed anion exchange ionomer (quaternized poly(arylene perfluoroalkylene), QPAF-4) for both the membrane and the catalyst layers (CLs) binder under practical gas flow rates conditions. The cell using the Fe-N-C cathode exhibited similar current-voltage (I-V) performance compared with those using Pt catalyst supported on carbon black. The power of this cell is 144~198 W s cm^{-2} L^{-1}, which is comparable to the 210 W s cm^{-2} L^{-1} of the highest current Pt-Ru/C and Pt/C catalyst-based cells [8], but the cell using the Fe-N-C catalyst showed I-V hysteresis between increasing and decreasing current. The hysteresis decreased with increasing back pressure. Based on the results of various I-V measurements, I conclude that the hysteresis is related to water supplied to the cathode using the Fe-N-C catalyst. Tafel slope component analysis revealed that a severe polarization occurred, amounting to slope octupling, with increasing current density, most likely due to the addition of water transport to the usual combination of gas and ionic transport. This severe polarization was alleviated after the cathode layer became sufficiently hydrated. I found from these results that water management is essential, due to the role of water as a reactant in the cathode reaction, for high-performance AEMFCs.

References

[1] H. Ono, T. Kimura, A. Takano, K. Asazawa, J. Miyake, J. Inukai, K. Miyatake, "Robust anion conductive polymers containing perfluoroalkylene and pendant ammonium groups for high performance fuel cells," *Journal of Materials Chemistry A,* 5 (2017) 24804-24812. DOI: 10.1039/c7ta09409d

[2] D. A. Tryk, M. S. Lee, M. Uchida, H. Uchida, M. Watanabe, "Tafel Slope Component Analysis of Polymer Electrolyte Fuel Cell Cathode Current-Potential Behavior," *The Electrochemical Society Transactions,* 35 (2011) 13-23. DOI: 10.1149/1.3643348

[3] M. L. Perry, J. Newman, E. J. Cairns, "Mass Transport in Gas-Diffusion Electrodes: A Diagnostic Tool for Fuel-Cell Cathodes," *Journal of The Electrochemical Society,* 145 (1998) 5-15. DOI: 10.1149/1.1838202

[4] D. R. Dekel, "Unraveling mysteries of hydrogen electrooxidation in anion exchange membrane fuel cells," *Current Opinion in Electrochemistry*, 12 (2018) 182-188. DOI: 10.1016/j.coelec.2018.11.013

[5] W. E. Mustain, M. Chatenet, M. Page, Y. S. Kim, "Durability challenges of anion exchange membrane fuel cells," *Energy & Environmental Science,* 13 (2020) 2805-2838, DOI: 10.1039/d0ee01133a

[6] T. J. Omasta, A. M. Park, J. M. LaManna, Y. Zhang, X. Peng, L. Wang, D. L. Jacobson, J. R. Varcoe, D. S. Hussey, B. S. Pivovar, W. E. Mustain, "Beyond catalysis and membranes: visualizing and solving the challenge of electrode water accumulation and flooding in AEMFCs," *Energy & Environmental Science*, 11 (2018) 551-558. DOI: 10.1039/c8ee00122g

[7] R. Gutru, Z. Turtayeva, F. Xu, G. Maranzana, B. Vigolo, A. Desforges, "A comprehensive review on water management strategies and developments in anion exchange membrane fuel cells," *International Journal of Hydrogen Energy,* 45 (2020) 19642-19663. DOI: 10.1016/j.ijhydene.2020.05.026

[8] N. U. Hassan, M. Mandal, G. Huang, H. A. Firouzjaie, P. A. Kohl, W. E. Mustain, "Achieving High-Performance and 2000 h Stability in Anion Exchange Membrane Fuel Cells by Manipulating Ionomer Properties and Electrode Optimization," *Advanced Energy Materials*, 10, (2020) 2001986, DOI: 10.1002/aenm.202001986

Chapter 3

Two approaches to suppress the performance hysteresis phenomenon in anion exchange membrane fuel cells with Fe-N-C cathode catalysts

3.1 Introduction

Continuing from Chapter 2, Chapter 3 focuses on effective water management in the AEMFC. In Chapter 2, I discovered the current density-voltage (I-V) hysteresis phenomenon that accompanies an increase or decrease in the current density (CD) of a cell that uses a Fe-N-C catalyst as a cathode catalyst. This suggested that the hysteresis phenomenon resulted from the difference in the absorption capacity of liquid water in the cathode CL and affected the water supply at the reaction sites of the cathode. By more detailed Tafel slope component analysis, this I-V behavior can be characterized as a direct transition from kinetic control to combined gas-ion-water transport control combination, with a unique 8× slope behavior, i.e., the intrinsic kinetic slope is multiplied by 8. These results also supported the importance of back-diffusing water.

In the case of Fe-N-C being used in the cathode catalyst layer, one of the methods for improving water management performance, i.e., improving the flux of back-diffusing water utilized from the anode, is the use of a thin electrolyte membrane. It has been reported that thinning the membrane shortens the distance of anion conduction and increases the flux of back-diffusing water, improving AEMFC performance. [1-4] Dekel

et al. and Yassin et al. reported that by reducing the membrane thickness from 28 μm to 10 μm and increasing the water diffusion coefficient of the membrane, not only the power generation performance was improved, but also the cell life was extended, based on model calculations. [5, 6] Also, Jiang et al. reported that the cell performance was improved by hydrophilizing the surface of the membrane via the creation of hydrophilic functional groups using a plasma. [7]

While thinner electrolyte membranes are necessary to reduce the overall transport resistance of water and OH^-, it tends to accelerate gas crossover as a problem and reduce the efficiency of making the system without some membrane strength, which leads to reduced durability. [19] This means that AEMFCs need thinner and more stable electrolyte membranes that can endure severe chemical and environmental conditions while meeting the durability goals of commercialization. In the case of hydrophilization of the electrolyte membranes by external treatments such as high concentration ozone for a long time, polymers with double carbon-carbon bonds in the main chain may readily react with ozone. [26, 27] In this regard, the above mentioned QPAF-4 has sufficient gas barrier properties and mechanical strength even in thin membrane formation. Moreover short-term low concentration hydrophilic modification occurs only at the top surface, and the hydrophilic effect at the interface may contribute to the bulk water mobility of the membrane.

In addition, for using Fe-N-C catalysts, the active reaction sites of the cathode must have a balanced hydrophilicity / hydrophobicity in order to be accessed by both oxygen gas and water for the ORR. To achieve high ORR performance for Fe-N-C catalysts, it is important to have a hierarchical pore structure with macro / mesopores for reactant access to the Fe-N-C active sites present in the micropores [8, 9]. Song et al. reported that Fe-N-

C catalyst particles synthesized using carbon with a high specific surface area carbon, specifically, refluxing Black Pearls (BP-2000, Asian-Pacific Specialty Chemicals Kuala Lumpur) with nitric acid increased the number of mesopores, and show ORR activity equivalent to that of a Pt/C [10].

In this Chapter 3, two methods to improve water management capacity were approached to control the I-V hysteresis phenomenon. First, I sought to increase the flux of back-diffusion water from the anode by both thinning and hydrophilizing a QPAF-4 AEM, and subjecting this membrane to hydrophilic treatment. Second, to develop a high ORR activity catalyst layer with a macro / mesopores layer accessible to both oxygen gas and water, I sought to improve the water supply to the reaction active sites by suppressing the absorption of water at the cathode by using a specially developed Fe-N-C catalyst provided by the Changchun Institute of Applied Chemistry (CIAC), Chinese Academy of Sciences.

3.2 Experimental

Preparation of MEAs

QAPF-4, which was used as an electrolyte membrane and binder, was synthesized based on the synthesis procedure of Ono et al. [11]. The catalyst inks for the anodes were prepared with Pt catalyst supported on carbon black (Pt/CB: TEC10E50E, Tanaka Kikinzoku Kogyo, K. K.), methanol and pure water by stirring for 30 minutes and use of a planetary ball mill containing 20 zirconia beads with a diameter of 5 mm. Subsequently, 5 wt.% QPAF-4-MeOH (IEC = 2.0 meq g^{-1}) binder solution was added to the slurry, and the mixture was further stirred with a planetary ball mill for 30 min. The weight ratio of QPAF-4 binder to support carbon was 0.8. In the same way, the catalyst inks for the cathodes were prepared with the Fe-N-Cc catalyst (synthesized and supplied by the CIAC from Black Pearls (BP-2000, Asian-Pacific Specialty Chemicals Kuala Lumpur)) and Fe-N-Cp catalyst (PMF-011904, supplied by Pajarito Powder), 5 wt.% QPAF-4-MeOH binder solution (IEC = 2.0 meq g^{-1}), methanol and pure water by use of a planetary ball mill. The weight ratio of QPAF-4 binder to support catalyst was set to 0.43. These catalyst inks were directly sprayed onto the microporous layers (MPLs) of the gas diffusion layers (GDLs) as the anode (W1S1010, Cetech Co., Ltd.) and cathode (29BC, SGL Carbon Group Co., Ltd.) by the pulse-swirl-spray (PSS, Nordson Co., Ltd.) technique to prepare the gas diffusion electrodes (GDEs). The electrode areas were 4.41 cm^2, the Pt loading of the CL was 0.20 ± 0.02 mg_{Pt} cm^{-2}, and these Fe-N-C loading of CLs were 0.50 ± 0.05 $mg_{cat.}$ cm^{-2}. The prepared GDEs were immersed in 1 M KOH 80 ◦C for 2 days before measurement to ion-exchange to the OH^- form. Similarly, the QPAF-4 electrolyte membranes (IEC = 2.0 meq g^{-1}, ca. 10 and ca. 30 μm) were also immersed in 1 M KOH aqueous solution at 80 °C for 2 days before measurement. To remove excess KOH

aqueous solution, the GDEs and the electrolyte membranes were sandwiched between Kim Towels (Nippon Paper Cresia Co., Ltd.). Next, the GDEs and the electrolyte membranes were immersed in ultrapure water for approximately on hour, being constrained so as not to float, and then sandwiched between Kim Towels again to remove the ultrapure water. After the KOH was thoroughly removed, each set of GDEs and QPAF-4 membrane was pressed together in-cell to form the membrane electrode assembly (MEA) without hot pressing. The MEAs were sandwiched between two single serpentine flow graphite plates and 200 μm silicone/poly(ethyl benzene-1, 4-dicarboxylat/silicone gaskets (SB50A1P, Maxell Kureha Co., Ltd.) and were fastened at 10 kgf cm^{-2} with four springs. For the reversible hydrogen electrode (RHE), a 5 mm diameter disk was cut from the Pt/CB 29BC GDE prepared above and applied to the membrane on the cathode side. The hydrogen source for the RHE was the anode outlet, supplied through a heated (90 °C) gas line. The CL surface of the RHE was in contact with the electrolyte membrane in the cell, and the GDL surface was in contact with gold wire, which was connected to the anode and cathode by terminals through a multi-input data logger (NR-500, KEYENCE Corp.) and a high voltage measurement unit (NR-HV04, KEYENCE Corp.), respectively, and the polarizations of the anode and cathode were measured.

Performance test of single cells

The cell voltages (V) as a function of current density (I) were measured with hydrogen and oxygen at 60 °C at various pressures. Hydrogen and oxygen gases were supplied to the anode and the cathode at a flow rate of 100 mL min^{-1}. The flow rates of all gases were controlled by mass flow controllers. These gases were humidified at 100% relative

humidity (RH) by bubbling through a hot water reservoir. The I-V curves were galvanostatically measured under steady-state operation by use of an electronic load (PLZ664WA and KFM2150, Kikusui Electronics Corp.) controlled by a measurement system (fuel cell characteristic evaluation device, Netsuden Kogyo Corp.). The measurement times in the direction of increasing current were 1 minute up to 0.02 A cm^{-2}, 3 minutes up to 0.1 A cm^{-2}, 5 minutes up to 0.2 A cm^{-2}, 7 minutes up to 0.3 A cm^{-2}, and 10 minutes up to 1.0 A cm^{-2}. The measurement times in the direction of decreasing current were just half those used for increasing current. Also, since resistances are difficult to measure with alternating current (AC) impedance at current densities below 0.1 A cm^{-2} (KFM2150, Kikusui Electronics Corp.), they were measured with a 1 kHz external resistance meter (MODEL 3566, Tsuruga Electric Corp.) For current densities of 0.1 A cm^{-2} or more, the membrane resistance was measured by AC impedance.

Characterization of membranes, catalyst and catalyst layers

An ozone/UV surface treatment device (EKBIO-1100, EBARA JITSUGYO Co., Ltd.) was used to hydrophilize the QPAF-4 electrolyte membrane. Ozone was generated by UV lamps (wavelengths of 245 nm and 185 nm) installed at the top of the chamber. The chamber temperature and water temperature were set at 40 ^{o}C, and the QPAF-4 membrane was placed 90 mm below the chamber ceiling. In an air atmosphere for 10 minutes, the back and front sides were turned over and hydrophilized twice in total. The ozone concentration in the chamber became steady after 2 minutes from the starting hydrophilization and showed a level of about 50 ppm.

For the surface-conduction analysis by current-sensing atomic force microscopy (CS-AFM) on the QPAF-4 membranes of ca. 10 μm thickness, the GDE was first prepared

by spraying a catalyst ink containing the Pt/CB and QPAF-4 binders (IEC = 2.0 meq g^{-1}) as a binder on the 29BC GDL using the PSS technique in the same manner as described above. The weight ratio of QPAF-4 binder to support catalyst was adjusted to 0.8. The Pt loading of the electrodes was 0.2 ± 0.02 mg_{Pt} cm^{-2}. The GDE was subsequently immersed in 1 M KOH aqueous solution at 80 °C for 2 days and then immersed in a saturated aqueous solution of $NaHCO_3$ aqueous solution at 40 °C for 2 days, and then dried to ion-exchange it to the HCO_3^- ion form. The membrane and the GDE in the HCO_3^- ion form were pressed at 10 kgf cm^{-2} and 140 ºC for 3 min. The ozone/UV surface treatment was carried out on the QPAF-4 membrane surface attached to the GDE.

The CS-AFM setup was prepared according to prior literature［12-18］making use of a commercial AFM system (SPM-5500, Agilent) equipped with a home-made environmental chamber under a purified (CO_2-free) air atmosphere at 40 ºC and 70% RH. A Pt/Ir-coated silicon tip (NanoWorld) was used for the CS-AFM measurements. The morphological and current images were obtained in the contact mode, with a contact force of 5 nN on the membrane surfaces and a tip bias voltage of -2.0 V [18]. Before measurements, humidified air was supplied to the environmental chamber (dead volume = 500 mL) at 100 mL min^{-1} for 2 h. During the AFM measurements, the flow rate was reduced to 10 mL min^{-1}.-To ensure that there was no tip damage of the surface and that it was free of airborne impurities such as dust, I obtained the first and second scanned images at the same position for each CS-AFM measurement. The tip bias voltage was kept at -2.0 V during the image acquisition.

An osmotic pressure evaluation of the electrolyte membrane was performed using an osmotic pressure experimental device (PP-5, Uchida Yoko Co., Ltd.). A 1 M sucrose solution in which 34.2 g of sucrose was dissolved in 100 mL of water was moistened

between a non-electrolyte solution and ultrapure water, and a QPAF-4 membrane, which was in the HCO_3^-form, was used as a permeable membrane. A capillary tube with both ends open was attached to the sealed sucrose side after each liquid level set same. The capillaries are equipped with a memory to read the water level, and as the water diffuses into the sucrose solution, the water level in the capillaries rises by the amount of water. The value of the memory was read out at each measurement time every 8, 16 and 24 hours. Osmotic pressures were calculated from the difference of height between sucrose solution and mercury (the height of the mercury column at 1 atm is 760 mmHg = 1.013×10^5 Pa). Moreover, since the density of mercury is 13.6 g mL^{-1}, osmotic pressures were calculated from the following Eq. 3-1.

$$\text{Osmotic pressure / Pa} = 1.013\times10^5\text{/ Pa} \times \frac{\text{Number of capillary from start position / mm}}{\text{760 / mm}} \times \frac{\text{Density of sucrose solution / g mL}^{-1}}{\text{13.6 / g mL}^{-1}} \quad \text{(Eq. 3-1)}$$

The electrochemical measurements were carried out with an Automatic Polarization System (HZ-5000, Hokuto Denko Co.) using the rotating disk electrode (RDE) method. A Pt mesh was used as the counter electrode and the RHE was used as the reference electrode. The working electrode was prepared as follows: the catalyst ink was prepared by mixing 1 mg of each catalyst with 0.025 mL of ultrapure water and 4.975 mL of ethanol via ultrasonication. A 1 μL droplet of this ink was deposited onto a glassy carbon electrode (GC area = 0.283 and 0.196 cm^2, Naito Rika Co. Ltd.) using a 1-μL syringe. The amounts of the Pt/CB ((4 μg_{Pt} cm^{-2}, TEC10E50E), Fe-N-Cp (11 μg cm^{-2}) and Fe-N-Cc (11 μg cm^{-2}) catalysts was controlled by the number of drops. Subsequently, Nafion diluent obtained by diluting a 5 wt.% Nafion solution with 75 vol.% of ethanol was pipetted on the

electrode surface, yielding an average thickness of 0.03 μm. The electrolyte solution, 0.1 M KOH, was prepared from reagent grade chemicals and ultrapure water. Polarization curves for the ORR were recorded in O_2-saturated electrolyte at 5 mV s^{-1} (positive potential scan) and several rotation rates from 1000 to 2500 rpm.

The wettability of QPAF-4 membranes with/without hydrophilization and CL surfaces were investigated by contact angle measurement (DM-501, Kyowa Interface Science Co., Ltd.). Reagents (wetting tension test mixture, Kanto Chemical Co., Inc.) having different surface tensions of 30, 40, 50, and 73 mN m^{-1} were pipetted on membranes and CL surfaces, and the contact angles were measured. The contact angle was evaluated by analysis software (FAMAS, Kyowa Interface Science Co., Ltd.) that can be used for the sessile drop method and a half-angle method. To reduce the measurement error, the measured value was calculated by averaging the values of 6 times measured the front and the back sides.

To investigate the pore structure of the CLs, N_2 adsorption was carried out. The N_2 physisorption experiments were measured at 77 K by use of an automated gas sorption analyzer (Autosorb iQ, Anton-Paar GmbH). All the samples (0.1 g or more) were degassed at 60 °C for 24 h in an onboard degassing port, prior to the adsorption experiments. The N_2 adsorption measurements were conducted in the P/P_0 range 0.025-0.997, where P represents the gas pressure and P_0 the saturation pressure. The specific surface areas and pore volume distributions were calculated by the Brunauer-Emmett-Teller (BET) and Barrett-Joyner-Halenda (BJH) methods, respectively. To obtain precise measurements of the values of the CLs and avoid the influence of the values of GDLs, catalyst-coated membranes (CCMs) were prepared by coating the catalysts on the QPAF-4 electrolyte membrane by the PSS method. The CCMs (6 cm × 6 cm) were divided into

three parts and placed in the measurement cell. The specific surface area and pore size distribution were calculated from the obtained adsorption isotherm curves.

Water vapor adsorption was also carried out to investigate the pore structure of CLs. The experiments of water vapor physisorption were measured at 60 °C with water vapor sorption analyzers (Vstar, Anton-Paar GmbH). All the samples (0.1 g or more) were degassed at 60 °C for 24 h in an onboard degassing port prior to the adsorption experiments. The values of water vapor adsorption were measured in the P/P_0 range 0.05-0.95. In the case of the CLs, these were formed on a PP film by the PSS method and were removed and filled into the cell.

3.3 Results and Discussion

Membrane improvement approach to suppress I-V hysteresis

In Chapter 2, it has been clarified that the supply of water to the catalytic active sites has a great influence on the hysteresis of the power generation performance of the cathode in the AEMFC. Therefore, in order to increase the supply of generated water to the reaction active site of the cathode, I sought to reduce the membrane thickness and increase the flux of back-diffusing of water.

Polarization performance of MEAs with reference electrode using various membranes

In Figures 3-1(a-e), the changes in the cell polarization curve, ohmic resistance, and anode cathode polarization curve using Pt/CB CL as the cathode CL are shown. As the thickness of the electrolyte membrane decreased from 33 μm to 11 μm by comparisons between circles and triangles in Figures 3-1(a) and 1(b), contrary to my expectations, there was a large difference in the potential between increasing and decreasing current, which was the phenomenon I have termed I-V hysteresis. These I-V hysteresis tended to be larger for thinner membranes, as shown in Figure 3-2. Based on the comparison in Figure 3-1(c), the ohmic resistance decreased from 0.088 Ω cm^2 to 0.066 Ω cm^2 at 1.0 A cm^{-2} as the membrane became thinner.

I hypothesized that one of the causes of I-V hysteresis was water transport at the interface between the membrane and the cathode, and therefore, to improve the transport, I hydrophilized the surface of the 11 μm membrane. In Figures 3-1(a) and 1(b), the hysteresis observed for the hydrophilized 11 μm membrane decreased, and the ohmic resistance of the hydrophilized membrane in Figure 3-1(c) was 0.080 Ω cm^2 at 1.0 A cm^{-}

^{2}, which was higher than that for the unmodified 11 μm membrane and less than that for the 33 μm membrane.

In order to investigate the cause of the I-V hysteresis in detail, the polarization contributions of the anode and cathode were measured independently. As shown in Figures 3-1(d-e), this I-V hysteresis occurred predominantly on the anode side and disappeared after hydrophilizing the membrane. The increase of I-V hysteresis for the 11 μm membrane with increasing CD is considered to be due to flooding by generated water in the anode.

Figures 3-1(f-l) show the results of investigating whether the effect of the hydrophilization is effective even in the case of cells using the Fe-N-Cp cathode catalyst. The cell using the Fe-N-Cp catalyst and the 11 μm QPAF-4 membrane showed hysteresis at both anode and cathode. However, as seen in Figures 3-1(f) and 1(g), the I-V hysteresis decreased even in the cell using the Fe-N-C CL when the hydrophilized 11 μm QAPF-4 membrane was used. Regarding the ohmic resistance in Figure 3-1(h), the resistance of the hydrophilized 11 μm membrane was 10% (increasing CD) and 20% (decreasing CD) smaller than that of the 33 μm membrane at 0.5 A cm^{-2} and increased significantly with increasing CD, in contrast with the case of the Pt/CB cathode in Figure 3-1(c). These phenomena can be explained by the fact that, in the case of the Fe-N-Cp cathode, water absorption was larger than that for Pt/CB and this led to the increasing ohmic resistance. In Figure 3-1(i), I-V hysteresis did not occur in the anodic polarization, and, in Figure 3-1(j), another instance of I-V hysteresis, in this case, for the Fe-N-Cp cathode polarization with the 33 μm membrane, was suppressed by use of the hydrophilized 11 μm membrane. Therefore, it was found that the improvement of the water transport at the interface between the membrane and the cathode by use of the hydrophilization treatment on a thin

electrolyte membrane is effective against the hysteresis phenomenon of both the anode and the cathode.

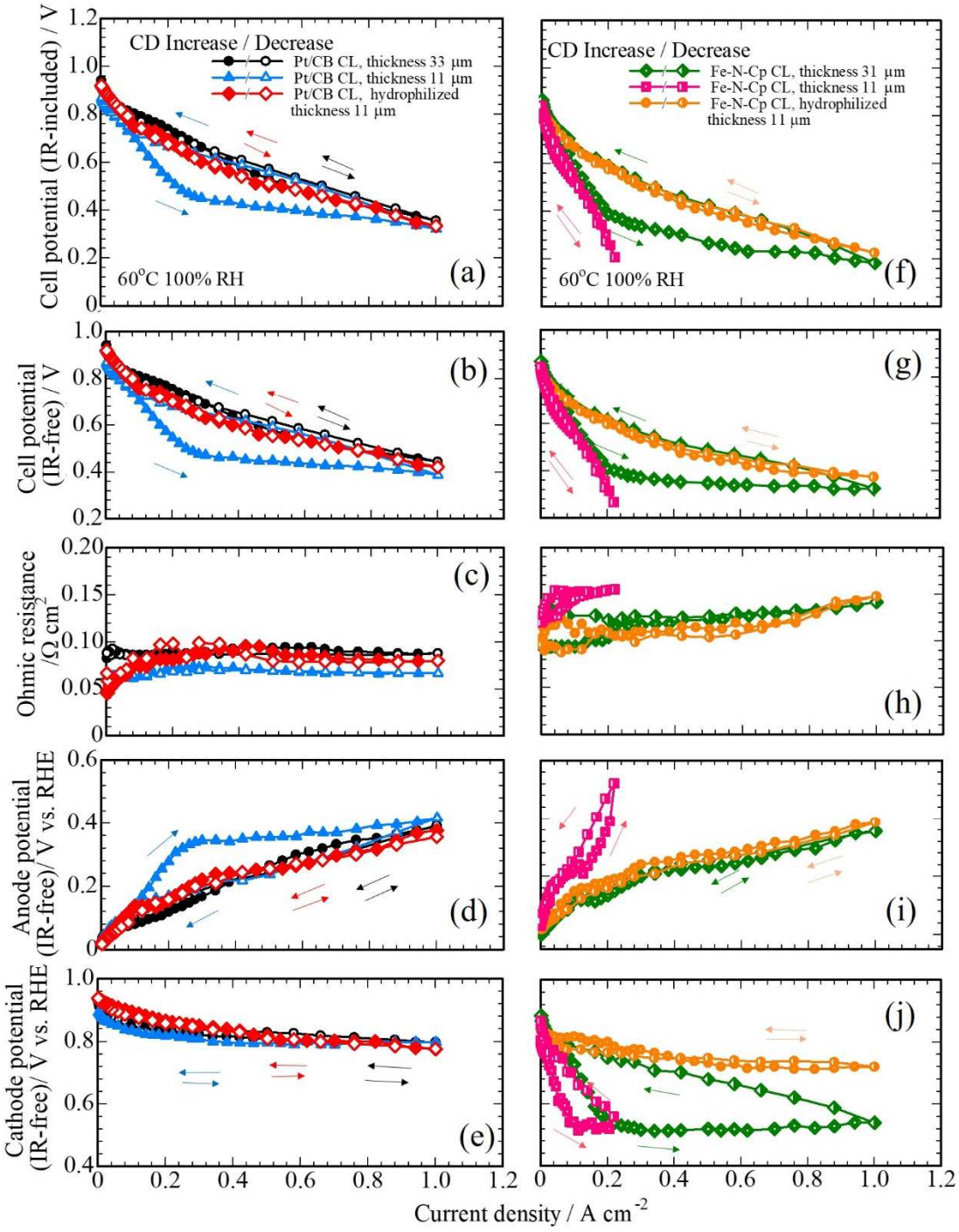

Figure 3-1. (a) IR-included polarization curves and (b) IR-free polarization curves, (c) Ohmic resistances, (d) IR-free anodic polarization curves, (e) IR-free cathode polarization curves using Pt/CB catalyst layer, and QPAF-4 membranes with a thickness of 33, 11,

hydrophilized 11 μm at 60 °C, 100% RH; anode H_2 (100 mL min^{-1}, 0 kPa_g); cathode O_2 (100 mL min^{-1}, 0 kPa_g). (f) IR-included polarization curves and (g) IR-free polarization curves, (h) Ohmic resistances, (i) IR-free anodic polarization curves, (j) IR-free cathode polarization curves using Fe-N-Cp catalyst layer, and QPAF-4 membranes with a thickness of 33 μm, hydrophilized 11 μm at 60 °C, 100% RH; anode H_2 (100 mL min^{-1}, 0 kPa_g); cathode O_2 (100 mL min^{-1}, 0 kPa_g).

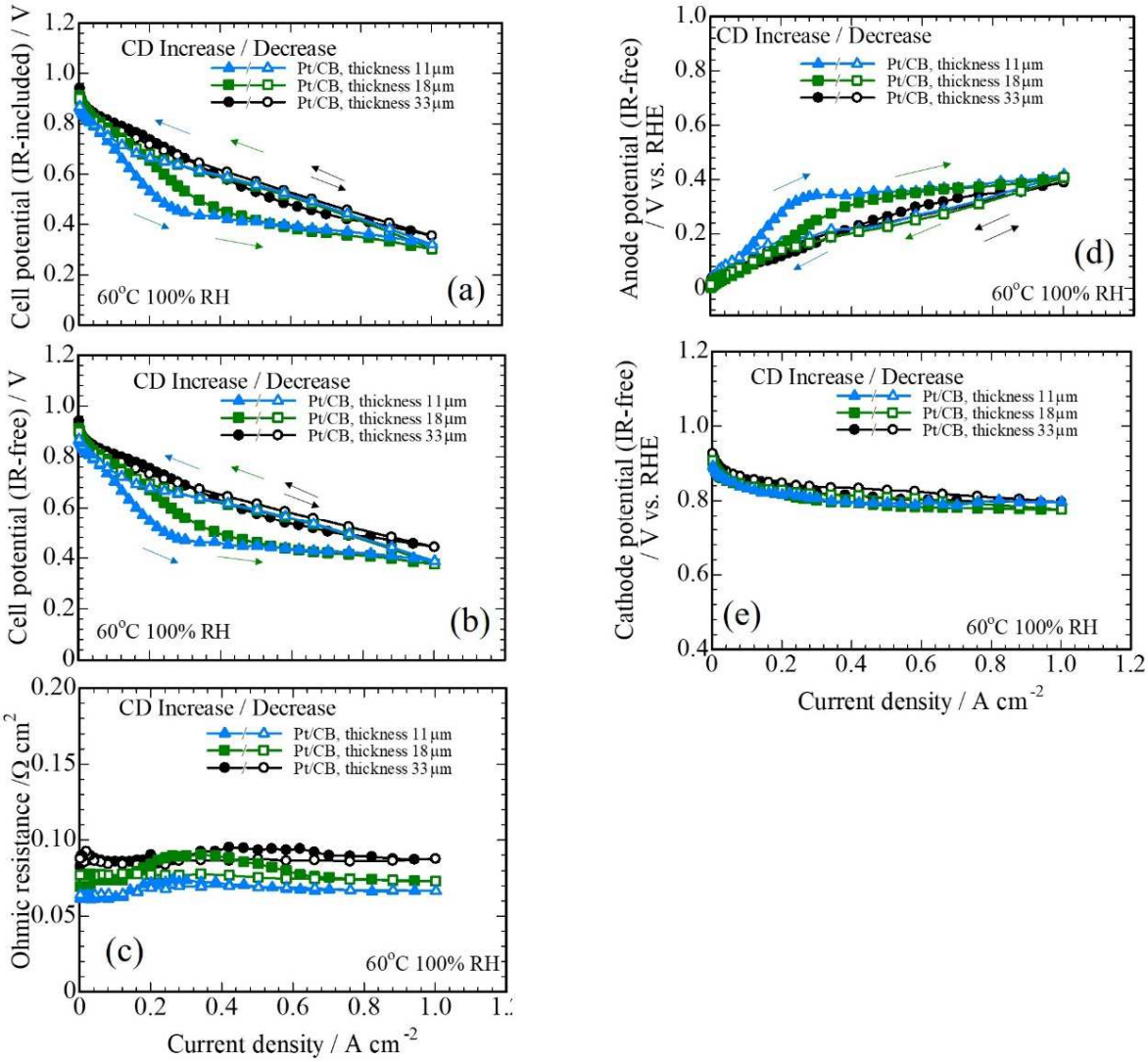

Figure 3-2. (a) IR-included polarization curves and (b) IR-free polarization curves, (c) Ohmic resistances, (d) IR-free anodic polarization curves, (e) IR-free cathode polarization curves using Pt/CB catalyst layer, and QPAF-4 membranes with a thickness of 33, 18, 11 at 60 °C, 100% RH; anode H_2 (100 mL min^{-1}, 0 kPa_g); cathode O_2 (100 mL min^{-1}, 0 kPa_g).

Analysis of various membrane surface structures

In Figure 3-3 and Figure 3-4, the change in contact angle for various reagents with different surface tensions used for each $MeOSO_3^-$ form membrane showed that the hydrophilicity of the membrane surface depended on the thickness, and those for the hydrophilized 11 μm QPAF-4 membrane were an average of 21° lower than those for the non-hydrophilized QPAF4 membrane. As for the reason for the change in contact angle depending on the thickness of the AEM, when the membranes were dried in the same casting method on a substrate, the hydrophobic substructure would be more stable and thus more prevalent at the the membrane/vapor interface, and the top surface were more hydrophobic. In a review of proton-based PFSA membranes, Kusoglu and Weber reported that at low hydration levels, the membrane/vapor interface layer was highly hydrophobic and resistive, and the fluorocarbon chains were oriented parallel to the membrane/vapor interface, which in some cases limits the mass transport of water and ions. [19] When imagined with a minimal molecular structure, i.e., two molecular chains, the ionic groups of the QPAF-4 AEM, which are hydrophilic, face inward, and the main chain structure, which is hydrophobic, faces outward. I estimate that the smaller the thickness of the bulk membrane, the more the hydrophobization would be enhanced. This result is also in agreement with the results of the OH^--form membrane, which is the same counter ion as that for the fuel cell evaluation. As shown in Figure 3-4, the contact angle also increased with decreasing membrane thickness, but the contact angle decreased for all membrane thicknesses after the membranes were subjected to hydrophilization. Hydrophilization of the membrane surface reduces impediments to water movement at the membrane-cathode interface. These results support the result of promoting the movement of water by the hydrophilization of the membrane surface and suppressing the

hysteresis of the I-V performance.

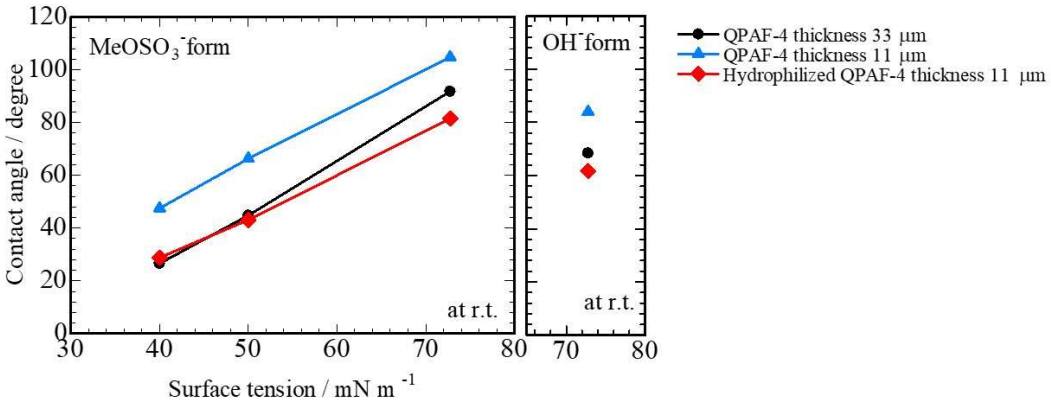

Figure 3-3 Contact angle changes for some reagents with different surface tensions using various QPAF-4 membranes with OH^- form and $MeOSO_3^-$ form, as well as 33, 11, and hydrophilized 11 μm.

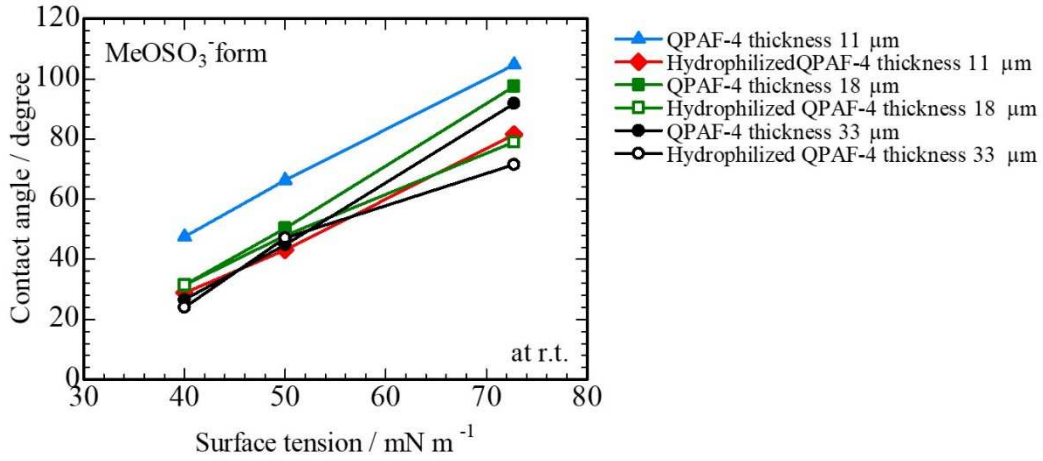

Figure 3-4. Contact angle changes for some reagents with different surface tensions using various QPAF-4 membranes with OH^- form and $MeOSO_3^-$ form, as well as 33, 18, 11 μm.

Figure 3-5 shows the results of CS-AFM analysis to investigate the effect of the hydrophilization on the 10 μm OPAF-4 membrane on the current distribution at the interface between the membrane and the cathode. There were no clear differences of more or less than 10 nm in the topography shown at the upper part of Figure 3-6(a), but in the current image in the lower part, it was found that the hydrophilization treatment clearly improved the uniformity of the current distribution. As shown in Figure 3-7, similar microscopic results were confirmed in other parts of the membrane surface. These results can also be clearly confirmed in the difference in the current profile on the lines shown in Figure 3-6(b). The results of the effect of the hydrophilization of the membrane surface

on the osmotic pressure in liquid water showed similar changes in Figure 3-8. Therefore, from these analysis results, I determined that hydrophilization does not improve the diffusivity of water inside the membrane but contributes to the improvement of the surface anion conduction and water pathways. The results of the membrane improvement approach show that hydrophilization of the QPAF-4 membrane surface was more effective than thinning in increasing the amount of back-diffusing water produced at the anode. I can conclude that a membrane with a hydrophilic surface can also function with the effect of reducing the membrane thickness. This effect was confirmed in the power generation performance results shown in Figure 3-1, even for the Fe-N-Cp catalyst.

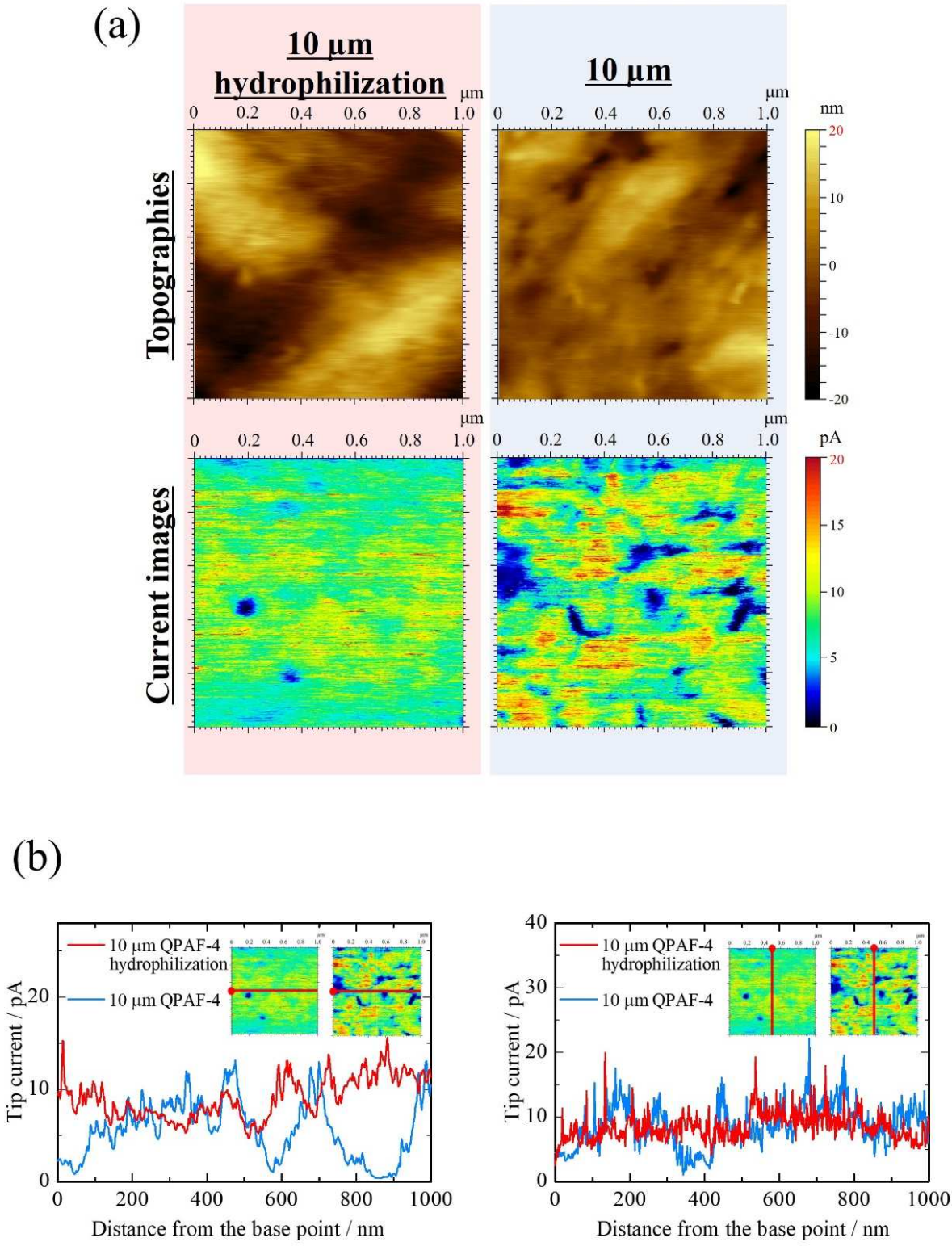

Figure 3-6. Topography (upper row) and current images (lower row) on 10 µm thick

QPAF-4 with hydrophilization (left column) and without hydrophilization (right column) under 40 °C, 70% RH, purified air conditions, and contact force = 5 nN, tip bias = -0.2 V, (b) line analysis in vertical and horizontal directions on current images with or without hydrophilization.

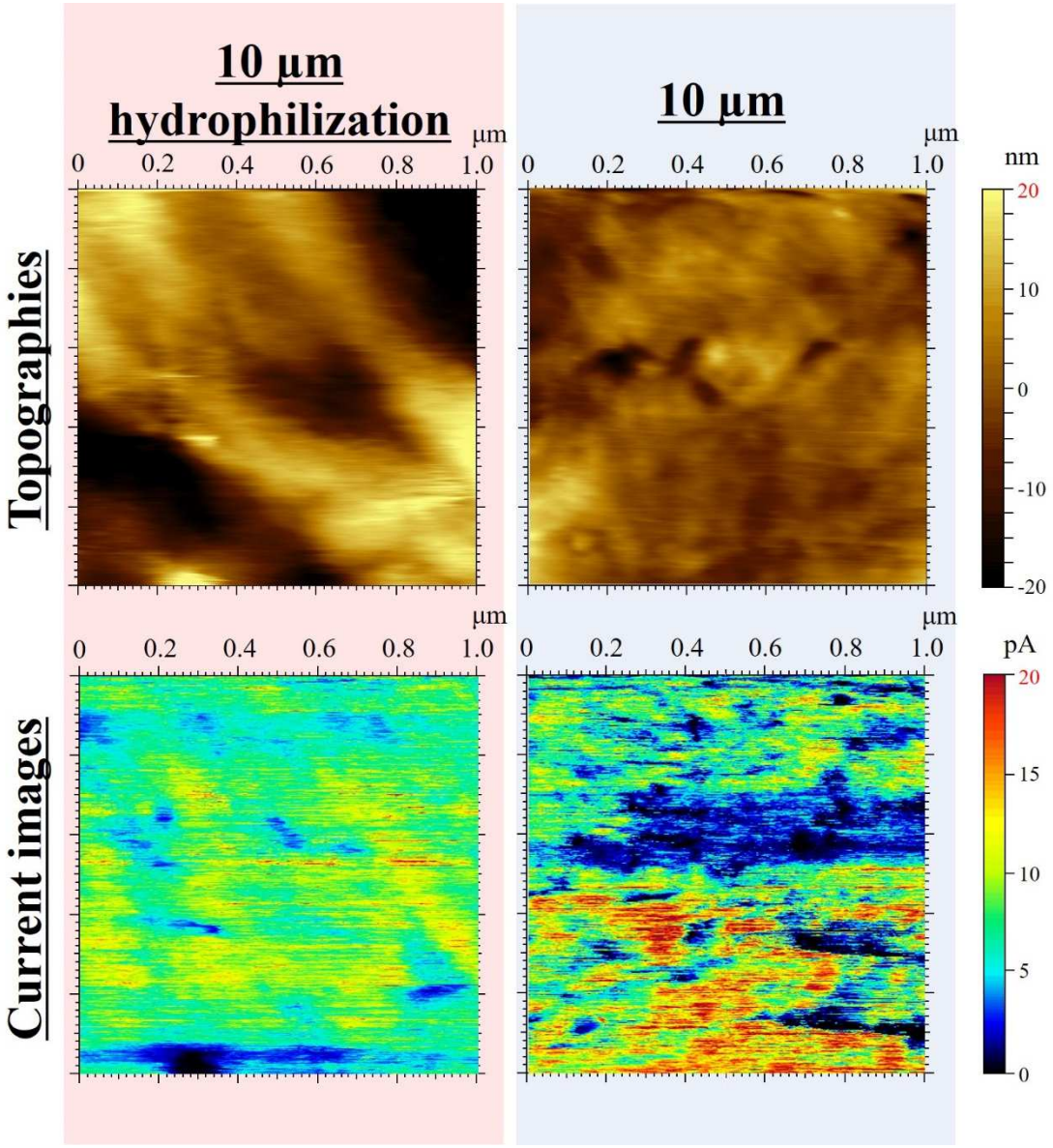

Figure 3-7. Topography (upper row) and current images (lower row) on 10-µm thick QPAF-4 with hydrophilic treatment (left column) and without hydrophilic treatment (right column) under 40 °C, 70% RH, purified air conditions, and contact force = 5 nN, tip bias = -0.2 V in a different field of view from that in Fig. 3(a).

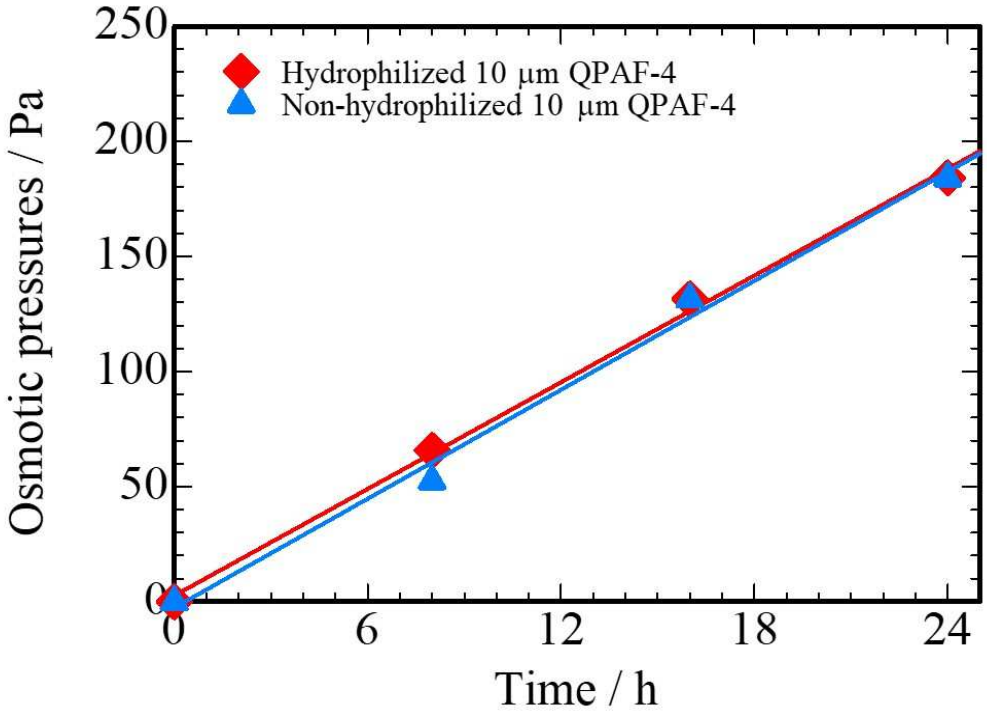

Figure 3-8. Osmotic pressures vs. time using 10 μm QPAF-4 membranes with or without hydrophilization.

Improvement approach of Fe-N-C catalysts to suppress I-V hysteresis

As a second approach to suppress the I-V hysteresis, I investigated the use of a new non-PGM catalyst that would have improved performance in comparison with that of the Fe-N-Cp material, used in the Chapter 2, by using the Fe-N-Cc catalyst developed at the CIAC Laboratory.

Analysis of CLs structure using Fe-N-C catalysts

Figure 3-9 shows the pore size distributions calculated by the BJH method and N_2 adsorption isotherms of these Fe-N-C catalysts and Pt/CB catalysts, respectively. In Figure 3-9, in the Fe-N-Cc CL, the hysteresis of the nitrogen adsorption/desorption isotherm is smaller than that for the Fe-N-Cp CL, suggesting that the pore volumes of the ink bottle structures [20, 21] were also lower. In addition, the isotherm on the low-pressure side near P = 0 had a larger slope than those for the other CLs, and the cumulative pore distribution and the log differential pore volume distributions calculated from the adsorption/desorption isotherms indicated many pores of ~5 and 40 nm. The Fe-N-Cc is synthesized from the high specific surface area carbon Black Pearls [10], and it is clear that the characteristics of the carbon material also affect the gas adsorption of the catalyst layer.

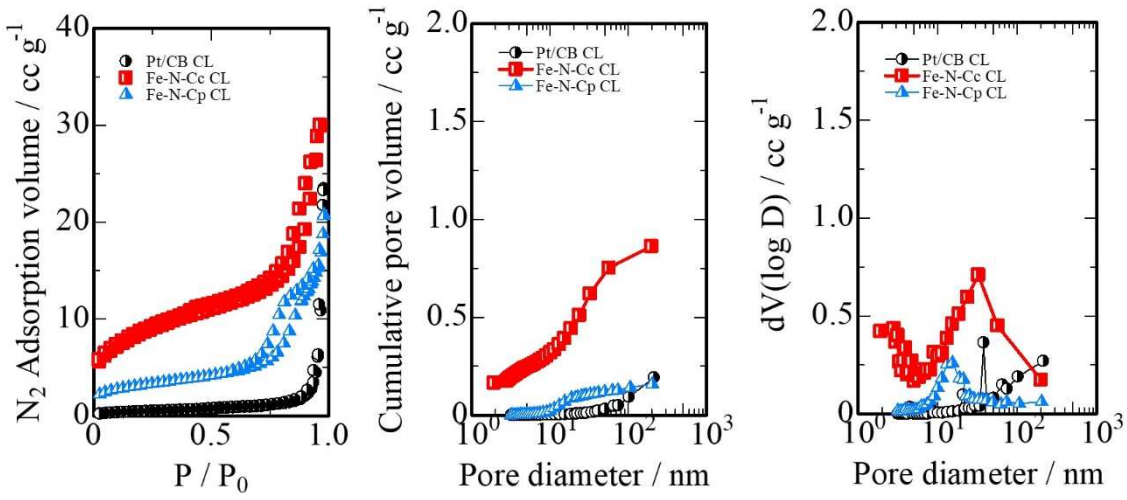

Figure 3-9. N_2 adsorption isotherms of Fe-N-Cc CL, Fe-N-Cp CL and Pt/CB CL, and pore size distribution calculated by the BJH method.

Figure 3-10 shows water vapor adsorption isotherms and contact angle changes of these Fe-N-C catalysts and Pt/CB catalysts, respectively. Comparing the water vapor adsorption isotherms of all of the CLs in Figure 3-10(a), on the low-pressure side near P = 0, where the first layer of water molecules was adsorbed, the amount of water vapor adsorbed by the Fe-N-Cc CL was as low as Pt/CB CL. On the high-pressure side near P = 1, the Fe-N-Cc CL had a similarly large adsorption amount as the Fe-N-Cp CL, and the water adsorbed value increased with increasing pressure applied. These results indicate that

water was not able to enter into the pores of the Fe-N-Cc CL despite the larger pore volume than that of the Pajarito CL at low pressure, close to a practical fuel cell condition. Figure 3-10(b) shows that the Fe-N-Cc CL was more hydrophobic than the Fe-N-Cp CL from the contact angle measurements of the CLs and the hydrophobicity was comparable to that of the Pt/CB CL. The high hydrophobicity of the Fe-N-Cc material is thought to be attributed to that of Black Pearls, a furnace black carbon similar to Kejten Black, the carbon support material for Pt/CB.

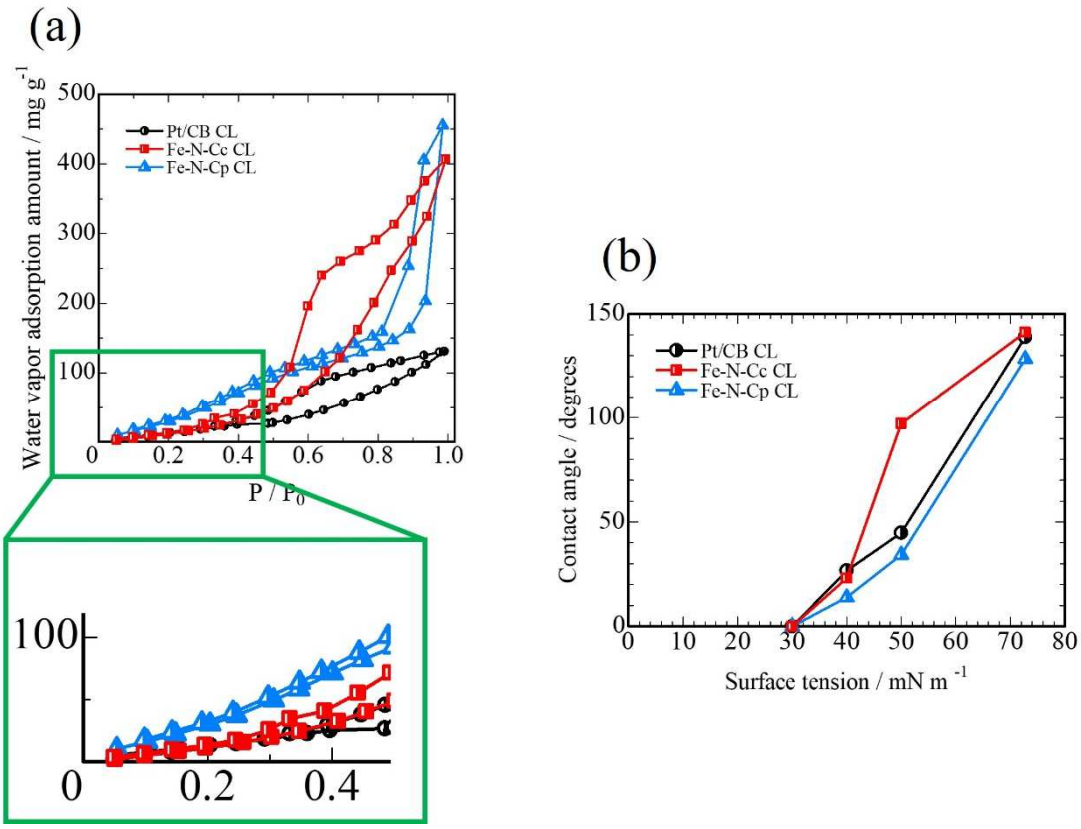

Figure 3-10. (a) Water vapor adsorption isotherms for the Fe-N-Cc CL, Fe-N-Cp CL and Pt/CB CL, (b) contact angle changes for some reagents with different surface tensions with the Fe-N-Cc CL, Fe-N-Cp CL and Pt/CB CL.

Polarization performance using Fe-N-C catalysts

Polarization performances for the Fe-N-Cc (11 μg cm^{-2}), Fe-N-Cp (11 μg cm^{-2}) and Pt/CB ((4 μg_{Pt} cm^{-2}, TEC10E50E) catalysts using the RDE technique are shown in Figures 3-11. The amounts of catalysts for the RDE were prepared at the same ratio used for the cathodes of the MEAs. The plateau currents for the Fe-N-C catalysts did not reach the limiting current density for the 4-electron ORR, because the amounts of the catalysts were very small, and thus there was a limitation due to mass transport between catalyst agglomerates on the electrode surface [22]. Nevertheless, the ORR activity can be compared in terms of the half-wave potentials: the Fe-N-Cc catalyst exhibited 0.81 V at 0.05 mA cm^{-2}, which was 0.18 V higher than that of the Pajarito catalyst but was 0.084 V lower than that of Pt/CB with the same catalyst ratio. Figure 3-12 shows the cell performance using each cathode CL with a 30 μm QPAF-4 membrane. Table 3-1 shows the voltages at three different current densities, 0.2, 0.5 and 0.8 A cm^{-2}. The voltage differences of the I-V hysteresis at 0.2 A cm^{-2} and 0.5 A cm^{-2} for the cell using the Fe-N-Cc CL were 0.05 V and 0.03 V, respectively, which were smaller than the corresponding values, 0.20 V and 0.15 V for the cell using the Fe-N-Cp CL, and the performance at current densities below 0.5 A cm^{-2} was comparable to that for the Pt/CB CL. In addition, the ohmic resistance of the Fe-N-Cc cell was 0.090 Ω cm^2 at 0.5 A cm^{-2}, which was similar to that of the Pt/CB CL.

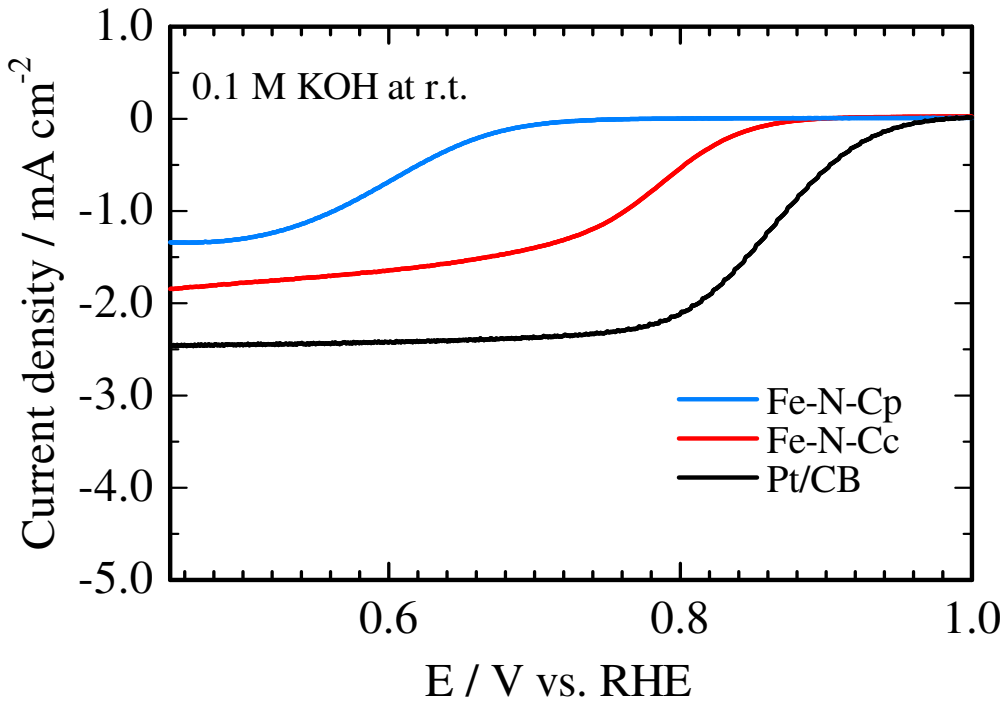

Figure 3-11. Hydrodynamic voltammogram of the Fe-N-Cc (11 µg cm^{-2}), Fe-N-Cp (11 µg cm^{-2}) and Pt/CB ((4 μg_{Pt} cm^{-2}, TEC10E50E) catalysts using RDE with a sweep rate of 5 mV s^{-1} and rotation rate of 1000 rpm in O_2-saturated 0.1 M KOH at ambient temperature.

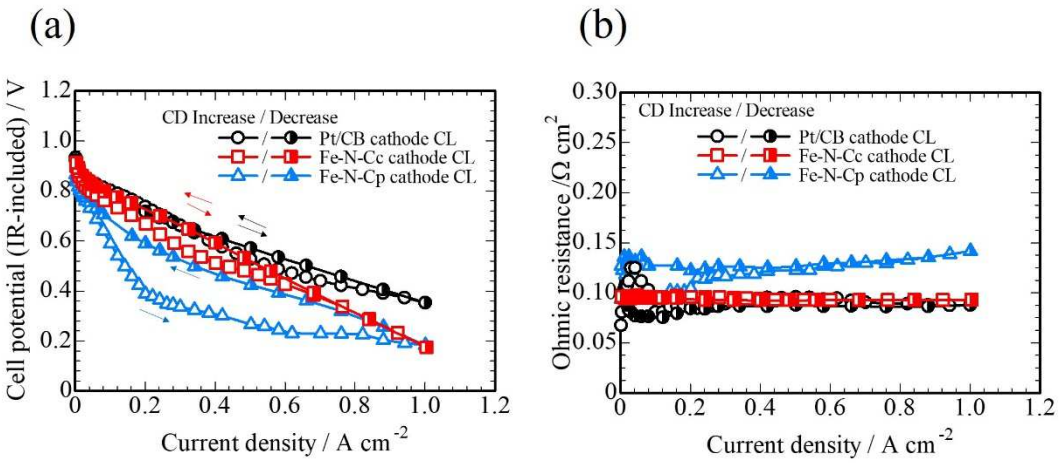

Figure 3-12. (a) I–V curves and (b) ohmic resistances using the Fe-N-Cc CL, Fe-N-Cp CL and Pt/CB CL at 60 °C, 100% RH; anode H_2 (100 mL min^{-1}, 0 kPa_g); cathode O_2 (100 mL min^{-1}, 0 kPa_g).

Table 3-1. Voltage changes at constant current density of cells using each catalyst layer

Cathode Catalyst	Current density					
	0.2 A cm^{-2}		0.5 A cm^{-2}		0.8 A cm^{-2}	
	Increase	Decrease	Increase	Decrease	Increase	Decrease
Pt/CB	0.74 V	0.73 V	0.53 V	0.57 V	0.41 V	0.43 V
Fe-N-Cc	0.67 V	0.73 V	0.47 V	0.52 V	0.31 V	0.32 V
Fe-N-Cp	0.39 V	0.59 V	0.27 V	0.42 V	0.23 V	0.29 V

The reason why I-V hysteresis was suppressed in the Fe-N-Cc CL can be rationalized as being due to its high hydrophobicity, so that the volume of water absorbed by the catalyst is reduced, and the water required for the reaction is secured. In addition, the reason why the ohmic resistance of the Fe-N-Cc cell was low is considered to be that there was little water absorbed by the catalyst, and the water content of the membrane increased. However, in the higher current density region, for example, 0.8 A cm^{-2}, the voltages of cell using the Fe-N-Cc CL decreased to 0.32 V compared with the case of 0.43 V using the Pt/CB CL and were nearly the same as those using the Pajarito CL (during decreasing current density). The reason for the performance decay at high current density is considered to be due to the fact that the catalyst layer was 3 times thicker than that of the Pt/CB, which was nearly the same as that of the Pajarito catalyst (Figure 3-13), and thus the diffusion overvoltages for oxygen and water required for the cathode reaction increased. On the other hand, with a thinner CL, there are fewer Fe active sites, and more oxygen is needed to penetrate the catalyst layer through the ionomer. [23] This may affect the performance and the use of ionomers with high gas permeability should be considered.

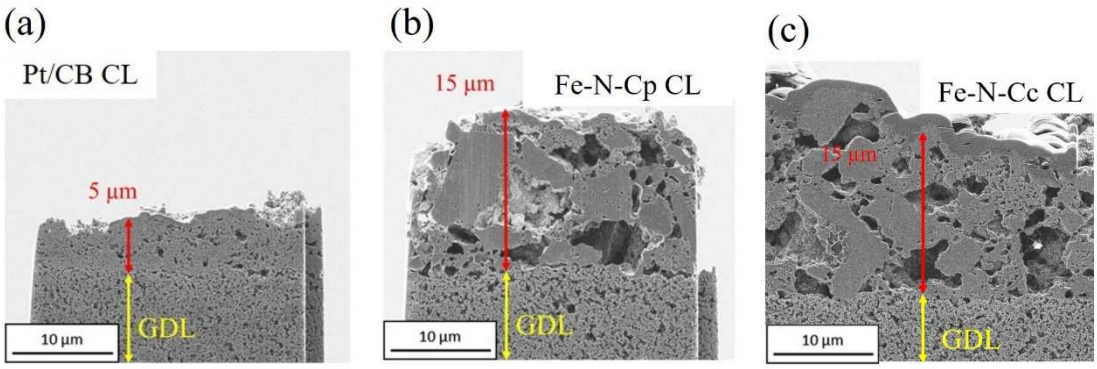

Figure 3-13. Images of cross-sectional structure with (a) Pt/CB CL, (b) Fe-N-Cp CL and (c) Fe-N-Cc CL by FIB-SIM.

Assumed mechanism of improvement effect of both membranes and Fe-N-C catalysts to suppress I-V hysteresis

The insights gained from the two approaches of the present Chapter 3 are summarized as schematic images of water management to suppress I-V hysteresis by use of the surface-hydrophilized electrolyte membrane in Figure 3-14(a) and by the use of the Fe-N-C catalyst with low water absorption in Figure 3-14(b). Figure 3-14(a) shows that I hydrophilized the surface of the QPAF-4 membrane, and this approach led to an improvement in performance due to the increased amount of water available for the ORR. By making the electrolyte membrane surface hydrophilic to improve the diffusivity of water at the surface rather than in the interior, it was possible to suppress the I-V hysteresis, even for the cell using the Fe-N-Cp catalyst, which has high water absorption. Therefore,

increasing the utilization of back-diffusing water from the anode is essential in the supply of water to reaction sites of the cathode [24, 25]. These results indicate that the water diffusivity, not only in the interior of both the membrane and CL, but also at the interface between membrane and cathode, is important.

Figure 3-14(b) shows diagrammatically the effect of changing the cathode catalyst from the Fe-N-Cp to the CIAC-developed counterpart. The Fe-N-Cc material exhibited lower water absorbability than the Pajarito material. The use of this material led to decreased absorption of the back-diffusing water into the interior of the carbon in the CL and an increased volume of water supplied to reaction sites on the surface of the carbon, which are those with the shortest oxygen diffusion distance. These improvements demonstrate that water transport is the main limitation responsible for the previously reported I-V hysteresis (Chapter 2) and provide strategies to achieve higher performance AEMFCs through proper water management and formation of water transport pathways.

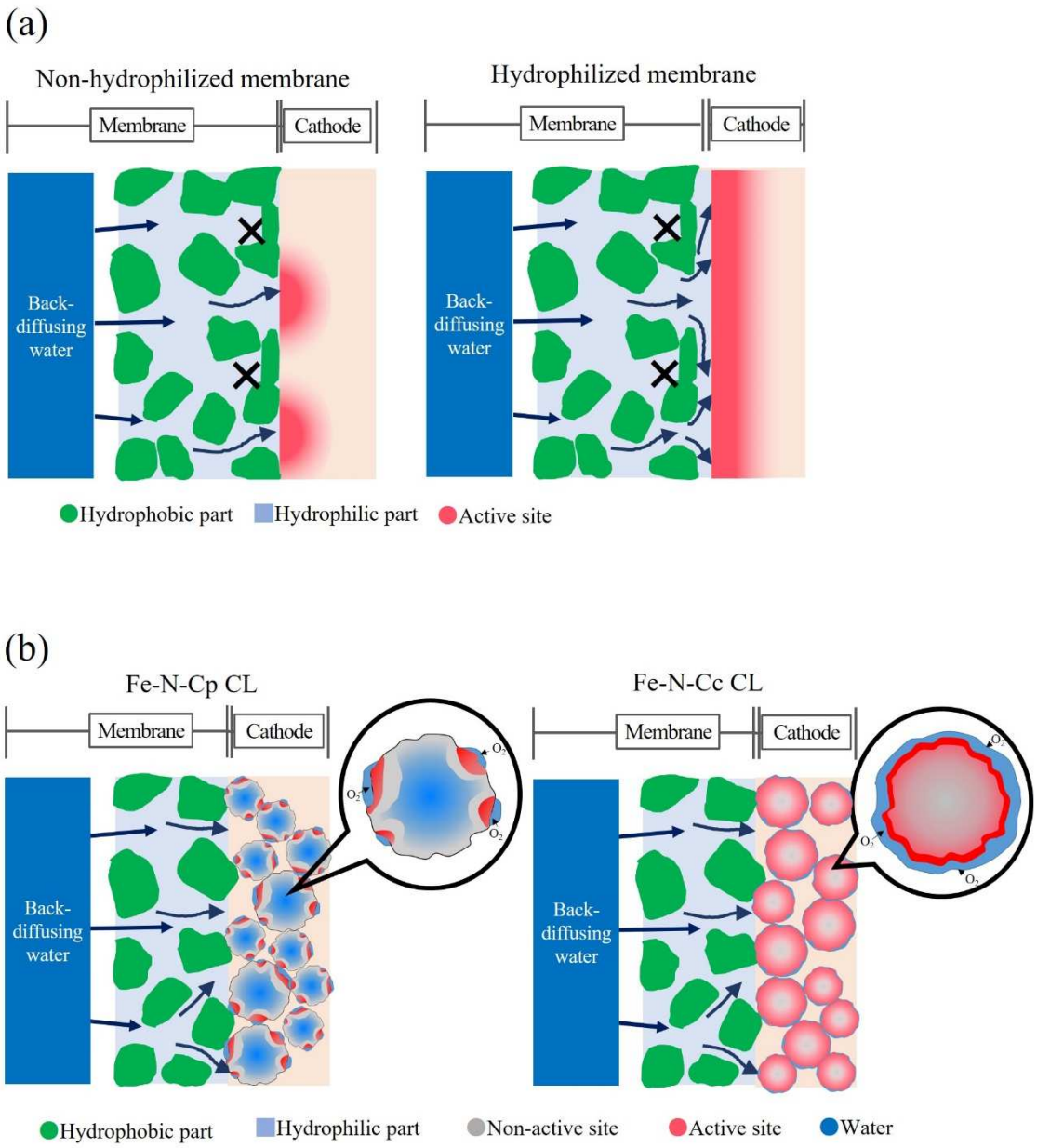

Figure 3-14. Schematic depiction of water management using (a) membranes with /without hydrophilization, and (b) the Fe-N-Cc CL and Fe-N-Cp CL.

3.4 Conclusions

In this Chapter 3, I have clearly identified the problem as being related to water management and developed two approaches to alleviating the problem: by use of a thin hydrophilized membrane, the diffusivity of water at the surface was improved, and the severe I-V hysteresis was suppressed, despite the cell using an Fe-N-C cathode catalyst with a high water absorption rate. The voltage loss was also alleviated by the use of a recently developed Fe-N-C catalyst with higher hydrophobicity, which decreased the absorption of back-diffusing water into the catalyst layer and increased the amount of water supplied to the reaction sites These improvements have demonstrated that water transport is the main limitation for the previously reported hysteresis and provide strategies to achieve higher performance AEMFCs through proper water management and formation of water transport pathways.

References

[1] G. Merle, M. Wessling, K. Nijmeijer, "Anion exchange membranes for alkaline fuel cells: a review," *Journal of Membrane Science,* 377 (2011) 1-35. DOI: 10.1016/j.memsci.2011.04.043

[2] J. R. Varcoe, P. Atanassov, D. R. Dekel, A. M. Herring, M. A. Hickner, P. A. Kohl, A. R. Kucernak, W. E. Mustain, K. Nijmeijer, K. Scott, T. Xu, L. Zhuang, "Anion-exchange membranes in electrochemical energy systems," *Energy & Environmental Science*, 7 (2014) 3135-3191. DOI: 10.1039/C4EE01303D

[3] W. E. Mustain, "Understanding how high-performance anion exchange membrane fuel cells were achieved: Component, interfacial, and cell-level factors," *Current Opinion in Electrochemistry*, 12 (2018) 233-239. DOI: 10.1016/j.coelec.2018.11.010

[4] T.B. Ferriday, P. H. Middleton. "Alkaline fuel cell technology - A review", *International Journal of Hydrogen Energy,* 46 (2021) 18489-18510. DOI: 10.1016/j.ijhydene.2021.02.203

[5] D. R. Dekel, I. G. Rasin, S. Brandon, "Predicting performance stability of anion exchange membrane fuel cells", *Journal of Power Sources,* 420 (2019) 118-123. DOI: 10.1016/j.jpowsour.2019.02.069

[6] K. Yassin, I. G. Rasin, S. Brandon, Dario R. Dekel, "Quantifying the critical effect of water diffusivity in anion exchange membranes for fuel cell applications", *Journal of Membrane Science*, 608 (2020) 118206. DOI: 10.1016/j.memsci.2020.118206

[7] Z. Jiang, Z. Jiang, "Plasma techniques for the fabrication of polymer electrolyte membranes for fuel cells", *Journal of Membrane Science*, 456 (2014) 85–106. DOI: 10.1016/j.memsci.2014.01.004

[8] S. Bae, J. Park, Y. Hwang, J. Park, J. Lee, B. Jeong, "Steam activation of Fe-N-C catalyst for advanced power performance of alkaline hydrazine fuel cells", *Journal of Energy Chemistry,* 64 (2022) 276–285 DOI: 10.1016/j.jechem.2021.04.029

[9] S. H. Lee, J. Kim, D. Y. Chung, J. M. Yoo, H. S. Lee, M. J. Kim, B. S. Mun, S. G. Kwon, Y. Sung, T. Hyeon, "Design Principle of Fe–N–C Electrocatalysts: How to Optimize Multimodal Porous Structures?", *Journal of the American Chemical*

Society, 141 (2019) 2035−2045. DOI: 10.1021/jacs.8b11129

[10] P. Song, H. M. Barkholtz, Y. Wang, W. Xu, D. Liu, L. Zhuang, "High-performance oxygen reduction catalysts in both alkaline and acidic fuel cells based on pre-treating carbon material and iron precursor", *Science Bulletin,* 62 (2017) 1602–1608. DOI: 10.1016/j.scib.2017.10.020

[11] H. Ono, T. Kimura, A. Takano, K. Asazawa, J. Miyake, J. Inukai, K. Miyatake, "Robust anion conductive polymers containing perfluoroalkylene and pendant ammonium groups for high performance fuel cells," *Journal of Materials Chemistry A,* 5 (2017) 24804-24812. DOI: 10.1039/c7ta09409d

[12] M. Hara, T. Kimura, T. Nakamura, M. Shimada, H. Ono, S. Shimada, K. Miyatake, M. Uchida, J. Inukai, M. Watanabe, "Effect of surface ion conductivity of anion exchange membranes on fuel cell performance", *Langmuir*, 32 (2016), 9557-9565 DOI: 10.1021/acs.langmuir.6b01747

[13] M. Hara, D. Hattori, J. Inukai, B. Bae, T. Hoshi, M. Hara, K. Miyatake, M. Watanabe, "Imaging individual proton-conducting spots on sulfonated multiblock-copolymer membrane under controlled hydrogen atmosphere by current-sensing atomic force microscopy", *The Journal of Physical Chemistry B*, 117 (2013) 3892-3899 DOI: 10.1021/jp312041c

[14] M. Hara, H. Daiki, J. Inukai, M. Hara, K. Miyatake, M. Watanabe, "Reversible/irreversible increase in proton-conductive areas on proton-exchange-membrane surface by applying voltage using current-sensing atomic force microscope", *Journal of Electroanalytical Chemistry,* 716 (2014) 158-163 DOI: 10.1016/j.jelechem.2013.11.035

[15] M. Hara, M. Hara, K. Miyatake, J. Inukai, M. Watanabe, "Effects of hot liquid-water treatment on local proton conductivity at surfaces of sulfonated poly(arylene ketone) block copolymer membrane for fuel cells studied by current-sensing atomic force microscopy", *Electrochimica Acta*, 143 (2014) 383-389 DOI: 10.1016/j.electacta.2014.08.031

[16] M. Hara, T. Miyahara, T. Hoshi, J. Ma, M. Hara, K. Miyatake, J. Inukai, N. Alonso-Vante, M. Watanabe, "Proton conductive areas on sulfonated poly(arylene ketone) multiblock copolymer electrolyte membrane studied by current-sensing atomic

force microscopy", *Electrochemistry,* 82 (2014) 369-375 DOI: 10.5796/electrochemistry.82.369

[17] J. Inukai, "Current-sensing atomic force microscopy for analyzing conformations and properties of polymer membranes for fuel cells", *Current Opinion in Electrochemistry,* 21 (2020) 345-350. DOI: 10.1016/j.coelec.2020.04.013

[18] T. Kimura, R. Akiyama, K. Miyatake, J. Inukai, "Phase separation and ion conductivity in the bulk and at the surface of anion exchange membranes with different ion exchange capacities at different humidities", *Journal of Power Sources,* 375 (2020) 397-403. DOI: 10.1016/j.jpowsour.2017.06.081

[19] A. Kusoglu and A. Z. Weber, "New Insights into Perfluorinated Sulfonic-Acid Ionomers", *Chem. Rev.,* 117 (2017) 987−1104. DOI: 10.1021/acs.chemrev.6b00159

[20] Y. Park, H. Tokiwa, K. Kakinuma, M. Watanabe, M. Uchida "Effects of carbon supports on Pt distribution, ionomer coverage and cathode performance for polymer electrolyte fuel cells", *Journal of Power Sources,* 315 (2016) 179-191. DOI: 10.1016/j.jpowsour.2016.02.091

[21] A. Kobayashi, T. Fujii, C. Harada, E. Yasumoto, K. Takeda, K. Kakinuma, M. Uchida, "Effect of Pt and Ionomer Distribution on Polymer Electrolyte Fuel Cell Performance and Durability", *ACS Applied Energy Materials*, 4 (2021) 2307−2317. DOI: 10.1021/acsaem.0c02841

[22] K. Miyatake, T. Omata, D. A. Tryk, H. Uchida, M. Watanabe, "Oxygen Reduction at the Pt/Carbon Black-Polyimide Ionomer Interface," *The Journal of Physical Chemistry C,* 113 (2009) 7772–7778. DOI: 10.1021/jp8095067

[23] P. G. Santori, A. N. Mondal, D. R. Dekel, F. Jaouen, "The critical importance of the ionomer on the electrochemical activity of platinum and platinum-free catalysts for anion-exchange membrane fuel cells", *Sustainable Energy Fuels,* 4 (2020) 3300-3307. DOI: 10.1039/D0SE00483A

[24] R. Gutru, Z. Turtayeva, F. Xu, G. Maranzana, B. Vigolo, A. Desforges, "A comprehensive review on water management strategies and developments in anion exchange membrane fuel cells," *International Journal of Hydrogen Energy,* 45 (2020) 19642-19663. DOI: 10.1016/j.ijhydene.2020.05.026

[25] T. J. Omasta, A. M. Park, J. M. LaManna, Y. Zhang, X. Peng, L. Wang, D. L.

Jacobson, J. R. Varcoe, D. S. Hussey, B. S. Pivovar, W. E. Mustain, "Beyond catalysis and membranes: visualizing and solving the challenge of electrode water accumulation and flooding in AEMFCs," *Energy & Environmental Science*, 11 (2018) 551-558. DOI: 10.1039/c8ee00122g

[26] J. S. Rugg, "Ozone Crack Depth Analysis for Rubber", *Analytical Chemistry,* 24 (1952) 818-821. DOI: 10.1021/ac60065a015

[27] S. D. Razumovsky, V. V. Podmasteriyev, G. Zaikov, "Kinetics of the growth of cracks on polyisoprene vulcanizates in ozone", *Polymer Degradation and Stability,* 16 (1986) 317-324. DOI: 10.1016/0141-3910(86)90088-1

Chapter 4

General conclusions and Future prospects

4.1 Conclusions

The purpose of this thesis is to evaluate the performance of AEMFCs under low flow conditions and with non-precious metal cathode catalysts, and to obtain a deeper understanding of water management in AEMFCs.

In Chapter 2, the cell performance for the AEMFC using a non-PGM catalyst (Fe-N-C) for the cathode and an in-house-developed anion exchange ionomer (QPAF-4) for both the membrane and the CL binder were investigated under practical gas flow conditions, i.e., high utilization. The cell using the Fe-N-C CL exhibited large hysteresis in the I-V curve under ambient pressures for both electrodes. Irrespective of the presence or absence of BP in the anode, the I-V hysteresis occurred but was not observed when only the cathode was pressurized to 100 kPa_g. In the cathode, decreasing amounts of liquid water due to a decrease of BP and relative humidity increased the ohmic resistance because of decreasing water content in the cathode ionomer and membrane. These results suggest that the difference of these hysteresis phenomena arises from the difference in the absorption capacity of liquid water for both CLs, affecting the supply of water at reaction sites in the cathode. The differences between Fe-N-C and Pt/CB was also clarified based on morphology analysis. The void volume of the Fe-N-C absorbed the generated water during increasing current density and led to an insufficiency of reactant water at the cathode reaction sites, so that water mass transport became a major limiting factor, causing the I-V hysteresis. The Tafel slope component analysis revealed that the I-V

behavior in this region can be characterized as a direct transition from kinetic control (56 mV slope) to combined gas-ion-water transport control, with a unique slope octupling behavior (448 mV slope). These results also support the importance of back-diffusing water from the anode for the rate of the cathode reaction.

In Chapter 3, based on the results of Chapter 2, this thesis examined two approaches for the improvement of the water management ability, with the aim of suppressing the I-V hysteresis phenomenon. First, to increase the supply of generated water to the reaction active sites of the cathode, I decreased the membrane thickness and hydrophilized the membrane surface in order to increase the flux of back-diffusing water. These improvements of the water transport at the interface between the membrane and the cathode by use of the hydrophilization on a thin electrolyte membrane were effective in eliminating the I-V hysteresis phenomenon at both the anode and the cathode. Based on various types of membrane characterization, including CS-AFM, contact angle and osmotic pressure, this research also clarified that hydrophilization does not improve the diffusivity of water in the interior but contributes to the improvement of surface anion conduction and water transport pathways. This effect was confirmed in the power generation performance measurements, even with the Fe-N-C catalyst with high water uptake that was associated with the initial observation of the I-V hysteresis. Second, from the viewpoint of the catalyst layer, to suppress the I-V hysteresis, I sought to improve the performance in comparison with that obtained for the Fe-N-Cp catalyst used in the previous research by using the recently developed Fe-N-Cc catalyst. The nitrogen adsorption results indicated that water was not able to enter into the pores of the Fe-N-Cc CL despite the larger pore volume than that of the Fe-N-Cp CL at low pressures, close to the practical fuel cell condition. From water vapor adsorption and contact angle

evaluation, the high hydrophobicity of the Fe-N-Cc catalyst was assigned to the hydrophobicity of Black Pearls, the furnace black carbon, which is similar in its characteristics to Kejten Black, which is the carbon support material of Pt/CB. From results, the reason for the I-V hysteresis suppression by the Fe-N-Cc CL was able to be assigned to its high hydrophobicity, so that the volume of water absorbed by the catalyst was decreased, and the water required for the reaction was secured. In addition, the reason for the low ohmic resistance of the Fe-N-Cc-based cell was considered to be that the volume of water absorbed by the catalyst was suppressed, and thus the water content of the membrane increased. These improvements have demonstrated that water transport is the main limitation responsible for the voltage drop observed as the current density is increased, with the resulting I-V hysteresis, and thus have provided strategies for achieving higher performance AEMFCs through proper water management and formation of water transport pathways. And the result obtained this time is one of the highest power efficiencies in AEMFC's water management so far (Figure 4-1). [1-21]

The importance of water balance is not new, as it has been mentioned in many previous reports. [22-35] However, this PhD research demonstrated and proposed that the water absorption of the catalyst and the impediments to water transport at the membrane catalyst layer interface make this important water management challenge more pronounced, and thus a more serious problem, at the lower flow rates and lower pressure drops that are easier to achieve in practical systems.

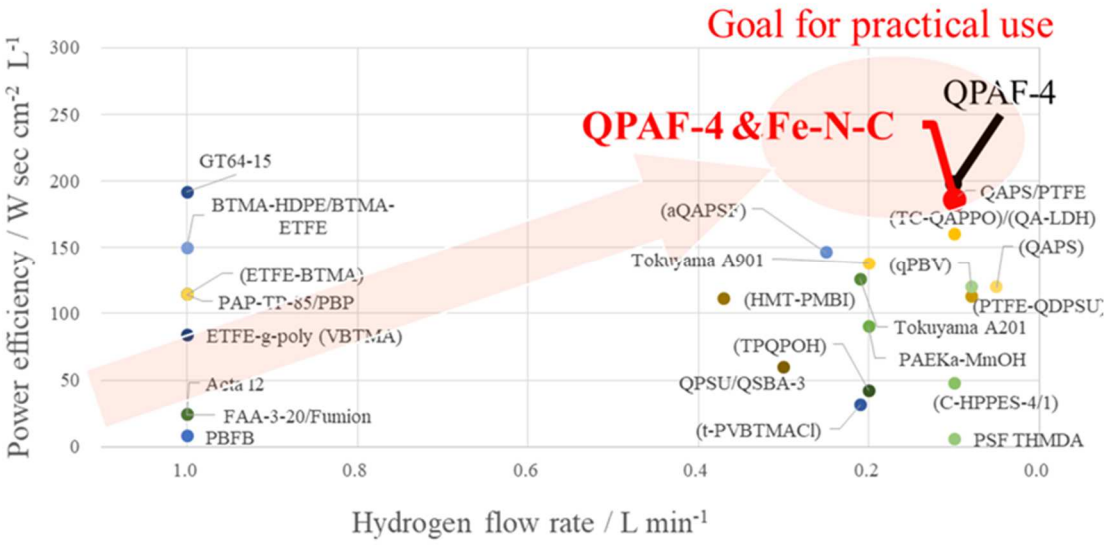

Figure 4-1. Positioning of this research and other researches. The legend indicates the name of the anionic electrolyte used in each paper.

4.2 Future prospects

The advantage of AEMFCs is that the alkaline conditions in the fuel cell system enable the use of non-PGMs catalysts, which the cost of AEMFCs can be lower than that of PEMFCs. In this thesis, changing only the cathode catalyst to non-PGMs was carried out because the cathode reaction, which is a water-consuming reaction, is considered to be an important factor for improving fuel cell performance and durability. In order to lower the cost and achieve practical use of AEMFCs, non-PGM catalysts must be used on the anode side as well. For anodes, mainly Ni-based non-PGM catalysts have been reported. [36-38] Water is produced in the reaction at the anode, and as the current density increases, the amount of water produced in the reaction increases, and the hydrogen gas does not

reach the reaction active site of the anode electrode, resulting in a decrease in performance, or in other words, flooding (Figure 4-2 [36]). There are several approaches to reduce this flooding, such as lowering the gas humidity, using a more hydrophobic GDLs, or using a more hydrophobic ionomer[25, 26, 39], and the water management methods for the anode as well as the cathode must be considered. Understanding the structure and fundamental properties of the electrode/electrolyte interface in AEMFCs will lead to advances in the design and development of highly active non-precious metal HOR electrocatalysts.

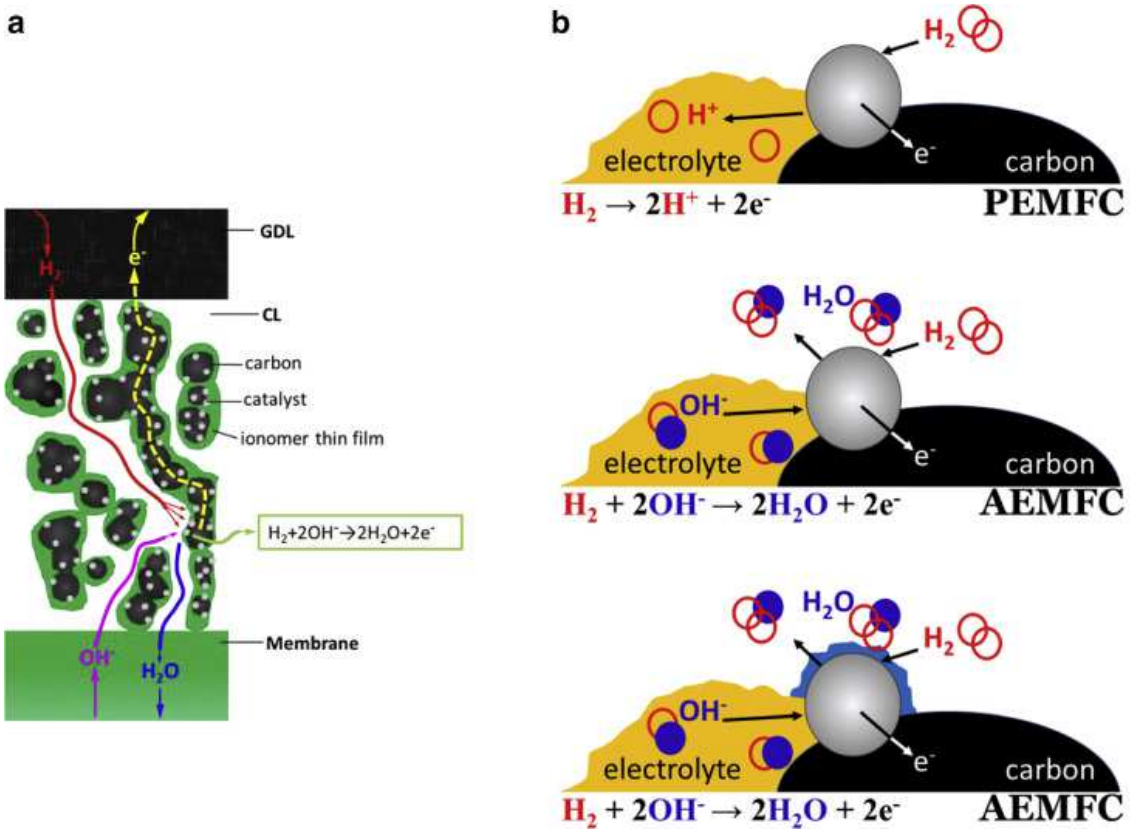

Figure 4-2. Schematic diagrams of the (a) AEMFC anode catalyst layer; and (b) a zoom-in into the triple-phase boundary of HOR, showing the differences between acidic and alkaline fuel cell environments.

The properties of the ionomers in the CL have been shown to significantly affect the water management of the electrode. Too little ionomer content interrupts the channels of hydroxide ion conduction at the CL and lowers the accessible electrochemical surface area, thus increasing IR losses and invalidating catalyst utilization. If there are too many ionomers, the ionomers are almost hydrophilic in nature, suppressing the electronic

conductivity of the CL and reducing the pore volume available for oxygen gas diffusion. [40] The optimal loading of ionomer was suggested to be 15% and 25%. [41] Therefore, it is important to consider the ratio of ionomer to catalyst when designing electrodes. More so, in AEMFCs, the ionomer layer should be uniformly formed on the catalyst surface.It is essential to improve the transport of water, gases and OH^- to the catalytically active sites, which is expected when using non-precious metal catalysts. Recently, Takahashi et al. and Cho et al. reported that the electrospray method can be used to form a dense catalyst layer structure and a uniform ionomer layer at the catalyst layer interface in PEMFC. [42-45] The application of this method to AEMFCs will lead to the development of high HOR and ORR active catalyst layers with macro/mesopore layers that are accessible to both gas and water.

These are issues to be considered that cannot be avoided for the practical application of AEMFCs.

4.3 Feasibility

In "Vision 2050," the Hydrogen Council predicts that the hydrogen market will reach US$2.5 trillion and create 30 million jobs worldwide by 2050. [46] Hydrogen can contribute to 18% of energy demand, 20% of CO_2 reduction, and 6 billion tons of CO_2 reduction per year. Hydrogen power generation will reach 1,500 TWh per year, and by storing surplus renewable energy, 500 TWh per year of renewable energy will be stored and used through hydrogen.

This thesis was the development of AEMFC, which is low cost for the widespread use of fuel cells. Figure 4-3 shows the cost breakdown and research priorities for fuel cells. More than 40% of this cost is for the Pt catalyst [47]; in the AEMFC, this catalyst cost will be less than 5% if we simply calculate the raw material cost. In addition, platinum, which will be almost exhausted by 2050 [48], requires recycling and reuse, while non-precious metal catalysts, such as Ni, Fe and Co, are more abundant than platinum. AEMFCs are more suitable for stationary power sources such as ENE-farms, where continuous power generation time is long and shutdown time is short, than for FCVs, where start-up and shutdown times are frequent. As ENE-farm's volume of installations increased, the average unit installation cost dropped 69% for PEFC, from JPY 3.03 million in 2009 to JPY 940,000 in 2018 (Figure 4-4). [49] In order to further reduce the cost, a breakthrough is needed by switching from the current use of PEMFC to the use of AEMFC.

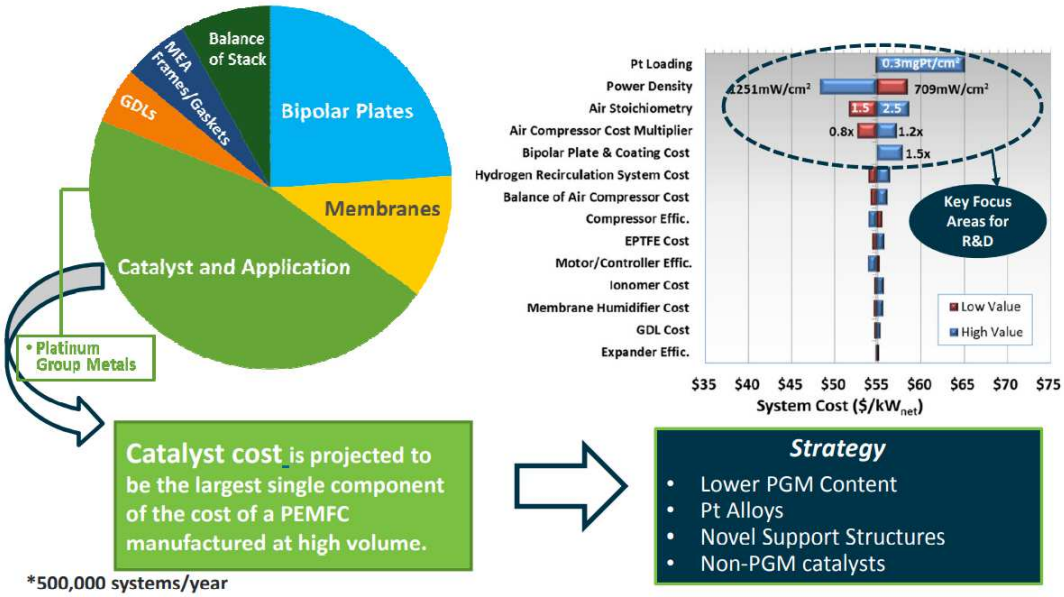

Figure 4-3. Fuel Cell R&D focus and priorities with PEFC stack cost breakdown and sensitivity analysis.

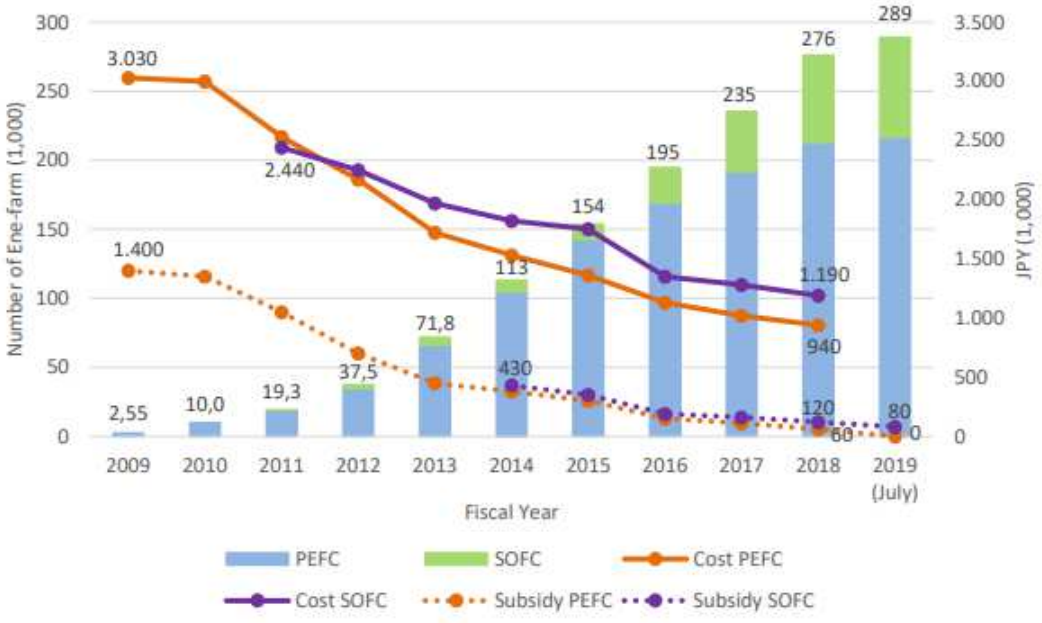

Figure 4-4. Dissemination of Ene-farms in Japan. Evolution of Costs and Subsidies

On the other hand, we need to focus not only on research for the widespread use of fuel cells, but also on hydrogen as a fuel. With fluctuating renewable energy capacity growing rapidly, supplementing solar and wind power generation facilities and using excess power that would otherwise be wasted to produce hydrogen can help maintain the flexibility of the power system and balance the grid. Unlike storage batteries, hydrogen can be stored on a large scale and on a long-term basis (Figure 4-5). [50] There are challenges to its widespread use, especially the high cost. At present, hydrogen is mainly produced from natural gas for industrial use (grey hydrogen), which emits a considerable amount of carbon dioxide. In doing so, a large amount of carbon dioxide is emitted. If the carbon emissions are captured and stored, or reused, then it is called “blue” hydrogen. Green hydrogen is the cleanest form of hydrogen. Green hydrogen is the cleanest form of hydrogen, produced by renewable energy sources with no carbon emissions. The main factor between gray and blue hydrogen is the fluctuating price of natural gas around the world.

Japan is an energy resource-poor country, but Green hydrogen will enable Japan to achieve its "3E+S" [51] goal by reducing carbon emissions in power generation, transportation, heating, and industrial processes. New Energy and Industrial Technology Development Organization (NEDO) estimates that the hydrogen market will reach 1 trillion yen in 2030 and 8 trillion yen in 2030, and is expected to reach 8 trillion yen in 2050 in Japan. [52]

Reverse-actuating AEMFCs results in the anion membrane water electrolyzer (AEMWEs). Unlike the current PEM type water electrolysis and alkaline water electrolysis, AEMWE eliminates the need to use catalysts such as platinum and the more costly iridium oxide, leading to lower costs for green hydrogen. Using the 5 MW base

alkaline water electrolysis and the PEM water electrolysis, AEMWE cost for 10 years of operation will be about 3 billion yen, which is 300 million yen less than the two water electrolysis. In addition, AEMWE is a recently conceived water electrolysis method, which is a promising market for future growth on a global scale towards a carbon neutral society. However, like the AEMFC, the AEMWE consumes water and involves a reaction to produce water, so water management is still an issue. Also, in AEMWE, there is a problem that the product gas inhibits the water electrolysis reaction, which increases the diffusion overvoltage and reduces the efficiency. It is clear that the technology and knowledge developed in AEMFC will be useful in addressing these issues.

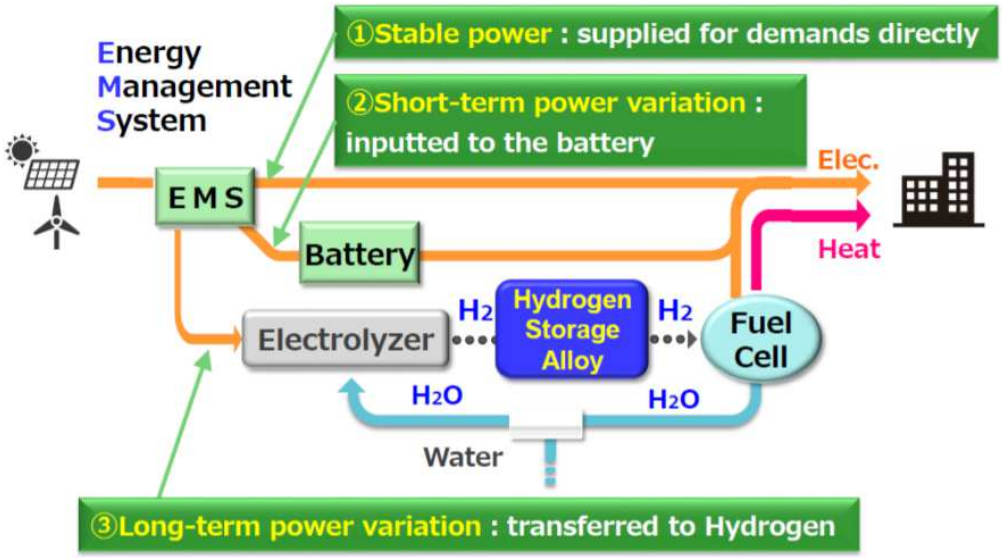

Figure 4-5. Hydrogen energy system.

References

[1] J. Liu, X. Yan, L. Gao, L. Hu, X. Wu, Y. Dai, X. Ruan, G. He, "Long-branched and densely functionalized anion exchange membranes for fuel cells", *Journal of Membrane Science,* 581 (2019) 82-92. DOI: 10.1016/j.memsci.2019.03.046

[2] X. Zhang, X. Chu, M. Zhang, M. Zhu, Y. Huang, Y. Wang, L. Liu, N. Li, "Molecularly designed, solvent processable tetraalkylammonium-functionalized fluoropolyolefin for durable anion exchange membrane fuel cells", *Journal of Membrane Science,* 574 (2019) 212-221. DOI: 10.1016/j.memsci.2018.12.082

[3] N. Chen, C. Long, Y. Li, D. Wang, H. Zhu, "High-performance layered double hydroxide/poly(2,6-dimethyl-1,4-phenylene oxide) membrane with porous sandwich structure for anion exchange membrane fuel cell applications", *Journal of Membrane Science,* 552 (2018) 51-60. DOI: 10.1016/j.memsci.2018.01.045

[4] T. J. Omasta, A. M. Park, J. M. LaManna, Y. Zhang, X. Peng, L. Wang, D. L. Jacobson, J. R. Varcoe, D. S. Hussey, B. S. Pivovar, W. E. Mustain, "Beyond catalysis and membranes: visualizing and solving the challenge of electrode water accumulation and flooding in AEMFCs," *Energy & Environmental Science*, 11 (2018) 551-558. DOI: 10.1039/c8ee00122g

[5] T. J. Omasta, L. Wang, X. Peng, C.A. Lewis, J.R. Varcoe, W.E. Mustain, "Importance of balancing membrane and electrode water in anion exchange membrane fuel cells," *Journal of Power Sources,* 375 (2018) 205-213. DOI: 10.1016/j.jpowsour.2017.05.006

[6] A.G. Wright, J. Fan, B. Britton, T. Weissbach, H.F. Lee, E.A. Kitching, T.J. Peckham, S. Holdcroft, "Hexamethyl-: P-terphenyl poly(benzimidazolium): a universal hydroxide-conducting polymer for energy conversion devices", *Energy & Environmental Science*, 9 (2016) 2130-2142. DOI: 10.1039/C6EE00656F

[7] A.N. Lai, D. Guo, C.X. Lin, Q.G. Zhang, A.M. Zhu, M.L. Ye, Q.L. Liu, "Enhanced performance of anion exchange membranes via crosslinking of ion cluster regions for fuel cells", *Journal of Power Sources,* 327 (2016) 56-66. DOI: 10.1016/j.jpowsour.2016.07.043

[8] C. Chen, J. Pan, J. Han, Y. Wang, L. Zhu, M.A. Hickner, L. Zhuang, "Varying the microphase separation patterns of alkaline polymer electrolytes", *Journal of Materials Chemistry A,* 4 (2016) 4071-4081. DOI: 10.1039/C5TA09438K

[9] R.B. Kaspar, M.P. Letterio, J.A. Wittkopf, K. Gong, S. Gu, Y. Yan, "Manipulating water in high-performance hydroxide exchange membrane fuel cells through asymmetric humidification and wetproofing", *Journal of The Electrochemical Society,* 162 (2015) F483. DOI: 10.1149/2.0131506jes

[10] P.S. Khadke, U. Krewer, "Performance losses at H2/O2 alkaline membrane fuel cell", *Electrochemistry Communications,* 51 (2015) 117-120. DOI: 10.1016/j.elecom.2014.12.006

[11] R. Zeng, J. Handsel, S.D. Poynton, A.J. Roberts, R.C.T. Slade, H. Herman, D.C. Apperley, J.R. Varcoe, "Alkaline ionomer with tuneable water uptakes for electrochemical energy technologies", *Energy & Environmental Science,* 4 (2011) 4925-4928. DOI: 10.1039/C1EE02349G

[12] X. Wang, M. Li, B.T. Golding, M. Sadeghi, Y. Cao, E.H. Yu, K. Scott, "A polytetrafluoroethylene-quaternary 1,4-diazabicyclo-[2.2.2]-octane polysulfone composite membrane for alkaline anion exchange membrane fuel cells", *International Journal of Hydrogen Energy,* 36 (2011) 10022-10026. DOI: 10.1016/j.ijhydene.2011.05.054

[13] Y.C. Cao, X. Wang, M. Mamlouk, K. Scott, "Preparation of alkaline anion exchange polymer membrane from methylated melamine grafted poly(vinylbenzyl chloride) and its fuel cell performance", *Journal of Materials Chemistry,* 21 (2011) 12910-12916. DOI: 10.1039/C1JM12068A

[14] M. Piana, M. Boccia, A. Filpi, E. Flammia, H.A. Miller, M. Orsini, F. Salusti, S. Santiccioli, F. Ciardelli, A. Pucci, "H_2/air alkaline membrane fuel cell performance and durability, using novel ionomer and non-platinum group metal cathode catalyst", *Journal of Power Sources,* 195 (2010) 5875-5881. DOI: 10.1016/j.jpowsour.2009.12.085

[15] J. Pan, S. Lu, Y. Li, A. Huang, L. Zhuang, J. Lu, "High-performance alkaline polymer electrolyte for fuel cell applications", *Advanced Functional Materials,* 20 (2010) 312-319. DOI: 10.1002/adfm.200901314

[16] S. Gu, R. Cai, T. Luo, Z. Chen, M. Sun, Y. Liu, G. He, Y. Yan, "A soluble and highly conductive ionomer for high-performance hydroxide exchange membrane fuel cells", *Angewandte Chemie International Edition,* 48 (2009) 6499-6502. DOI: 10.1002/anie.200806299

[17] Y. Zhao, J. Pan, H. Yu, D. Yang, J. Li, L. Zhuang, Z. Shao, B. Yi, "Quaternary ammonia polysulfone-PTFE composite alkaline anion exchange membrane for fuel cells application", *International Journal of Hydrogen Energy,* 38 (2013) 1983-1987. DOI: 10.1016/j.ijhydene.2012.11.055

[18] E. Vijayakumar, D. Sangeetha, "A quaternized mesoporous silica/polysulfone composite membrane for an efficient alkaline fuel cell application", RSC Advances, 5 (2015) 42828- 42835. DOI: 10.1039/C5RA04144A

[19] M. Iravaninia, S. Azizi, S. Rowshanzamir, "A comprehensive study on the stability

and ion transport in cross-linked anion exchange membranes based on polysulfone for solid alkaline fuel cells", *International Journal of Hydrogen Energy,* 42 (2017) 17229-17241. DOI: 10.1016/j.ijhydene.2017.05.200

[20] N. Chen, H. H. Wang, S. P. Kim, H. M. Kim, W. H. Lee, C. Hu, J. Y. Bae, E. S. Sim, Y. Chung, J. Jang, S. J. Yoo, Y. Zhuang, Y. M. Lee, "Poly(fluorenyl aryl piperidinium) membranes and ionomers for anion exchange membrane fuel cells", Nature Communications, 12 (2021) 2367. DOI: 10.1038/s41467-021-22612-3

[21] J. Wang, Y. Zhao, B.P. Setzler, S. Rojas-Carbonell, C. Ben Yehuda, A. Amel, M. Page, L. Wang, K. Hu, L. Shi, S. Gottesfeld, J. Xu B, Y. Yan, "Poly(aryl piperidinium) membranes and ionomers for hydroxide exchange membrane fuel cells", *Nature Energy*, 4 (2019) 392-398. DOI: 10.1038/s41560-019-0372-8

[22] C. E. Diesendruck, D. R. Dekel, "Water – A key parameter in the stability of anion exchange membrane fuel cells," *Current Opinion in Electrochemistry,* 9 (2018) 173-178. DOI: 10.1016/j.coelec.2018.03.019

[23] W. Youa, K. J. T. Noonan, G. W. Coates, "Alkaline-stable anion exchange membranes: A review of synthetic approaches," *Progress in Polymer Science*, 100 (2020) 101177 DOI: 10.1016/j.progpolymsci.2019.101177

[24] R. Gutru, Z. Turtayeva, F. Xu, G. Maranzana, B. Vigolo, A. Desforges, "A comprehensive review on water management strategies and developments in anion exchange membrane fuel cells," *International Journal of Hydrogen Energy,* 45 (2020) 19642-19663. DOI: 10.1016/j.ijhydene.2020.05.026

[25] R. B. Kaspar, M. P. Letterio, J. A. Wittkopf, K. Gong, S. Gu, Y. Yan, "Manipulating Water in High-Performance Hydroxide Exchange Membrane Fuel Cells through Asymmetric Humidification and Wetproofing," *Journal of The Electrochemical Society*, 162 (2015) F483-F488. DOI: 10.1149/2.0131506jes

[26] W. E. Mustain, M. Chatenet, M. Page, Y. S. Kim, "Durability challenges of anion exchange membrane fuel cells," *Energy & Environmental Science,* 13 (2020) 2805-2838, DOI: 10.1039/d0ee01133a

[27] D. R. Dekel, S. Willdorf, U. Ash, M. Amar, S. Pusara, S. Dhara, S. Srebnik, C. E. Diesendruck, "The critical relation between chemical stability of cations and water in anion exchange membrane fuel cells environment," *Journal of Power Sources,* 375 (2018) 351-360. DOI: 10.1016/j.jpowsour.2017.08.026

[28] D. R. Dekel, I. G. Rasin, M. Page, S. Brandon, "Steady state and transient simulation of anion exchange membrane fuel cells," *Journal of Power Sources,* 375 (2018) 191-204. DOI: 10.1016/j.jpowsour.2017.07.012

[29] T. J. Omasta, L. Wang, X. Peng, C.A. Lewis, J.R. Varcoe, W.E. Mustain,

"Importance of balancing membrane and electrode water in anion exchange membrane fuel cells," *Journal of Power Sources,* 375 (2018) 205-213. DOI: 10.1016/j.jpowsour.2017.05.006

[30] T. J. Omasta, A. M. Park, J. M. LaManna, Y. Zhang, X. Peng, L. Wang, D. L. Jacobson, J. R. Varcoe, D. S. Hussey, B. S. Pivovar, W. E. Mustain, "Beyond catalysis and membranes: visualizing and solving the challenge of electrode water accumulation and flooding in AEMFCs," *Energy & Environmental Science*, 11 (2018) 551-558. DOI: 10.1039/c8ee00122g

[31] D. R. Dekel, "Review of cell performance in anion exchange membrane fuel cells," *Journal of Power Sources,* 375 (2018) 158-169. DOI: 10.1016/j.jpowsour.2017.07.117

[32] M. Mamlouk, J. A. Horsfall, C. Williams, K. Scott, "Radiation grafted membranes for superior anion exchange polymer membrane fuel cells performance," *International Journal of Hydrogen Energy,* 37 (2012) 11912-11920. DOI: 10.1016/j.ijhydene.2012.05.117

[33] J. Ponce-González, D. K. Whelligan, L. Wang, R. Bance-Soualhi, Y. Wang, Y. Peng, H. Peng, D. C. Apperley, H. N. Sarode, T. P. Pandey, A. G. Divekar, S. Seifert, A. M. Herring, L. Zhuang, J. R. Varcoe, "High performance aliphatic-heterocyclic benzyl-quaternary ammonium radiation-grafted anion-exchange membranes," *Energy & Environmental Science*, 9 (2016) 3724-3735. DOI: 10.1039/c6ee01958g

[34] L. Wang, E. Magliocca, E. L. Cunningham, W. E. Mustain, S. D. Poynton, R. Escudero-Cid, M. M. Nasef, J. Ponce-González, R. Bance-Souahli, R. C. T. Slade, Da. K. Whelligan, J. R. Varcoe, "An optimised synthesis of high performance radiation-grafted anion-exchange membranes," *Green Chemistry,* 19 (2017) 831-843. DOI: 10.1039/c6gc02526a

[35] Y. Wang, G. Wang, G. Li, B. Huang, J. Pan, Q. Liu, J. Han, L. Xiao, J. Lu, L. Zhuang, "Pt–Ru catalyzed hydrogen oxidation in alkaline media: oxophilic effect or electronic effect?," *Energy & Environmental Science,* 8 (2015) 177-181. DOI: 10.1039/c4ee02564d

[36] D. R. Dekel, "Unraveling mysteries of hydrogen electrooxidation in anion exchange membrane fuel cells," *Current Opinion in Electrochemistry*, 12 (2018) 182-188. DOI: 10.1016/j.coelec.2018.11.013

[37] S. T. Thompson, D. Peterson, D. Ho, D. Papageorgopoulos, "Perspective—The Next Decade of AEMFCs: Near-Term Targets to Accelerate Applied R&D," *Journal of The Electrochemical Society*, 167 (2020) 084514. DOI: 10.1149/1945-

7111/ab8c88

[38] A. Roy, M. R. Talarposhti, S. J. Normile, I. V. Zenyuk, V. D. Andrade, K. Artyushkova, A. Serov, P. Atanassov, "Nickel–copper supported on a carbon black hydrogen oxidation catalyst integrated into an anion-exchange membrane fuel cell," *Sustainable Energy Fuels,* 2 (2018) 2268-2275. DOI: 10.1039/c8se00261d

[39] M. Hu, Q. Li, H. Peng, H. Ma, L. Xiao, G. Wang, J. Lu, L. Zhuang, "Alkaline polymer electrolyte fuel cells without anode humidification and H_2 emission", *Journal of Power Sources,* 472 (2020) 228471. DOI: 10.1016/j.jpowsour.2020.228471

[40] W. Vielstich, A. Lamm, H.A. Gasteiger, "Handbook of fuel cells: fundamentals, technology and applications," vol. 2, Wiley, New York (2003)

[41] D. Yang, H. Yu, G. Li, Y. Zhao, Y. Liu, C. Zhang, W. Song, Z. Shao, "Fine microstructure of high performance electrode in alkaline anion exchange membrane fuel cells", *Journal of Power Sources*, 267 (2014) 39-47. DOI: 10.1016/j.jpowsour.2014.04.053

[42] K. Takahashi, K. Kakinuma, M. Uchida, "Improvement of Cell Performance in Low-Pt-Loading PEFC Cathode Catalyst Layers Prepared by the Electrospray Method", *Journal of The Electrochemical Society,* 163 (2016) F1182-F1188. DOI: 10.1149/2.0611610jes

[43] [20] K. Takahashi, R. Kobayashi, K. Kakinuma, M. Uchida, "Improvement of Cell Performance in Low-Pt-Loading PEFC Cathode Catalyst Layers with Pt/Ta-SnO 2 Prepared by the Electrospray Method", *Journal of The Electrochemical Society,* 164 (2017) F235-F242. DOI: 10.1149/2.0251704jes

[44] S. Cho, K. Tamoto, M. Uchida, "Effect of an Electrospray-Generated Ionomer Morphology on Polymer Electrolyte Fuel Cell Performance", *Energy Fuels*, 34 (2020) 14853-14863. DOI: 10.1021/acs.energyfuels.0c02337

[45] M. Uchida, "PEFC catalyst layers: Effect of support microstructure on both distributions of Pt and ionomer and cell performance and durability", *Current Opinion in Electrochemistry,* 21 (2020) 209-218. DOI: 10.1016/j.coelec.2020.02.019

[46] Hydrogen scaling up: A sustainable pathway for the global energy transition,

published by Hydrogen Council November 2017, https://hydrogencouncil.com/wp-content/uploads/2017/11/Hydrogen-scaling-up-Hydrogen-Council.pdf

[47] Overview of Fuel Cell Activities with a focus on AEMFC R&D, published by U.S. Department of Energy Fuel Cell Technologies Office, April, 2016 https://www.energy.gov/sites/prod/files/2016/04/f30/fcto_2016_amfcw_1-papageorgopoulos.pdf,

[48] Resource depletion risk in rare metal and rare earth special feature, published by National Institute for Materials Science (NIMS). https://www.nims.go.jp/research/elements/rare-metal/probrem/dryness.html

[49] J. Arias, “hydrogen and fuel cells in Japan”, Tokyo, October 2019 https://www.eu-japan.eu/sites/default/files/publications/docs/hydrogen_and_fuel_cells_in_japan.pdf

[50] Tatsuoki Kono,“Hydrogen from Regional Energy Management to Global Network of Renewable Production”, French-Japanese seminar for cooperation on hydrogen development, June 2019. https://www.tresor.economie.gouv.fr/Articles/120903c7-34bc-49b1-a324-b1f6ba0dbf53/files/84e67d9a-a641-4624-b8c4-5b7e64cc9ba4

[51] 3E+S in "10 Questions to Understand Energy Today," Japan's Energy 2020 Edition, published by Agency for Natural Resources and Energy of Japan. https://www.enecho.meti.go.jp/about/pamphlet/energy2020/005/

[52] NEDO Hydrogen Energy White Paper Chapter 4: Current Status and Prospects of the Hydrogen Energy Market, published by NEDO. https://www.nedo.go.jp/content/100639757.pdf

List of Publications

1. Performance hysteresis phenomena of anion exchange membrane fuel cells using an Fe–N–C cathode catalyst and an in-house-developed polymer electrolyte

K. Otsuji, N. Yokota, D. A. Tryk, K. Kakinuma, K. Miyatake, M. Uchida

Journal of Power Sources, 487 (2021) 229407. DOI: 10.1016/j.jpowsour.2020.229407

2. Effect of water management in membrane and cathode catalyst layers on suppressing the performance hysteresis phenomenon in anion-exchange membrane fuel cells

K. Otsuji, Y. Shirase, T. Asakawa, N. Yokota, K. Nagase, W. Xu, P. Song, S. Wang, D. A. Tryk, K. Kakinuma, J. Inukai, K. Miyatake, M. Uchida

Journal of Power Sources, 522 (2022) 230997. DOI: 10.1016/j.jpowsour.2022.230997

Supplemental articles

3. High Hydroxide Ion Conductivity with Enhanced Alkaline Stability of Partially Fluorinated and Quaternized Aromatic Copolymers as Anion Exchange Membranes.

A. M. A. Mahmoud, A. M. M. Elsaghier, K. Otsuji, K. Miyatake

Macromolecules, 50 (2017) 256. DOI: 10.1021/acs.macromol.7b00401

4. Structurally Well-Defined Anion Conductive Aromatic Copolymers: Effect of the Side-Chain Length

R. Akiyama, N. Yokota, K. Otsuji, K. Miyatake

Macromolecules, 51, (2018) 3394. DOI: 10.1021/acs.macromol.8b00284

5. Structurally Well-Defined Anion-Exchange Membranes Containing Perfluoroalkyl and Ammonium-Functionalized Fluorenyl Groups

M. Ozawa, T. Kimura, K. Otsuji, R. Akiyama, J. Miyake, M. Uchida, J. Inukai, K. Miyatake

ACS Omega, 3 (2018) 16143. DOI: 10.1021/acsomega.8b02742

6. Partially fluorinated copolymers containing pendant piperidinium head groups as anion exchange membranes for alkaline fuel cells

D. Koronka, A. Matsumoto, K. Otsuji, K. Miyatake

RSC Advances, 9 (2019) 37391. DOI: 10.1002/pola.29360

7. Durability of Newly Developed Polyphenylene-Based Ionomer Membranes in Polymer Electrolyte Fuel Cells: Accelerated Stress Evaluation

R. Shimizu, K. Otsuji, A. Masuda, N. Sato, M. Kusakabe, A. Iiyama, K. Miyatake M. Uchida,

Journal of The Electrochemical Society, 166 (2019) F3105. DOI: 10.1149/2.0131907jes

Meeting Abstracts

1. The 6th International Seminar for Special Doctoral Program "Green Energy Conversion Science and Technology", Nagano, Japan (2017, 9)

K. Otsuji, N. Yokota, N. Yoshimura, K. Miyatake, M. Uchida

2. The 58th Battery Symposium in Japan, Hukuoka, Japan (2017, 11)

K. Otsuji, N. Yokota, N. Yoshimura, K. Miyatake, M. Uchida

3. 22nd Topical Meeting of the International Society of Electrochemistry, Tokyo, Japan (2018, 4)

K. Otsuji, M. Shimada, N. Yokota, D. A. Tryk, K. Kakinuma, K. Miyatake, M. Uchida

4. The 7th International Seminar for Special Doctoral Program "Green Energy Conversion Science and Technology", Yamanashi, Japan (2018, 8)

K. Otsuji, N. Yokota, N. Yoshimura, K. Miyatake, M. Uchida

5. The 8th International Fuel Cell Workshop 2018, Yamanashi, (2018, 8)

K. Otsuji, N. Yokota, K. Miyatake, M. Uchida

6. The 59th Battery Symposium in Japan, Osaka, Japan (2018, 11)

K. Otsuji, N. Yokota, K. Miyatake, M. Uchida

7. The 86th Electrochemical Society of Japan spring Meeting, Kyoto, Japan (2019, 3)

K. Otsuji, N. Yokota, K. Kakinuma, K. Miyatake, M. Uchida

8. The 8th International Seminar for Special Doctoral Program "Green Energy Conversion Science and Technology", Yamanashi, Japan (2019, 10)

K. Otsuji, N. Yokota, K. Kakinuma, K. Miyatake, M. Uchida

9. The 60th Battery Symposium in Japan, Kyoto, Japan (2019, 11)

K. Otsuji, N. Yokota, K. Kakinuma, K. Miyatake, M. Uchida

10. PRiME 2020, Honolulu, USA (2020, 10)

K. Otsuji, N. Yokota, D. A. Tryk, K. Kakinuma, K. Miyatake, M. Uchida

11. 240th ECS Meeting, Orlando, USA (2021. 10)

K. Otsuji, N. Yokota, D. A. Tryk, K. Kakinuma, K. Miyatake, M. Uchida

Acknowledgments

For this thesis, researches have been carried out at Fuel Cell Nanomaterial Center, Clean Energy Center and Interdisciplinary Graduate School of Medicine, Engineering, and Agricultural Science in University of Yamanashi.

This project was partly supported by the New Energy and Industrial Technology Development Organization (NEDO) Japan through funds for the "Advanced Research Program for Energy and Environmental Technologies," by the Japan Society for the Promotion of Science (JSPS) and the Swiss National Science Foundation (SNSF) under the Joint Research Projects (JRPs) program, and by the Japan Science and Technology (JST) through Strategic International Collaborative Research Program (SICORP).

I am deeply grateful to Pajarito Powder supplying the Fe-N-Cp catalyst.

I would like to express my great gratitude to **Professor Makoto Uchida** of University of Yamanashi, academic supervisor of this work, for his continuous guidance, invaluable suggestions, and warm encouragements throughout this work. I'm proud that I have worked with him.

I would like to express my science thanks to **Professor Kenji Miyatake** of University of Yamanashi and Waseda University for his helpful suggestion, excellent technical advices and continuous guidance to this work. He provided me a great opportunity to earn essential things as a science.

I would like to express my science appreciation to **Professor Katsuyoshi Kakinuma, Professor Donald Alexander Tryk** of University of Yamanashi for valuable suggestions and warm encouragement

I would like to express my science gratitude to **Professor Hiroyuki Uchida, Professor Akihiro Iiyama** and **Professor Junji Inukai** of University of Yamanashi for valuable suggestions and warm encouragement.

I would like to express my appreciation to **Professor Kazutoshi Higashiyama, Professor Tomio Omata, Professor Manuel Eduardo Brito, Professor Toshihiro Miyao, Assosiate Professor Junpei Miyake, Assosiate Professor Shinji Nohara, Assistant Professor Hanako Nishino, Assistant Professor Teppei Kawamoto** of University of Yamanashi, for valuable support and professional guidance

I am grateful thanks to **Professor Thomas J. Schmidt, Professor Emiliana Fabbri, Ms. Cordelia Gloor, Dr. Dino Aegerter, Dr. Casy Beall, Dr. Alexander Muroyama and Dr. Bernhard Pribyl** for their kind support in Switzerland.

I am grateful to **Dr. Koichiro Asazawa, Mr. Yui Kuwabara, Mr. Aoi Takano** and **Ms. Eriko Nishino** of Daihatsu Motor Co., Ltd. for their kind support and encouragement.

I am grateful to **Dr. Hiroshi Senoh and Dr. Masese Titus Nyamwaro** of AIST for their kind support and encouragement.

My deeply appreciation is expressed to **Dr. Ryo Akiyama, Dr. Akinobu Matsumoto, Dr. Hideaki Ono, Dr. Manai Shimada, Dr. Naoki Yokota, Dr. Katsuya Nagase** for valuable support and professional guidance

I am grateful to **Dr. Hiromichi Nishiyama, Dr. Hideaki Ohno, Dr. Ryo Shimizu, Dr. Taro Kimura, Dr. Ibuki Hosaka**, **Dr. Shun Kobayashi, Dr. Keisuke Shiino, Dr. Yu Kakizawa** of University of Yamanashi, for valuable support and professional advice.

I am also grateful to **Mr. Takayuki Asakawa, Ms. Mika Kodama, Ms. Setsuko Mori, Ms. Toshiko Gomyo** of University of Yamanashi for assistance of SEM and TEM measurement.

I am also grateful to **Ms. Nozomi Toyoda, Ms. Tomomi Hashizume, Ms. Kaori Ichinose** and all staffs of Fuel Cell Nanomaterial Center and Clean Energy Research Center for kind support and help.

I would like to thank **Dr. Yuya Yamashita, Dr. Kento Takahashi, Dr. Kazuhiro Takanohashi, Dr, Kazuki Shimura, Dr. Yoshiyuki Ogihara, Dr. Ahmed Mohamed Ahmed Mahmoud, Dr. Ryosuke Nishikawa, Dr. Ahn Jinju, Dr. Zhi Long, Dr. Daniel Koronka, Mr. Ryo Shirasaka, Mr. Shigefumi Shimada. Mr. Shota Miyashita, Ms.Mizuki Ozawa, Mr. Kohei Uyama, Mr. Yuta Oishi, Mr. Koki Ueno, Ms. Mizuki Hayashi, Mr. Takayuki Watanabe, Mr. Takatoshi Sawano, Mr. Yuto Shirase, Ms. Fumika Ishihara, Ms. Aki Kobayashi, Mr. Takumi Nagasaka, Mr.**

Yoshihiro Ozawa, Mr Yuto Shikano, Mr. Makoto Yonenaga, Mr. Ryohei Tomiyama, Mr. Ren Kumao, Mr. Ryuji Ohno, Mr. Keijiro Nagahara, Ms. Sayaka Takahashi, Ms. Masako Tanabe for their grateful support.

I would like to my university classmate, **Mr. Shunsuke Ishikawa, Mr. Junya Yamada, Mr. Takahiro Matsumoto, Mr. Akihiro Kamei, Ms. Chinatsu Takayama, Mr. Ryo Kobayashi, Mr. Takeshi Kawamura, Mr. Daiki Hasegawa** for giving me happy days.

I would like to offer my special thanks to **Mr. Toshiki Tanaka** without their encouragements, my doctoral program would not have been possible.

I would like to thank deeply all member of Fuel Cell Nanomaterials Center, Clean Energy Research Center, and Special Doctoral Program for Green Energy Conversion Science and Technology for their kind helps and supports.

Finally, I greatly appreciate the support of my family, **Toshihiro Otsuji, Mayumi Otsuji, Hiroto Otsuji, Toshitaka Otsuji, Hiroko Otsuji, Takashi Ueda, Youko Ueda, near relatives** and **animal friends.**

Kanji Otsuji

March 2022